Synthesis and Rheology of
Model Comb Polymer Architectures

Zur Erlangung des akademischen Grades eines

DOKTORS DER NATURWISSENSCHAFTEN

(Dr. rer. nat.)

Fakultät für Chemie und Biowissenschaften

Karlsruher Institut für Technologie (KIT) - Universitätsbereich

genehmigte

DISSERTATION

von

Dipl.-Chem. Michael Kempf

aus

Landau in der Pfalz

Dekan: Prof. Dr. M. Bastmeyer
Referent: Prof. Dr. M. Wilhelm
Korreferent.: Prof. Dr. C. Barner-Kowollik

Tag der mündlichen Prüfung: 15.12.2011

Every opportunity we take brings us forward.
Every chance we miss draws us back.
Every time we do not act we stand still.

Contents

Chapter 1

Introduction

1.1 Branching in commercial polymers

The worldwide demand for polyethylenes is increasingly high, due to their mechanical properties and the wide spreaded field of applications. Polyethylenes are used e.g. for bags, cling and agricultural films, milk carton coatings, electrical cable coatings, bottles, pipes and many more. The total global production of polyethylenes, including low density polyethylene (LDPE), linear low density polyethylene (LLDPE) and high density polyethylene (HDPE) accounted for about 77 million tons in 2008 [Malpass 10].

High density polyethylene (HDPE) consists of rarely branched (0.3-3 short-chain branches per 1000 C-Atoms), linear chains, Fig. 1.1a. Due to the highly linear structure and the extremely low level of defects a high degree of crystallinity is achieved, which results in a high density and stiffness of the polymer. Linear low density polyethylene (LLDPE) consists of linear polyethylene backbones with randomly attached short alkyl branches, Fig. 1.1b. The short branches are introduced via copolymerization of ethylene with 1-alkenes. Common is the introduction of ethyl, butyl, or hexyl groups as comonomer, the typical content is about 2-4 mol-%. The short branches suppress crystallization, leading to a reduction of the density. Low density polyethylene (LDPE) contains a substantial amount of alkyl (primarily ethyl and butyl) groups together with long-chain branches (15 - 30 branches per 1000 C-Atoms), Fig. 1.1c. The long-chain branches can themselves be branched. The short-chain branches reduce the degree of crystallinity, resulting in a flexible polymer with a low melting point. Whereas the long-chain branches influence the processing properties. The viscosity is lowered and the occurence of strain-hardening strengthens the stability during extensional flow, e.g. for the film-blowing process [Peacock 00].

The macroscopic properties of polyolefins in solid and melt state are determined by the

(a)

(b)

(c)
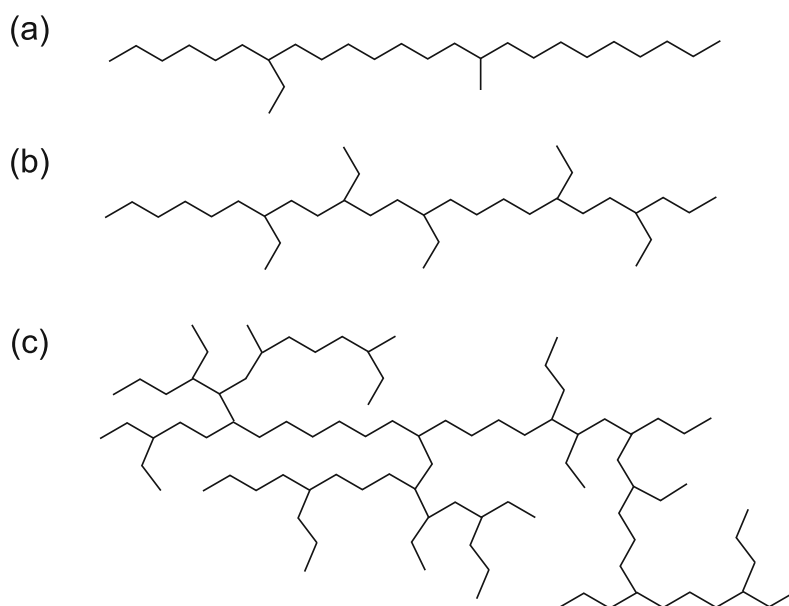
Figure 1.1: Schematic illustration of the different polyethylene structures: (a) High density polyethylene (HDPE), (b) linear low density polyethylene (LLDPE) and (c) low density polyethylene (LDPE).

underlying molecular structure, the molecular weight and the molecular weight distribution. Long chain branches (LCB), which are generally longer than the entanglement molecular weight have major effects on the flow and processing behavior. In contrast, short chain branches (SCB) influence the solid-state properties, due to the decrease of the melting point (T_m), the degree of crystallinity and the density [Peacock 00].

1.2   Motivation

The influences on the macroscopic properties, described above, can be so far related qualitatively to a certain kind (mainly amount and length) of branching. Whereas the correlation between the properties and the underlying molecular structure in polyethylenes is still far away from being understood. Several polymer characterization techniques have been applied for the determination of the branching degree, e.g. the combination of size-exclusion chromatrography (SEC) and fourier transform infrared spectroscopy (FT-IR) [DesLauriers 07], temperature-rising elution fractionation (TREF) [Monrabal 94], differential scanning chromatography (DSC) [Zhang 03], melt state ^{13}C-NMR spectroscopy [Klimke 06], and many more. However those techniques were mostly used to quantify the amount of short chain branches, they are not suitable for the determination of long-chain branching. Rheology, in contrast, is a promising method for the investiga-
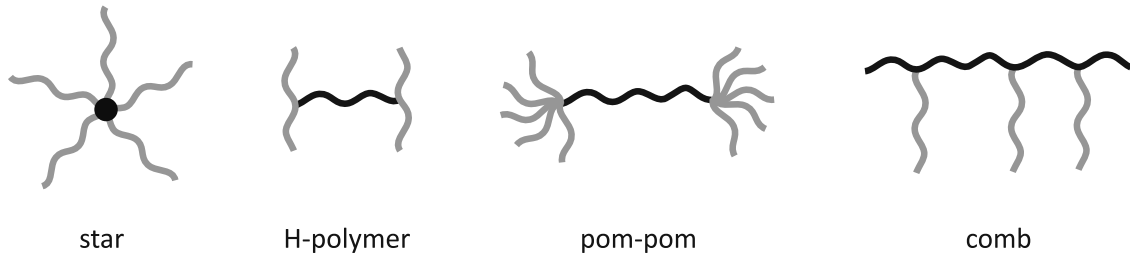
Figure 1.2: Overview of different topologies for branched structures.

tion of the influences and for the quantification of long-chain branching (LCB). Due to its high sensitivity towards the molecular structure, influences on viscoelasticity, even for low branching degrees, can be determined [Dealy 06]. However the rheological quantification of branching is still a challenging task. The topic of this thesis is therefore the application of rheological techniques towards the quantification of long-chain branching and the correlation with the mechanical properties.

A better control of the level and type of LCB is possible using metallocene catalysts, in contrast to free radical polymerization or Ziegler-Natta catalysts. Since the rheological properties of a specific structure are unknown, a control of the branching is not of interest so far. Therefore the success of metallocene catalysts is dependent on the quantitative understanding of the correlation between the long-chain branching and the rheological properties to compete with the well-established synthesis methods. As a result polyethylenes with defined mechanical properties could be amenable [Dealy 06].

In commercial PE it is very difficult to achieve quantitative correlations between the rheological data and the topology, due to the unknown underlying (branching) structure. This is further complicated by the use of additives to improve the rheological properties
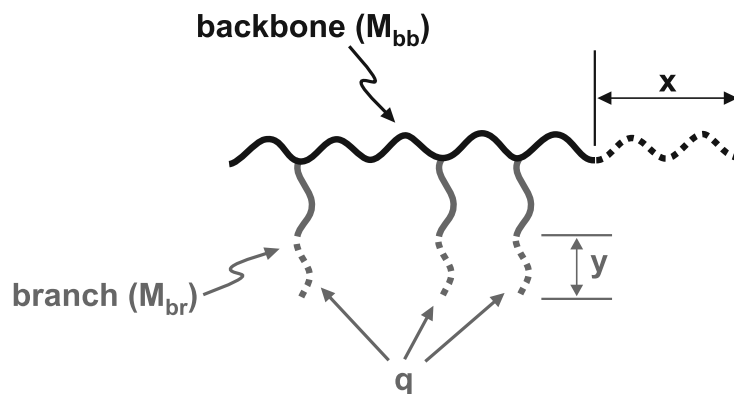
Figure 1.3: Schematic of a model comb polymer, consisting of a backbone with molecular weight M_{bb} and polydispersity x and a variable number of branches q, with molecular weight M_{br} and polydispersity y.

of the polymer for processing purposes and by the high polydispersities. The synthesis of branched model polymers with defined and well-known structures, which are comparable to the branching in polyethylenes is therefore indispensable.

Different kinds of model branched polymer topologies can be considered, e.g. star-, H-, Pom-Pom- and comb structures, Fig. 1.2. The comb topology is the appropriate structure to be used, due to its similarity to the polyethylene structure. To fulfill the requirements of a model comb polymer, Fig. 1.3, the molecular weight and molecular weight distribution of the backbone and of the branches as well as the number of branches of the comb have to be well controlled. Therefore different synthesis methods for model comb polymers were established and their rheological properties determined, within the framework of this study.

The objectives of this thesis are:

- The development of new syntheses methods for model branched polymers with well-defined structures. In contrast to previous methods, a low degree of long chain branching (< 1 mol-%) is aspired to determine the sensitivity of the rheological methods. Furthermore an upscaling ability is desired to apply the model combs to processing steps.

- The establishment of rheological measurement techniques for the determination of the branching structure of branched polymers to evaluate polymer properties.

- The comparison of the rheological methods regarding their possibilities and limitations/detection limits for the investigation of branched polymer topologies.

- The identification of optimal branching degrees, e.g. for maximum strain-hardening for processes in extensional flow. The results can be applied to the optimization of the synthesis conditions for polyethylenes to achieve a certain type of branching with desired rheological and processing properties.

- The results will likewise help to develop a non-linear model for complex architectures, which is so far not available. The knowledge of the non-linear behavior of branched polymers is of substantial interest, since during the polymer processing large and rapid deformations are applied which result in a highly non-linear behavior. Rheological properties and processing conditions can be thereby predicted.

The knowledge of the correlation between the molecular structure on the mechanical properties is of utmost importance for polymer processing and engineering applications, Fig. 1.4.
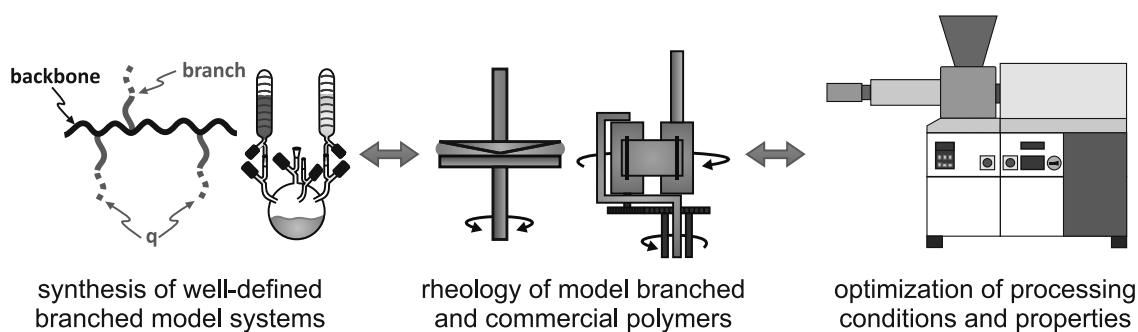
Figure 1.4: Graphical illustration of the objective of this study, the correlation between the polymer topology and the rheological properties for the improvement of the processing conditions of polyolefins.

1.3   Synthesis and rheology of model combs - State of the art

The rheological properties and processing abilities of branched polymers are highly affected by the degree of long chain branching. This induced a strong interest for a better understanding of the influences of branching on the rheological properties especially for commercial branched polymers [Gahleitner 01].

A major problem in the rheology of model (comb) polymers is the lack of sufficient sample quantities to perform various rheological experiments. The commonly used synthesis route for polystyrene based homopolymer model combs involves the chloromethylation of the polystyrene backbone to introduce branching points [Roovers 79]. The disadvantages of this method are the formation of highly toxic chloromethyl methyl ether as well as crosslinking side reactions during the functionalization reaction, which makes the synthesis of high amounts (several grams) difficult. The synthesis of polyisoprene (PI) and polybutadiene (PBD) model comb homopolymers can be accomplished using the macromonomer method [Koutalas 05] or by hydrosilylation [Hadjichristid 00b, Fernyhough 01]. In the case of the macromonomer method, side chains produced by anionic polymerization are terminated with a polymerizable endgroup and are copolymerized with the monomer (isoprene or butadiene) via anionic polymerization. By hydrosilylation a chlorosilane group is introduced at the pendant vinyl groups of the polymer backbone, the side chains are grafted via nucleophilic attack of living PI/PBD at the chlorosilane group. In both cases a low polydispersity of the backbone and the side chains can be achieved by the use of living polymerization, but the number of branching points is difficult to control. The PI and PBD samples have to be stabilized by radical scavengers and stored at low temperatures (approx. -20 °C) to prevent crosslinking.

Several approaches for the quantification of branching in commercial polymers have

been conducted. Due to the high complexity of commercial branched polymers mostly several analysis methods have been combined. Wood-Adams et al. [Wood-Adams 00a, Wood-Adams 00b] was able to estimate the degree of long chain branching in polyethylenes using linear viscoelastic (LVE) data in combination with molecular weight distribution (MWD) determined by size exclusion chromatography. They distinguished the effects of MWD and LCB on the LVE behavior by comparison of the MWD, calculated by the complex viscosity curve data, with the MWD obtained by the SEC measurements. The difference of the two MWDs is related to the branching degree of LCB. Similar approaches were conducted by Shaw and Tuminello [Shaw 94] as well as by Janzen and Colby [Janzen 99]. It is worth to mention that those methods were only concentrated on the number of branches, but not on their molecular weight or distribution along the backbone.

The determination of the effect of branching is difficult for commercial branched polymers, since their detailled topology is almost unknown and the additional complication by high polydispersities and additives. For this reason, rheological measurements alone do not give accurate results for the degree of branching, a combination with other analytical methods (SEC, NMR, viscosimetry, etc.) has to be applied. To circumvent those issues, several model systems e.g. stars [Graessley 79, Islam 01, Pryke 02], H-polymers [Roovers 84] and combs [Fujimoto 70, Roovers 81, Yurasova 94, Ferri 99, Daniels 01, Hepperle 05, Kapnistos 05, Lee 05, Hepperle 06, Inkson 06, Chambon 08, Kirkwood 09] with known architecture and low polydispersities have been synthesized and their melt rheological properties analyzed in the past.

For the quantification of long chain branching, shear rheology in the linear regime can be used, Trinkle et al. [Trinkle 01, Trinkle 02] suggested the reduced van Gurp-Palmen plot [Gurp 98] for the correlation of linear rheological data with the topology of different branched polymers and developed a topology map to assign different topologies. Liu et. al [Liu 11] used a branch-on-branch constitutive model (BoB-model) to calculate different topological structures with the aim to find characteristic points in the van Gurp-Palmen plot to construct a topology map using theoretically calculated points, implementing experimental data of various topologies as well.

Besides the rheological properties in the linear regime, the non-linear properties are as well highly influenced by long chain branching. In comparison to linear polymers an increased shear thinning behavior in long chain branched polyethylenes or polystyrenes was found [Lohse 02]. The occurance of strain hardening in extensional flow is also well known for long chain branched polymers, which is an important factor in processing, e.g. thermoforming [Yamaguchi 02, Münstedt 06], foaming [Spitael 04] and especially

film-blowing [Münstedt 06]. The experimental determination of the melt extensional viscosity is more difficult [Schulze 01], but nevertheless highly sensitive for distinguishing between different topologies in case of low degrees of long-chain branching (LCB). There have been noticeable results as for example in correlating the departure from linear extensional behavior (strain hardening) and its dependence on the applied strain rate, with the presence of various degrees of molecular branching in polyethylene [Gabriel 03]. This has also been recently studied for polyethylene samples, in which the molar mass distribution and the long-chain branching were varied systematically. The degree of strain hardening was found to vary with the different branching degrees, which could be well described in the context of a Cayley-tree, a model system for highly-branched polymers [Stadler 09]. In contrast to the investigations in the linear viscoelastic regime only a few experimental studies on the non-linear rheological properties in extensional flow of model (comb) architectures have been performed so far. Hepperle et al. [Hepperle 06] studied branched polystyrenes in shear and elongational flow in the non-linear regime. The branched polystyrenes were synthesized by radical copolymerisation of anionically synthesized macromonomer side chains and styrene, leading to a variety of structures with a high polydispersity (PDI = 1.4 - 2.4) of the polymer backbone. They could show that elongational flow measurements are more sensitive to differences in molecular structure than shear flow. Even graft-polystyrenes with branches below the entanglement molecular weight ($M_e \approx 15$ kg/mol) display some degree of strain hardening. The step strain experiment is frequently used to study the nonlinear response of polymer systems in the absence of flow. In various studies on combs of short as well as long branches [Vega 07, Kapnistos 09, Kirkwood 09]. Kapnistos et al. [Kapnistos 09] presented stress relaxation mastercurves covering the entire relaxation of the comb and demonstrated that the hierarchy of relaxation processes seen in the linear regime still exists under strong non-linear deformations. Both Kapnistos et al. [Kapnistos 09] as well as Vega and Milner [Vega 07] utilized the hierarchical relaxation picture to suggest that if the comb backbone remains well-entangled after dynamic dilution due to the arm relaxation process, the backbone should follow the Doi-Edwards [Doi 86] prediction for a linear chain, with no dependence on architecture.

A further method for rheological measurements in the non-linear regime is to apply medium- (MAOS) or large amplitude oscillatory shear (LAOS) as a test method. When the shear amplitude γ_0 and/or the shear frequency $\omega_1/2\pi$ are increased in a MAOS/LAOS experiment, non-linear effects start to appear on the shear stress response. This is because the applied shear rates become higher than the inverse of their characteristic relaxation times. An oscillatory excitation at a frequency $\omega_1/2\pi$ within

the non-linear regime generates mechanical harmonics on the stress response at $3\omega_1$, $5\omega_1$, $n\omega_1$ (with odd integer values of n > 1), with different intensities and phases [Giacomin 98, Wilhelm 98, Wilhelm 02]. In the literature the analysis of the stress response is usually performed using Lissajous figures. However, when the relative intensities of the harmonics are small (I_n/I_1 < 5 %) this approach presents some disadvantages for the quantification of their intensities and phases. In order to overcome this problem, the relative phase differences of the harmonics can be determined. The relative phase difference of the nth harmonic is given by $\Phi_n = \Phi_n\text{-}n\Phi_1$, where Φ_n and Φ_1 are the phases of the nth harmonic and of the fundamental frequency respectively [Neidhöfer 03]. This allows more precise and quantitative data because Φ_n is defined relative to the stress response [Neidhöfer 04]. The relative intensity of the nth harmonic is given by $I_n/I_1 = I_{n/1}$, which corresponds to the intensity of the nth harmonic (I_n) normalized to the intensity of the fundamental frequency (I_1). In contrast to other methods, FT-Rheology [Wilhelm 02] has several advantageous aspects. It is a very sensitive method, which can even detect very weak non-linearities ($I_{n/1} < 10^{-4}$), it is as well very sensitive for the detection of LCB and the distinction between branched and linear homopolymer topologies [Neidhöfer 04, Schlatter 05, Vittorias 07b, Hyun 09]. Neidhöfer et al. [Neidhöfer 04] were able to differentiate between branched and linear topologies under non-linear oscillatory shear using the relative intensity of the third harmonic ($I_{3/1}$) and the phase angle of the third harmonic (Φ_3) as a function of frequency at a fixed strain amplitude. Schlatter et al. [Schlatter 05] investigated $I_{3/1}$ and Φ_3 of linear and sparsely branched polyethylene melts and they observed that FT-Rheology is sensitive regarding the polymer topology. Vittorias et al. [Vittorias 07a, Vittorias 07b] found optimal conditions for the differentiation of linear and branched polyethylenes, they observed higher non-linearity for long chain branched polyethylenes in comparison to linear polyethylenes with similar molecular weight. Hyun et al. [Hyun 09, Hyun 10] studied monodisperse linear and comb polystyrene melts under LAOS conditions. A quadratic dependency of the relative intensity of the third harmonic ($I_{3/1}$) on the strain amplitude was concluded from constitutive equations and theoretical considerations. Consequently the instrinsic non-linear parameter Q_0 was introduced, which reflects the relaxation processes of the polymer chain and makes it possible to differentiate linear from branched topologies.

1.4   Outline

In the present study, monodisperse comb architectures with different branching degrees were examined to determine the effect of branching on the rheological properties. The

determination of the number and molecular weight of the branches is of special interest. Therefore well-defined polystyrene based comb polymers with narrow polydispersities with a controlled, but low number (0.1-1 mol-% per backbone) of branches were synthesized and compared with data of polystyrene combs of the Roovers series [Roovers 81] with higher number of branches (> 1 mol-% branches per backbone). The number and molecular weight of the branches was systematically varied to investigate the influence of slightly and fully entangled branches, section 2.4. In the linear regime, using the reduced van Gurp-Palmen plot, the influence of the molecular weight and the number of branches, in terms of critical points in the plots was investigated, see section 3.3. Uniaxial extensional measurement were further conducted to investigate the non-linear behavior in extensional flow, section 4.3. For the non-linear rheological shear measurements the intrinsic non-linear parameter Q_0 under Large Amplitude Oscillatory Shear (LAOS) in combination with FT-Rheology was used, section 5.2. For the modeling of the experimental data obtained from extensional rheological measurements and for the comparison with commercial branched polymers the molecular stress function (MSF) model was used, section 6.1. By means of the pom-pom model correlations between the branching degree and molecular weight of the branches with the strain hardening factor and the non-linear parameter Q_0 were performed. The validity of the reptation time, obtained from the intrinsic non-linear mastercurve was further shown, section 6.2.

Chapter 2

Synthesis of model comb homopolymers

2.1 Fundamentals of anionic polymerization

2.1.1 Introduction

The anionic polymerization is a living polymerization, which is after the definition of Szwarc [Szwarc 68]: "A living polymerization is a chain growth reaction, which takes place in the absence of termination or chain transfer reactions." The main advantages of the anionic polymerization are accessibility to high molecular weights (> 1000 kg/mol) simultaneously with low polydispersities (PD < 1.1).

The dependency of the polymerization degree P_n as function of the monomer conversion is schematically illustrated in Fig. 2.1 [Odian 04, Hsieh 96].
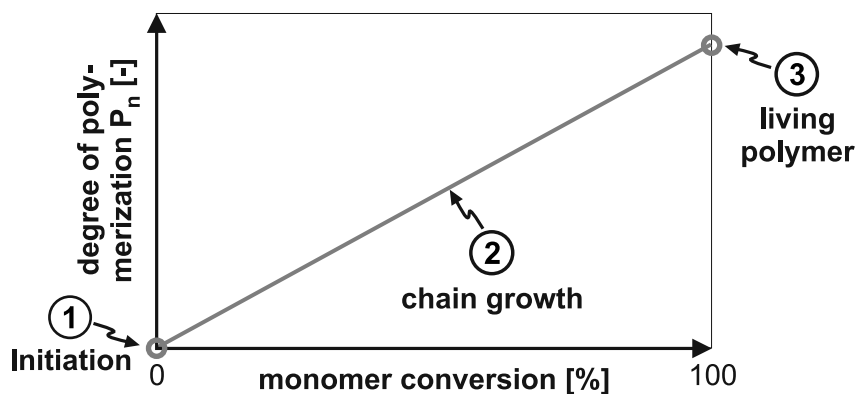
Figure 2.1: Schematical illustration of the dependency of the polymerization degree P_n as function of the monomer conversion for a living polymerization.

In the initiation step (1), the transfer of the active center of the initiator I^- to a monomer

molecule M takes place.

$$I^- + M \rightarrow IM^- \tag{2.1}$$

To achieve polymers with a narrow molecular weight distribution, the initiation step must occur much faster than the actual chain growth, so that all chains start approximately at the same time.

In the chain growth step (2) the polymerization degree P_n increases linearly with conversion. In the ideal case, no termination (anions cannot recombinate, due to charge repulsion) or chain transfer reactions take place, all chains grow with the same rate and consequently polymer chains with almost similar chain length can be obtained. For the chain growth reaction holds:

$$IM_n^- + M \rightarrow IM_{n+1}^- \tag{2.2}$$

Since in the ideal case no termination or chain transfer reactions occur, the concentration of the active species $[IM_n^-]$ is identical to the concentration of the initiator $[I]_0$.

The chain growth rate is therefore

$$v_p = -\frac{[M]}{dt} = k_p\,[M]\,[IM_n^-] = k_p\,[M]\,[I]_0 \tag{2.3}$$

with the polymerization rate constant k_p. The polymerization degree P_n at the time t is given by

$$P_n = \frac{[M]_0 - [M]_t}{[I]_0} \tag{2.4}$$

with $[M]_0$ = as the monomer concentration at the beginning of the polymerization and with $[M]_t$ = monomer concentration at time t.

At the end of the polymerization (3) all monomer molecules have been consumed $[M]_t$ = 0, which results for the polymerization degree in

$$P_n = \frac{[M]}{[I]_0} \tag{2.5}$$

The polymerization degree P_n or the molecular weight respectively can be therefore controlled by the stoichiometry of the monomer concentration $[M]$ and the initiator concentration $[I]_0$.

The living chain ends stay active after the polymerization step, so that after further addition of monomer molecules, the polymerization can be continued.

As a result of the similtaneous initiation of all chains, in absence of termination reactions, a narrow molecular weight distribution can be obtained, which corresponds to a *Poisson distribution*[Elias 05].

2.1.2 Applicable Monomers

For the anionic polymerization, two types of monomers are suitable. On one hand monomers $CH_2{=}CHX$ with a substituent X at the double bond, which is able to stabilize the resulting negative charge, Fig (2.2), and on the other hand cyclic monomers, which can be ring-openend via nucleophilic addition [Hsieh 96].

$$X \ = \ \text{-NO}_2 \ > \ \text{-}\overset{\displaystyle \|}{\underset{\displaystyle O}{C}}\text{-R} \ > \ \text{-CN} \ \geq \ \text{-COOR} \ > \ \text{Ph} \ > \ \text{-CH=CH}_2$$
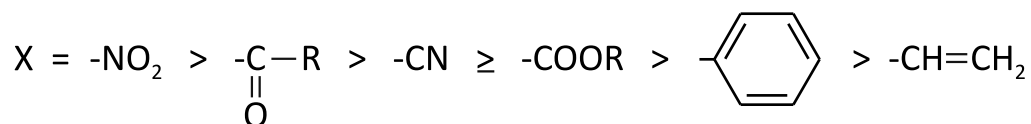
Figure 2.2: Substituents with decreasing electronic stabilization (-I, +M)

The substitutent has to be stable towards the reactive anionic species, to avoid termination reactions. Due to this, acidic or electrophilic functional groups (e.g. amino-, halogen-, hydroxy- or carboxy groups) should not be present or need to be protected appropriately [Hsieh 96].

A further aspect is the relationship between the reactivity of the monomers and the stability of the anion, which can be related to the pK_a value of the conjugated acid of the anion. This correlation is important for the choice of the initiator. Monomers, which form the least stable anions, posses the highest pK_a value for the corresponding conjugated acid and are therefore the least reactive monomers for the anionic polymerization. For such unreactive monomers (e.g. styrene), highly reactive initiators (e.g. organolithium compounds) have to be used [Hsieh 96].

2.1.3 Initiation

The initiation occurs after the addition of a base B^- (nucleophil) at the $C{=}C$ double bond of the monomer $CH_2{=}CHX$ [Odian 04]. The active center (the anion) is transfered from the initiator to the monomer in this step, Eq. 2.6.
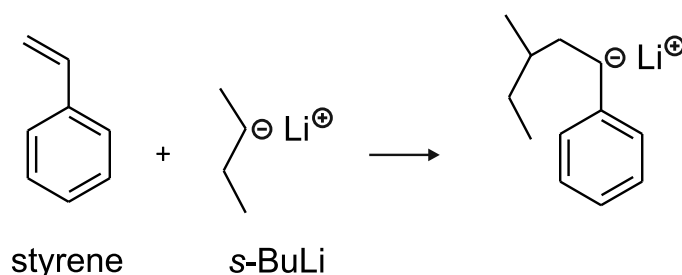
styrene   *s*-BuLi

Figure 2.3: Initiation reaction at the example of styrene with *s*-BuLi.

$$M^+ B^- \ + \ CH_2 = CHX \ \rightarrow B - CH_2 - CHX^- M^+ \tag{2.6}$$
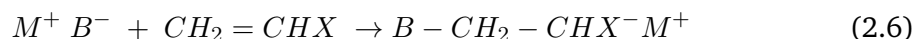
The initiation process is illustrated in Fig. 2.3, by the example of the initiation of styrene with sec-butyllithium (s-BuLi).

2.1.4 Propagation

The chain growth proceeds, according to Eq. 2.7, in a continuous regeneration of the active species, by insertation of the monomer between the metal cation Me^+ and the carbanion $P_i^{\ominus}$.

$$P_i^{\ominus} \ Me^+ + M \rightarrow P_i - M^{\ominus} \ Me^+ = P_{i+1}^{\ominus} \ Me^+ \tag{2.7}$$
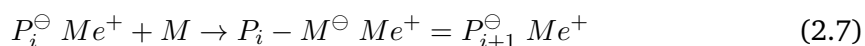
In Fig. 2.4 the propagation reaction is illustrated on the example of styrene.
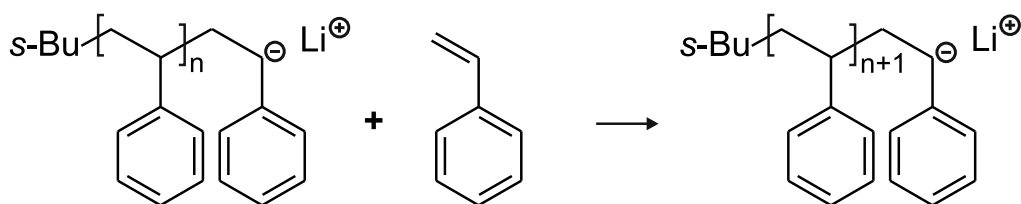
Figure 2.4: Propagation reaction on the example of polystyrene.

2.1.5 Termination

The deactivation of the active species results in the termination of the living chain, this is exemplarily shown in Eq. 2.8 for the termination with protic agents:

$$P_i^{\ominus} + H^+ \rightarrow P \tag{2.8}$$

To obtain the final polymer, the anions of the living chains are deactivated by the addition of protic agents (e.g. water or methanol), Fig. 2.5.
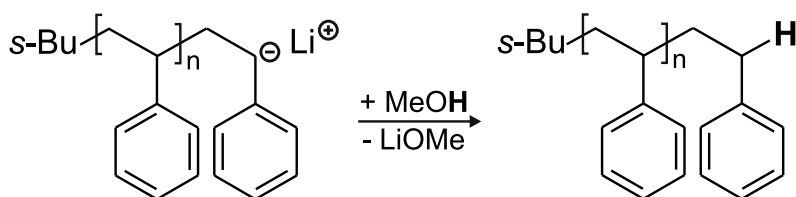
Figure 2.5: Termination reaction of living polystyrene with methanol.

The anionic polymerization is highly sensitive towards impurities, e.g. traces of protic agents (water), carbon dioxide or oxygen, which are major causes for the termination of the polymerization. The major termination reactions, caused by impurities, are illustrated in Fig. 2.6.
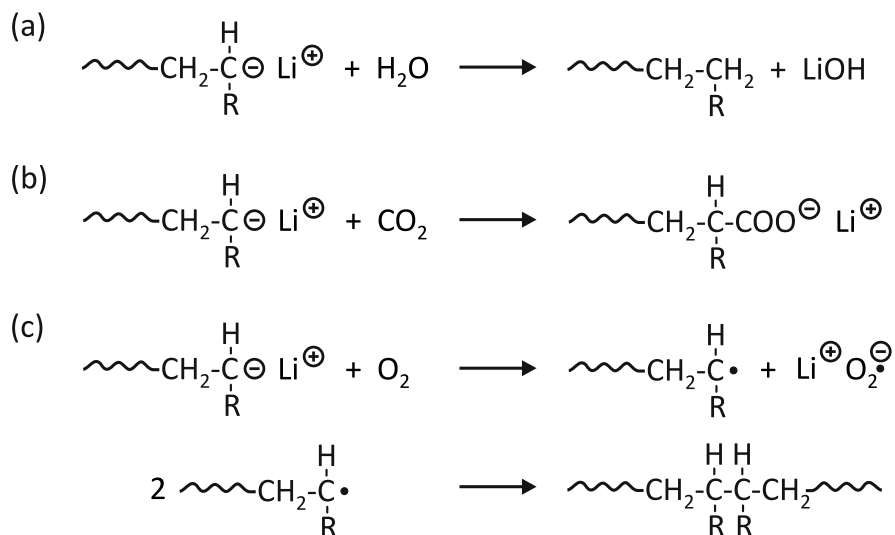
Figure 2.6: Termination reactions, caused by impurities, like water, carbon dioxide or oxygen [Quirk 82].

Water leads to a termination via proton transfer, Fig. 2.6a, the formed hydroxy-ion is in most cases not nucleophilic enough to reinitiate the polymerization. Carbon dioxide leads to carboxy endgroups, Fig. 2.6b, which are also not reactive enough to reinitiate the polymerization. By the addition of carbon dioxide and subsequent termination with e.g. methanol, carboxylic acids at the chain end can be achieved [Quirk 82]. Oxygen leads in contrast to different termination products, due to the radical mechanism involved [Quirk 84], Fig. 2.6c. The major termination product with oxygen is a dimer of two polymer chains connected via a peroxy-group. The product of the dimerization shows the double molecular weight of the main product and can be well observed in SEC measurements. Therefore the anionic polymerization steps are performed under inert gas atmosphere or high vacuum conditions [Hadjichristid 00a].

2.1.6 Solvent effects

The initiation and propagation rate depends substantially on the type of solvent, which is a result of the influence on the aggregation degree of the organolithium compounds and the living chains.

Polar solvents (e.g. THF) coordinate with the lithium cation, leading to a break up of the

aggregates. As a result, less aggregated or monomeric living species are present, which possess a higher initation or propagation rate.

The polymerization in aliphatic/non-polar solvents is in contrast to polar solvents much slower, since the living species are only partially dissoziated. It can be assumed that the initiation process is performed by the direct insertion of the monomer into the aggregated organolithium species, which leads to mixed aggregates between initiator and growing chain [Hsieh 96].

In Fig. 2.7 the initiation step of s-BuLi, which exists as a tetrahedral aggregate, and a monomer with a stabilizing substituent X is illustrated. The first step is the coordination of the double bond of the monomer with a lithium cation, which inserts in a second step in the sec-butyllithium bond. The aggregates change from solely sec-butyllithium bonds to mixed aggregates with incorporated living chains [Hsieh 96].
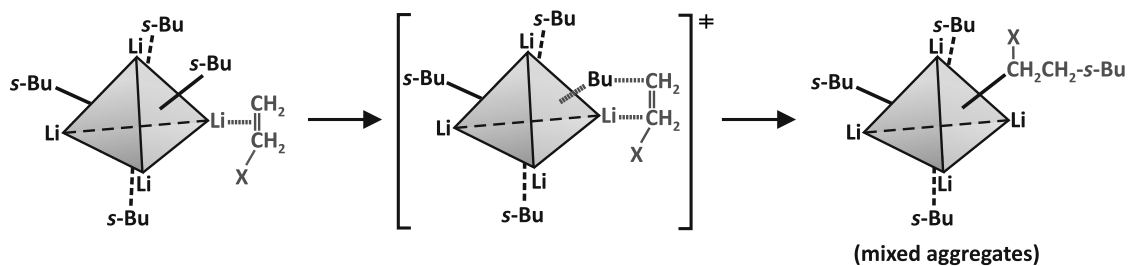
Figure 2.7: Schematic illustration of the initation step in non-polar solvent with s-BuLi as initiator and a monomer with a stabilizing substituent X [Hsieh 96].

The initiation in non-polar solvents is slow at the beginning, but due to the formation of mixed aggregates a self-acceleration of the reaction takes place. The steric hinderance of the growing chain in the mixed aggregates decreases the degree of aggregation, which leads to an increase of the concentration of monomeric active species and to an

| TMEDA | Tetraglyme | 18-crown-6 | 2.2.2-cryptand |
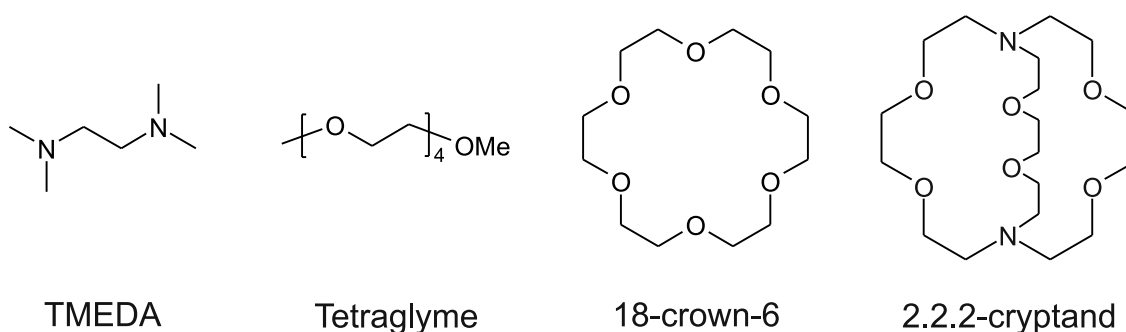
Figure 2.8: Examples of Lewis-bases used for the acceleration of the initiation step: (a) TMEDA, (b) Tetraglyme, (c) 18-crown-6 (d) 2.2.2-cryptand.

acceleration of the propagation [Morton 70, Worsfold 72, Odian 04].

For the acceleration of the initiation step, Lewis-bases, like TMEDA (N,N,N',N'-Tetra-methylethylendiamin), Tetraglyme (Tetraethylenglycoldimethylether), crown ether (e.g. 18-crown-6) oder cryptands (e.g. 2.2.2-cryptand) can be used, Fig. 2.8. Those coordinate analogous to the lithium cation and break up the aggregates [Odian 04].

2.2 Comb formation techniques

Comb structures can be made by three different methods, by grafting-from, grafting-through or grafting-onto processes [Hong 99]. The following section gives an overview over the different methods and their advantages and disadvantages.

2.2.1 Grafting-from

For the grafting-from method, active centers are generated directly at the backbone, which are able to initiate the monomer of the prospective branches, which grow away from the backbone, Fig. 2.9.
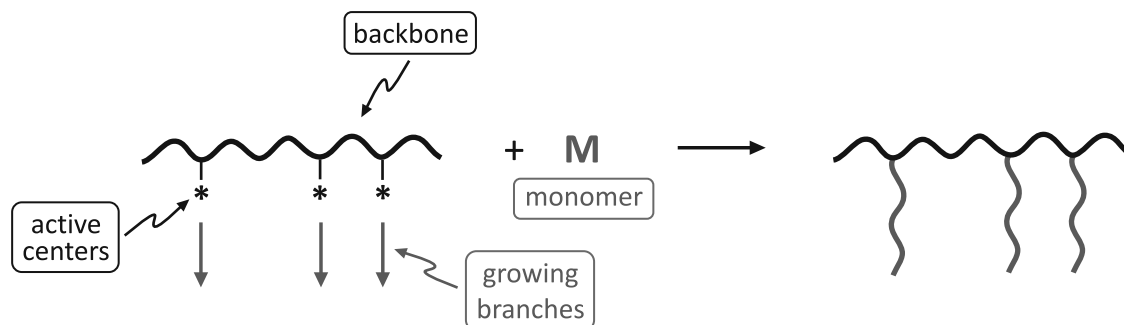
Figure 2.9: Schematic illustration of the grafting-from method.

In most cases anionic centres are generated at the polymer backbone, e.g. by metalation of the C-H bond, using organometallic compounds. The best known metalation process for the grafting-from method uses the combination of s-BuLi and TMEDA [Chalk 69, Falk 73, Clouet 79], whereby allylic, benzylic or aromatic C-H bonds can be metalated [Hsieh 96].

The grafting-from method has a series of disadvantages. The metalation generates active centers with different reactivity, which results in varying rates of initiation and therefore in branches with different length. This can also occur for active centers with identical reactivity, but slow initiation in comparison with the propagation.

Side reactions can take place, e.g. crosslinking, leading to unsoluable backbones or incomplete metalation, leading to homopolymerization of the monomer by unreacted organometallic compounds. The quantification of the final number, molecular weight and polydispersity of the branches is quite difficult, so that the number and average molecular weight is calculated from the total molecular weight of the branched polymer, elucidated e.g. via static-light scattering experiments.

2.2.2   Grafting-through or macromonomer method

In the case of the grafting-through or also called macromonomer method, the branches are synthesized independently and are endfunctionalized with a polymerizable endgroup. In most cases an olefinic endgroup is used. The endgroup of the macromonomer allows the copolymerization with the comonomer desired for the backbone, Fig. 2.10 [Hsieh 96].
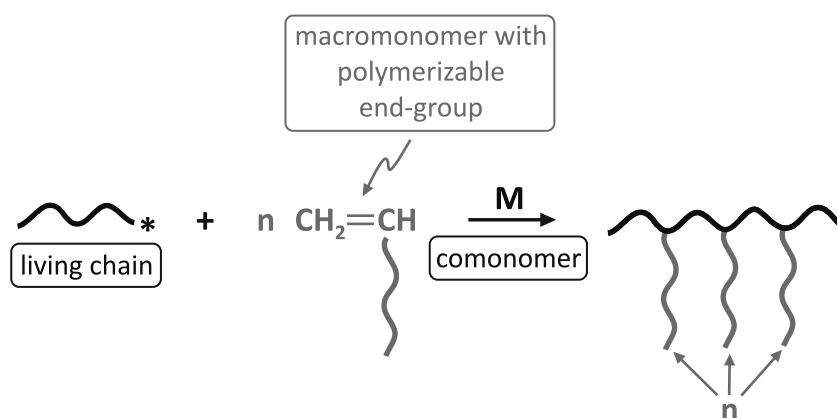
Figure 2.10: Schematical illustration of the grafting-through method.

To use the macromonomer method efficiently, the copolymerization behavior has to be well controlled, since the difference of the reactivities between macromonomer and comonomer has a much bigger influence on the copolymerization in the case of the ionic polymerization than for the free radical polymerization. Therefore it is difficult to control the implementation of macromonomers along the backbone [Hong 99].

In case the reactivity of the comonomer is higher than the reactivity of the macromonomer, the implementation of the comonomer is favored, after decreasing comonomer concentration, the copolymerization of the macromonomer takes place. The statistical distribution of the branches is therefore not assured anymore.

To achieve an ideal random copolymerization, the comonomer and the macromonomer must possess similar reactivities. For the copolymerization with styrene, the living branches can be converted with vinylbenzylbromide to achieve a vinylbenzyl-endgroup

at the macromonomer, which exhibits a similar reactivity in comparison with styrene [Gnanou 89].

The living polystyryllithium-chains (PSLi) are first endcapped with 1,1-diphenylethylene (DPE) to lower the reactivity and to minimize the occurance of side reactions. Afterwards it is converted to the endfunctionalized macromonomer by the addition of vinylbenzyl-bromide, Fig. 2.11.
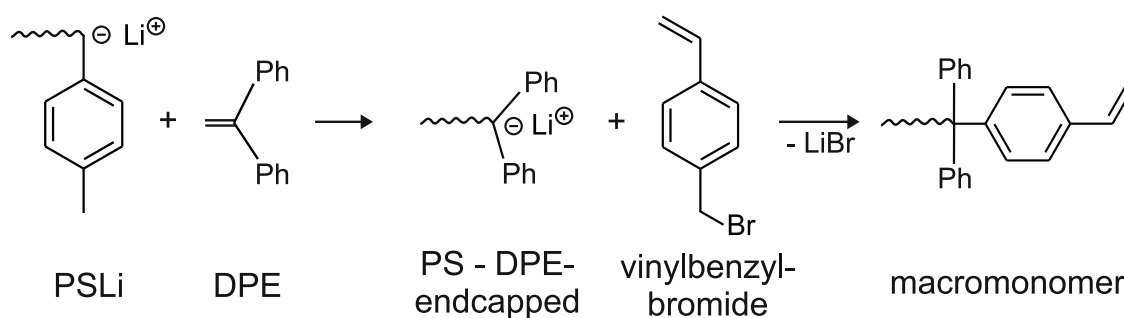
Figure 2.11: Preparation of vinylbenzyl-endfunctionalized macromonomers.

The endfunctionalization process is one of the disavantages of the macromonomer method, since on one side an excess of the endfunctionalization reagent (e.g. vinyl-benzylbromide) cannot be completely converted, so that the excess can react with living chains and leads consequently to a termination during the copolymerization. The excess can be deactivated by the addition of triphenylmethyllithium, which is not reactive enough to initiate the comonomer, but the formed product will also be implemented into the backbone, Fig. 2.12 [Hirao 96, Radke 96].
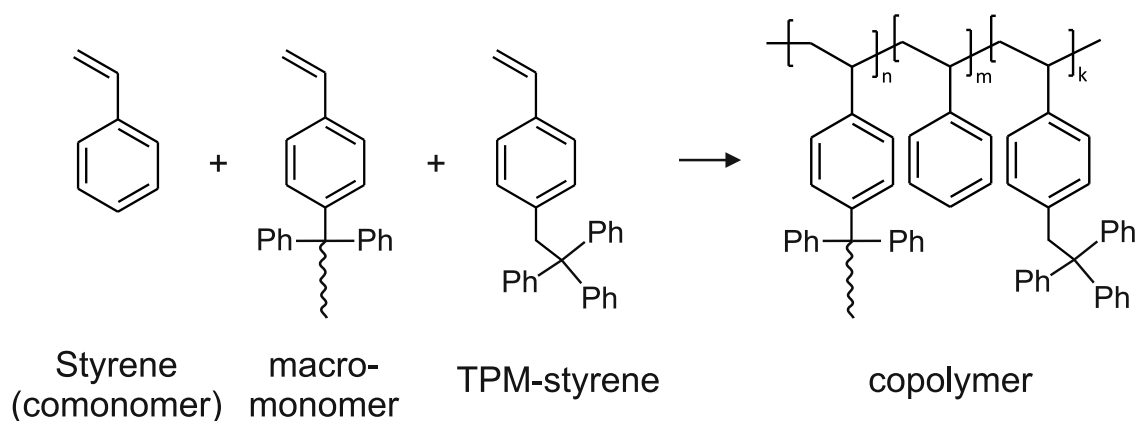
Figure 2.12: Schematic of the copolymerization of a macromonomer with the comonomer styrene. The triphenylmethylstyrene (TPM-styrene) created by the deactivation of excess vinylbenzylbro-mide is copolymerized as well.

On the other side a deficient amount of the endfunctionalization reagent (e.g. vinylben-zylbromide) would lead to an incomplete conversion of the living branches and would consequently lead to the consumption of the comonomer by the living branches, before the copolymerization would have even started by the addition of the initiator.

In the case of the macromonomer method, the average number of implemented branches per backbone results only by the stoichiometry of the added macromonomers. So that the number of branches as well as the backbone molecular weight and polydispersity cannot be determined directly, since only the molecular weight of the branched polymer and the macromonomer is known. The synthesis of well-defined structures is indeed possible, but the well characterization of the system is not.

2.2.3   Grafting-onto

In the grafting-onto method the backbone exhibits statistically distributed functional groups X, which can react with branches, possessing a corresponding functional group Y, Fig. 2.13 [Hsieh 96]. In most cases the reaction takes place between the nucleophilic chain end of living branches with electrophilic groups along the backbone [Hong 99].
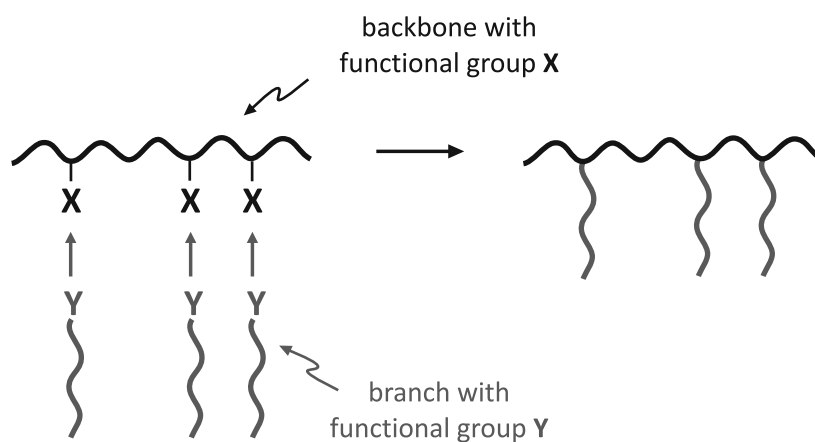
Figure 2.13: Schematic illustration of the grafting-onto method.

The main advantage of this method is the possibility of the independent synthesis and characterization of the backbone and the branches. Due to the independent characterization, the molecular weight and the polydispersity of the branches and of the backbone as well as the number of branching points is known. Using the grafting-onto method well defined comb polymer systems can be obtained.

Disadvantageous are occuring side reactions during the comb formation leading to crosslinking or incomplete conversion, see section 2.4.6.   Mostly used was the reac-

tion of living branches with chloromethylated [Pepper 53, Altares Jr. 65, Roovers 75] or dimethylchlorosilyloxymethylated backbones [Rahlwes 77, Cameron 81].

2.3 Characterization of comb polymers

2.3.1 Size exclusion chromatography (SEC)

The size exclusion separation is based on the effective hydrodynamic volume of the measured polymer. In contrast to linear polymers, branched polymers of similar molecular weight are more dense than the linear ones, leading to a lower effective hydrodynamic volume. Branched polymers will therefore elute later than a linear polymer of the same molecular weight. The detected molecular weight will be lower than the true value, when using a standard calibration [Wu 04]. This is illustrated in Fig. 2.14, where the molecular weight of the branched polymer M_B is higher than of the linear one M_L, but due to the similar hydrodynamic volume, both are eluated at the same time. For branched polymers a molecular weight determination using a standard calibration curve (calibration performed with linear polymer standards) is therefore not appropriate. A calibration with branched polymer standards would be possible, however such are not commercially available. An efficient method for the determination of the absolute molecular weights of branched polymers is the additional use of a light-scattering detector on the SEC system.

$$V_H^B \qquad V_H^L$$

$$V_H^B = V_H^L$$
$$M_B > M_L$$

branched polymer (M_B)　　　linear polymer (M_L)
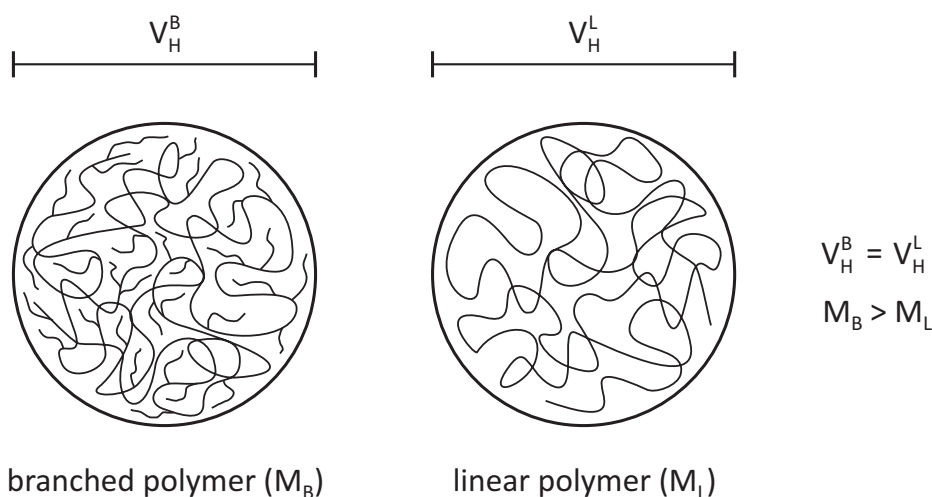
Figure 2.14: Comparison of the hydrodynamic volumes of branched and linear polymers. A branched polymer is more dense than the linear polymer of similar molecular weight, which leads to a lower effective hydrodynamic volume.

2.3.2   SEC coupled with Multi Angle Light Scattering (MALS)

The determination of the absolute molecular weight of polymers using a combination of SEC with a Multi Angle Light Scattering (MALS) detector follows the same fundamental principles as a static light scattering (SLS) experiment. The molecular weight of a polymer is related to the scattering intensity of the polymer solution over that of the pure solvent by [Zimm 48b, Wu 04]

$$\frac{Kc}{R\theta} = \frac{1}{M_w P(\theta)} + 2A_2 c \tag{2.9}$$

with c as the polymer concentration, M_w weight-average molecular weight of the polymer, A_2 second virial coefficient (measure of the compatibility between polymer solution and the solvent), $R\theta$ the excess Rayleigh ratio (measured excess scattering intensity of the solution over that of the pure solvent), $P(\theta)$ the particle scattering function (angular dependence of the excess Rayleigh ratio), and K an optical constant for the scattering system, given by

$$K = \frac{4\pi^2 n_0^2 (dn/dc)^2}{\lambda_0^4 N_A} \tag{2.10}$$

with N_A as the Avogadro number, n_0 refractive index of the solution at the incident wavelength λ and *dn/dc* specific refractive index increment, which reflects the change in solution refractive index with change in solute concentration. The particle scattering function is defined as:

$$\frac{1}{P(\theta)} = 1 + \left(\frac{4\pi}{\lambda}\right)^2 sin^2\left(\frac{\theta}{2}\right)\frac{\langle R_g^2\rangle_z}{3} \tag{2.11}$$

with $<R_g^2>$ the mean-square radius of gyration and θ as the scattering angle.
When the light-scattering detector is used online with a SEC setup, the light-scattering intensity is measured at a single concentration at several angles, for each molecular weight fraction. Since the measurement is performed at only one concentration, an extrapolation to zero angle for the determination of the second virial coefficient A_2 cannot be performed. For the determination of the molecular weight, according to Eq. 2.9, the second virial coefficient A_2 must be either known or assumed to be zero. Setting the second virial coefficient A_2 to zero is in most cases an appropriate approximation, because the polymer concentration is usually so low that the concentration is assumed to be zero and the second term vanishes thereby. The molecular weight and the mean-square radius of gyration can be generally determined by a Zimm-plot (where Kc/Rθ is plotted against $sin^2(\theta/2+kc)$), Fig. 2.15 [Zimm 48a]. The extrapolation at zero concentration intercepts the Kc/Rθ axis, which is equal to the inverse of the molecular weight:

$$\left(\frac{Kc}{R\theta}\right)_{c\to 0} = \frac{1}{M_w} \tag{2.12}$$

The initial slope of the graph at zero concentration, divided by the intercept, is proportional to the mean-square radius of gyration [Mori 99, Wu 04].

The determination of the branching degree of polymers with unknown branching structure using MALS has long been of major interest since the first publication of this topic was released by Zimm and Stockmeyer [Zimm 49]. The amount of branching can be assigned to the so-called branching ratio g [Zimm 49, Burchard 80, Podzimek 01a]:

$$g = \frac{1/M \int r_b^2 \, dm}{1/M \int r_l^2 \, dm} = \frac{\langle R_{g,b}^2 \rangle}{\langle R_{g,l}^2 \rangle} \tag{2.13}$$

with the mean square radii of the branched $\langle R_{g,b}^2 \rangle$ and the linear $\langle R_{g,l}^2 \rangle$ polymer at the same molar mass. The problem hereby is the requirement of linear and branched polymers with identical molar masses for the comparison [Mori 99, Wu 04].

The advantage of the SEC-MALS system is the fast determination of the absolute molecular weight, of the mean square radius and of the polydispersity of the polymer. The time consuming independent measurement of the *dn/dc* and the preparation of multiple concentrations in the case of classic static light scattering experiments are not necessary. While the results of the polydispersity determined by SEC-MALS have been criticized in the literature for being to small, because of the decreasing sensitivity for decreasing molecular weight. Podzimek et al. [Podzimek 01a, Podzimek 01b] concluded that SEC-MALS leads to most plausible values for the polydispersity.
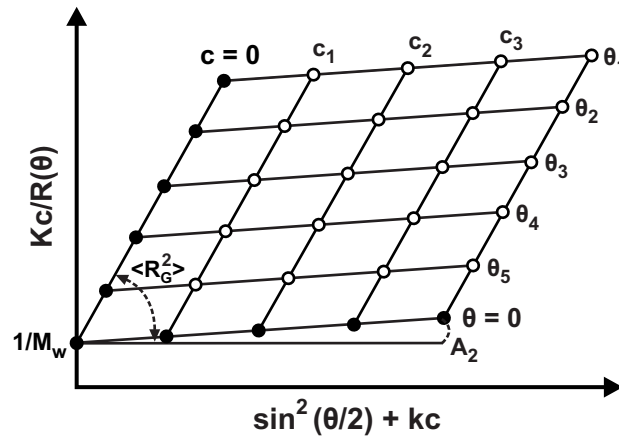
Figure 2.15: Schematic of a Zimm-plot derived from static light scattering, in the case of the SEC-MALS measurement only the c=0 values at different scattering angles are obtained.

2.4   Synthesis strategy for homopolymer comb architectures

2.4.1   Introduction

As already pointed out in section 2.2, the grafting-onto approach is the method of choice for the synthesis of model comb architectures. It allows the independent and full characterization of the comb components to determinate the molecular weight and polydispersity of the backbone and of the branches as well as the number of branching points. Although model comb homopolymers of polyisoprene (PI) and polybutadiene (PBD) have been synthesized in the past [Cameron 81, Hadjichristid 00b, Fernyhough 01, Koutalas 05], polystyrene (PS) and poly(p-methylstyrene) (PpMS) was choosen instead for the synthesis of model comb structures. The major advantages of PS/PpMS over PI/PBD are the possibilities for selective mono-functionalization at the aromatic and benzylic position respectively, the long-term stability of the polymer without occurent crosslinking as well as the high activation energy and no crystallinity, which makes a wide temperature/frequency range in rheology accessible.

Polyisoprene (PI) and polybutadiene (PBD) based combs can be synthesized via the grafting-onto method, e.g. by the introduction of chlorosilane groups at the pendant vinyl groups of the polymer backbone via hydrosilylation [Hadjichristid 00b, Fernyhough 01]. The branches are grafted via nucleophilic attack of living PI/PBD at the chlorosilane group. In both cases a low polydispersity of the backbone and the branches can be achieved by the use of living polymerization, but the number of branching points is difficult to control via hydrosilylation. To prevent crosslinking the PI and PBD samples need to be stabilized by radical scavengers and stored at low temperatures (approx. -20°C). The commonly used synthesis route for polystyrene based homopolymer model combs involves the chloromethylation of the polystyrene backbone to introduce branching points [Roovers 79]. Disadvantageous is the formation of highly toxic and carcinogenic chloromethyl methyl ether (CMME) during the functionalization reaction. Side reactions, like crosslinking do also occur during the functionalization, which broadens the polydispersity. The synthesis of high amounts (several grams) is therefore difficult.

Thus it was necessary to develop new approaches for the synthesis of styrene based model comb architectures with the ability for high molecular weight backbones (> 200 kg/mol), low polydispersity of the backbone and the branches and the possibility to introduce a low number of branching points (< 1 mol-% per backbone). The type of functional group to be introduced has to be choosen appropriately to ensure a quantitative conversion during the comb formation reaction. Those are critical conditions to be fulfilled by the reaction, since the molecular weight of the backbone and of the branches, the polydispersity and

the number of branches have an influence on the rheological properties of the sample.

2.4.2 Reaction overview

An overview of the different reaction steps for the synthesis of polystyrene and poly(p-methylstyrene) based model combs is given in Fig. 2.16 and Fig. 2.17 respectively. The reaction steps are described in detail in the following sections. The molecular characteristics of the synthesized and rheologically analyzed samples are listed in table (2.1). The following nomenclature is used for the comb samples: xk-y-zk, with x = backbone weight average molecular weight $M_{w,bb}$, y = number of branches and z = branch weight average molecular weight $M_{w,br}$. The polymer type is described by the prefix PS for polystyrene or PpMS for poly(p-methylstyrene). When appropriate, the sample name listed in table (2.1) is used instead.

Table 2.1: Molecular characteristics of the model comb samples.

sample name	$M_{w,bb}$ [kg/mol] backbone	$M_{w,br}$ [kg/mol] branch	q (branches/ backbone)	$M_{w,total}$ [kg/mol]	PDI (comb) (SEC-MALLS)	polymer type
CK106	197	42	14	765	1.07	PpMS
CK123	275	42	5	495	1.02	PS
CK128	197	15	14	404	1.02	PpMS
CK132	197	15	29	607	1.09	PpMS
CK158	262	17	2	304	1.01	PS
CK159	262	37	2	322	1.01	PS
C632[a]	275	26	25	913	-	PS
C642[a]	275	47	29	1630	-	PS

[a]: model comb samples synthesized by Roovers [Roovers 79]
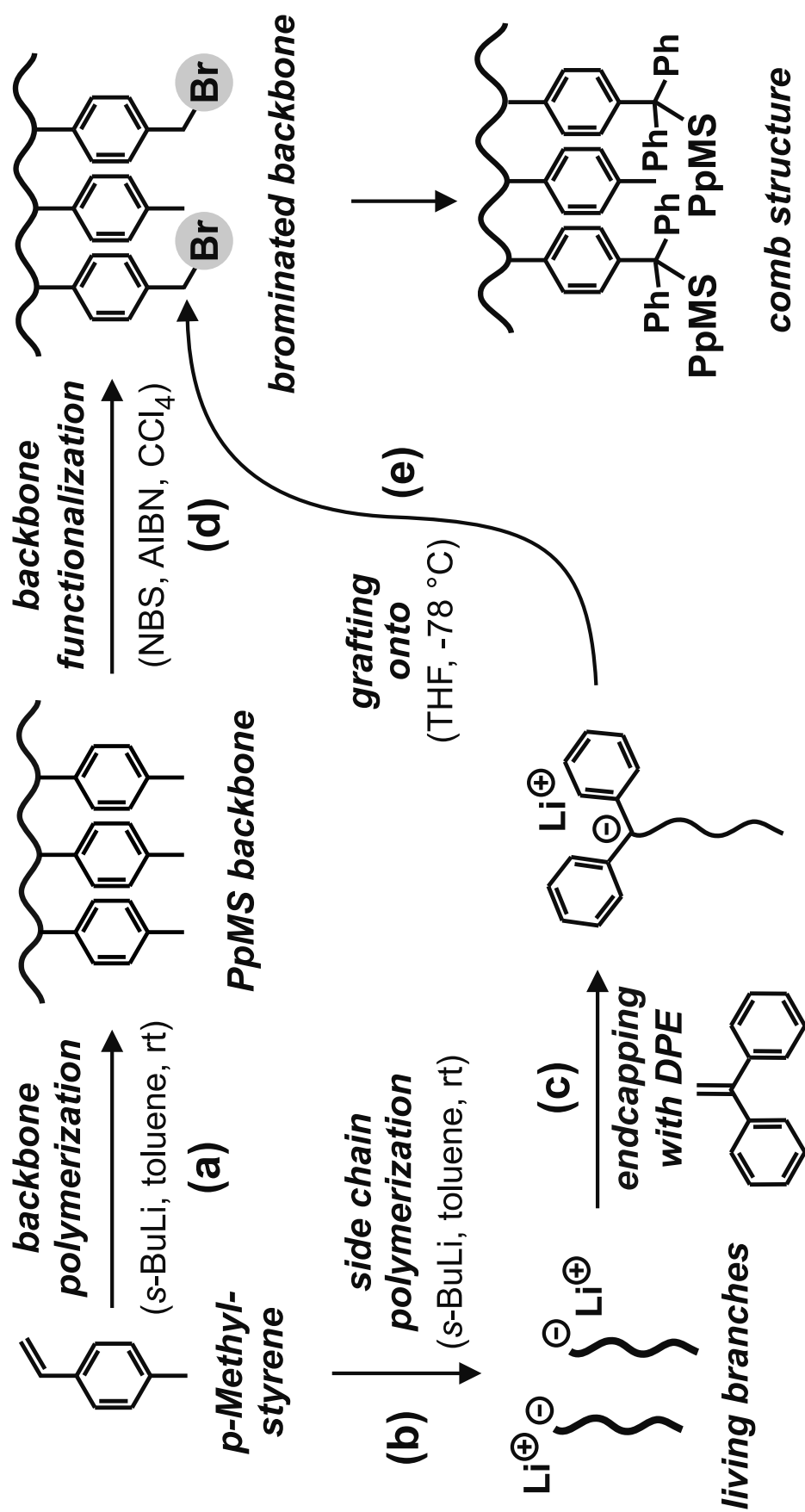
Figure 2.16: Scheme of the synthesis route for poly(p-methylstyrene) based model combs.
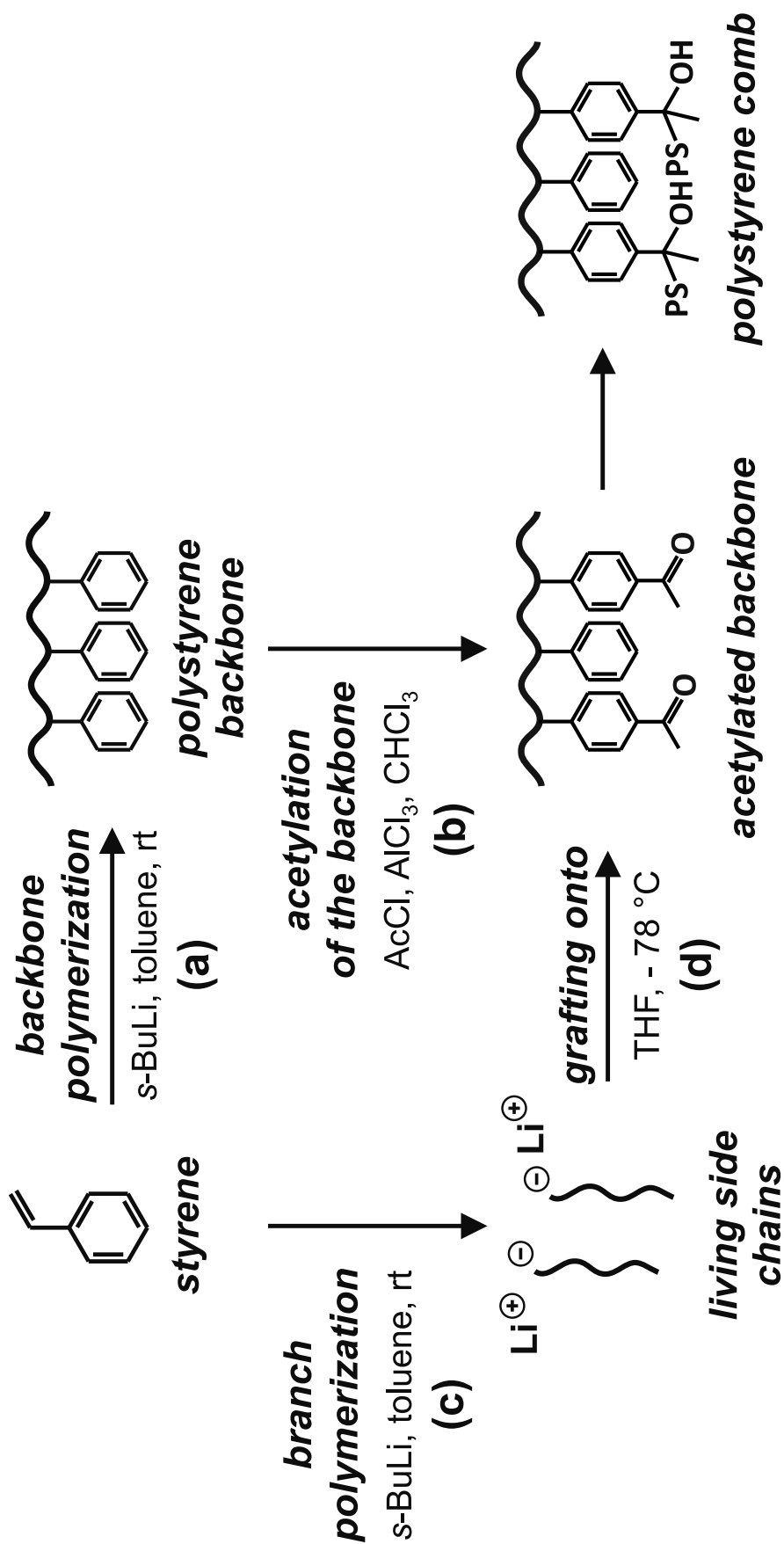
Figure 2.17: Scheme of the synthesis route for polystyrene based model combs.

2.4.3 PS/PpMS backbone and branch polymerization

The polystyrene and poly(p-methylstyrene) backbones and branches were prepared by anionic polymerization at room temperature from styrene or p-methylstyrene with s-BuLi as initiator and toluene as solvent, Fig. 2.18.
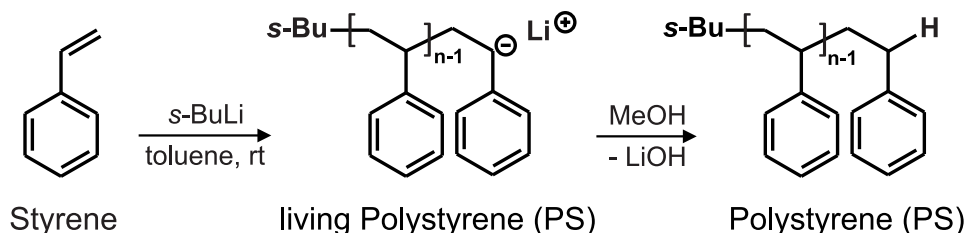
Figure 2.18: Scheme of the polymerization route for polystyrene backbones and branches.

Since the polymerization in non-polar solvents, like toluene, is much slower than in polar solvents, e.g. THF, the resulting reaction enthalphy is lower for non-polar solvents, additional cooling is not necessary in this case. In the case of molecular weights up to 200 kg/mol the polymerization in toluene is prefered over THF. For higher molecular weights, THF is used as solvent to avoid an increase in polydispersity. In the synthesis of the backbones, the residual anions were terminated using degassed methanol, after complete conversion of the monomer. The polymerization of the branches was performed in an ampoule with high-vacuum PTFE stopcocks and ground glass joints. For further characterization of the branches a sample was removed using a syringe and terminated with degassed methanol after completion of the polymerization. The PpMS polymers exhibit a slightly higher polydispersity than PS, this is related to a termination side reactions caused by protonation of the living chain by the slightly protic methyl group of p-methylstyrene. In the case of high molecular weight PpMS the polydispersity index (PDI) is slightly above
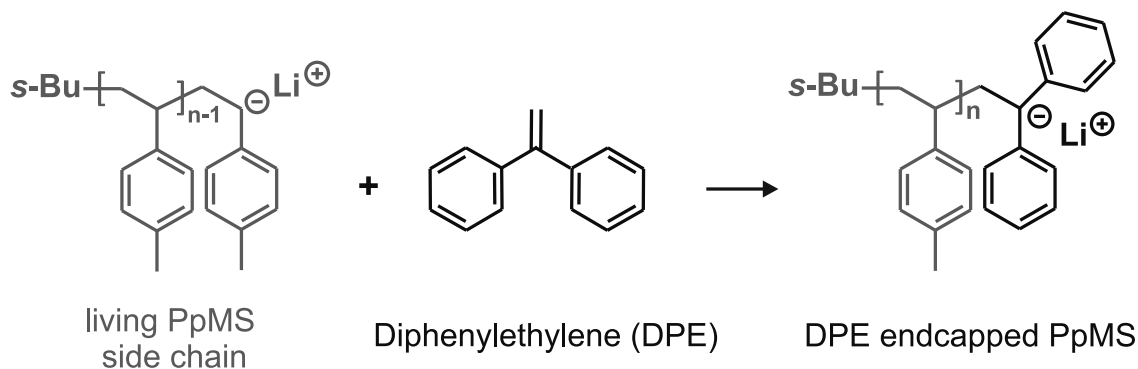
Figure 2.19: Scheme of the endcapping reaction of living PpMS branches and 1,1-diphenyl-ethylene (DPE).
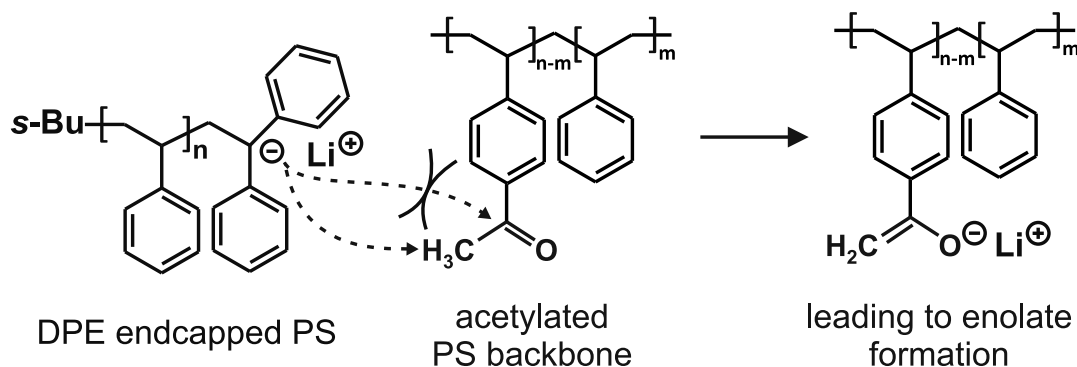
Figure 2.20: Schematic illustration of the nucleophilic attack of an DPE-endcapped polystyrene branch at the acetylated polystyrene backbone. Due to the steric hinderance of the DPE-endgroup, the living branch is not acting as a nucleophilic, but as a base instead, leading to enolate formation.

1.1, while for the branches of PpMS and PS as well as for the backbones of PS a PDI < 1.1 was achieved. To reduce the amount of side reactions, the nucleophilicity of the living branches is reduced using 1,1-diphenylethylene (DPE) as an endcapping agent, Fig. 2.19. The second aromatic ring of the DPE stabilizes the anion additionaly and lowers its reactivity. Due to the steric hinderance of the two phenyl groups, DPE cannot homopolymerize and only one DPE monomer is added [Quirk 03, Quirk 07]. By adding an excess of DPE a quantitative endcapping of the living branches can be assured. The excess of DPE does not have an influence on the further comb formation reaction.

The endcapping of living polystyrene branches with DPE is not recommended. The nucleophilic attack of the living branch at the carbonyl-C-atom is in this case sterically hindered Fig. 2.20. Instead it is acting as a base, leading to deprotonation of the methyl-group and consequently to an enolate formation [Li 01].

To determine the influence of the molecular weight on the rheological properties, backbones with molecular weights between 200 and 300 kg/mol and branches with 15 to 40 kg/mol were polymerized. Depending on the molecular weight of the backbone and the branches, the polymer chains are able to entangle, which can be observed in the rheological measurements. The entanglement molecular weight M_e of polystyrene is about 17 kg/mol, section 3.1.4. This value corresponds to the choosen minimal limit for the molecular weight of the branches. Full entanglement takes place for branch molecular weights above the critical molecular weight M_c ($M_c \approx$ 2-3 M_e), which corresponds to the comb structures with high molecular weight of the branches. Thereby the influence of the branch molecular weight and its ability to entangle slightly or fully with other branches or backbones can be investigated in the rheological measurements.

2.4.4   Poly(p-methylstyrene) based combs

2.4.4.1   Introduction of bromomethyl-groups as branching points

To enable the grafting of the living nucleophilic branches, an electrophilic centre has to be available at the polymer backbone, which can be created e.g. by introducing a halomethylgroup. A common method is the chloromethylation of polystyrene with chloromethyl methyl ether (CMME) and $SnCl_4$ proceeding in a Friedel-Crafts electrophilic aromatic substitution reaction [Camps 87]. The disadvantage of this procedure is the highly volatile and carcinogenic CMME used in the reaction. Additionally the undesired crosslinking of polymer chains takes place as a side reaction, leading to higher polydispersities (PD > 1.2). Therefore PpMS was used as a polymer basis for the introduction of a halomethylgroup at the benzylic position by the bromination with N-Bromosuccininimide (NBS) [Janata 02, Radke 05]. To introduce the bromomethyl group, the backbone is dissolved in carbon tetrachloride (CCl_4), N-Bromosuccinimide and a small amount of azobisisobutyronitrile (AIBN) were added, Fig. 2.21. AIBN was used to facilitate the radical formation. The SEC measurements before and after the bromination reaction did not show tailing, higher molecular weight fragments or increase in polydispersity. At the low functionalization degrees of 1 mol-% or lower, used here, crosslinking can be excluded.

The average number of functional groups was determined using high field (500 MHz) ^{1}H NMR-spectroscopy. The number of bromomethyl groups can be calculated by comparing the integrals of the aromatic protons (δ = 6 - 7.5 ppm, m, 4H, Phenyl-H) and the protons of the bromomethyl group (δ = 4.40 ppm, s, 2H, -CH_2Br). High accuracy even at low amounts of functional groups was achieved. The NMR spectrum of a partially brominated PpMS backbone (M_w = 197 kg/mol) with in average 14 bromomethyl groups is shown in Fig. 2.22. Even for low functionalization degrees of about 1 mol-% and lower (in this case 0.8 mol-% with 14 groups out of approx. 1700 monomers) the number of bromomethyl
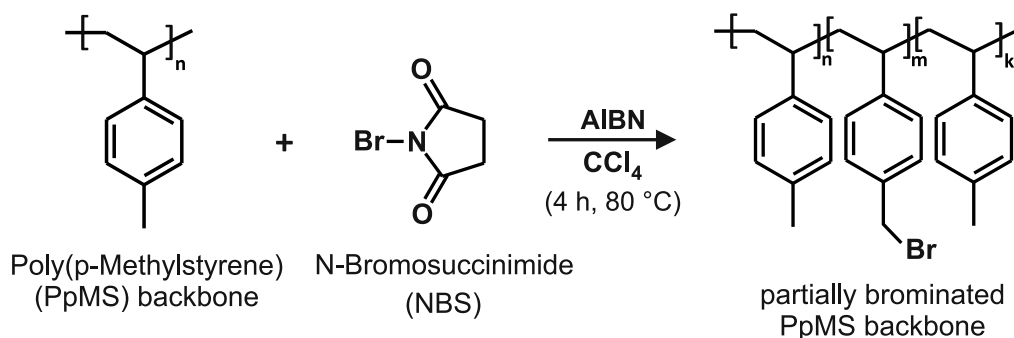
Figure 2.21: Reaction scheme for the introduction of a bromomethyl-group on the PpMS backbone
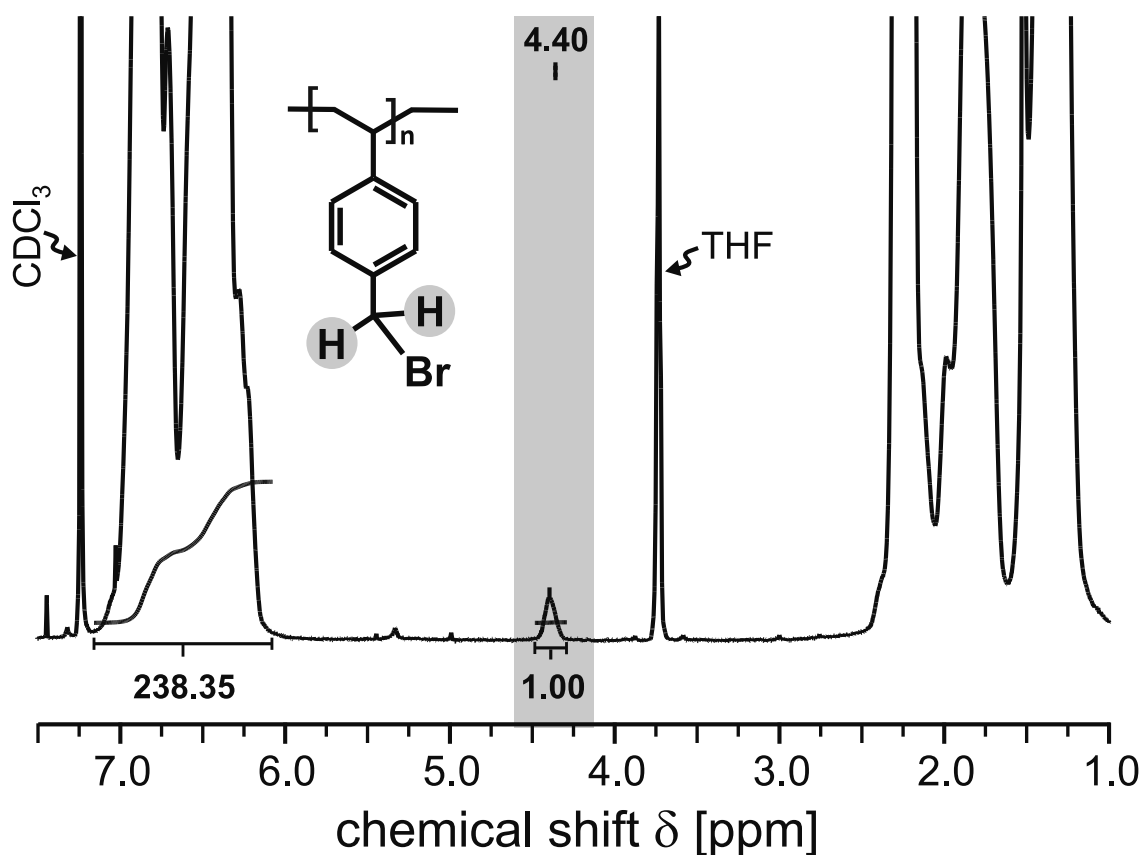
Figure 2.22: ^{1}H-NMR spectra of partially brominated poly(p-methylstyrene), M_w = 197 kg/mol, PDI = 1.22, average number of functional groups per main chain (FG) = 14 (1 FG per 240 C-atoms), measured in CDCl$_3$ at 500 MHz with 512 scans.

groups can be accurately set by the reaction conditions (desired number of bromomethyl groups was 15) and determined via proton NMR.

2.4.4.2 Comb formation

The grafting of the branches is conducted in THF as solvent to ensure a fast reaction. THF is acting as a Lewis base, stabilizing the charge of the Li-cation and leading to non aggregated living branches. Side reactions, e.g. ring-opening of THF are reduced by conducting the grafting reaction at low temperatures, $\approx$ - 70 °C. The grafting is performed by the addition of living branches to the backbone solution. In this case the backbone could be "titrated" until full conversion is indicated by the color change of the solution from colorless to red. The red color is caused by an excess of the living branches, due to their carbanionic state. However due to metal-halogen exchange a crosslinking of the backbones occurs, leading to a multimodal distribution. To prevent those coupling reactions, the functionalized backbone is slowly added to an excess of living branches.
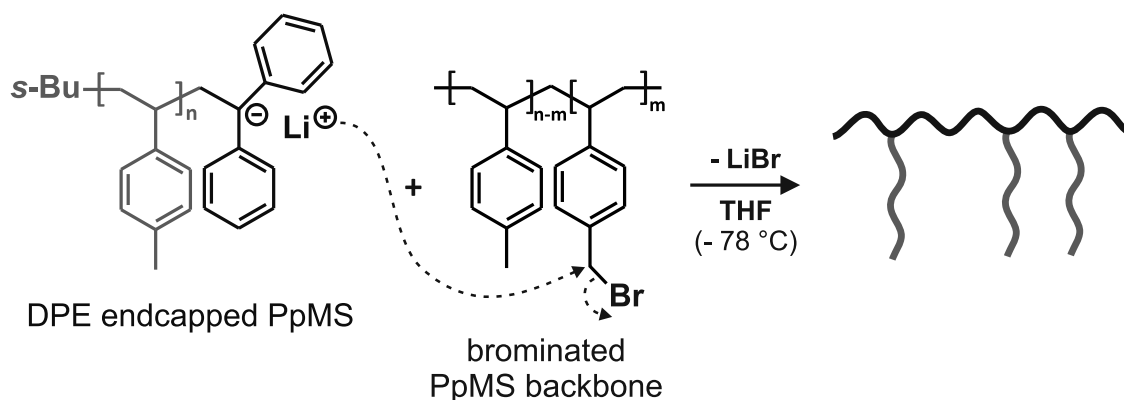
Figure 2.23: The comb formation is realized by the addition of the brominated PpMS backbone to an excess of living DPE-endcapped PpMS branch at $\approx$ - 70 °C to reduce side reactions. The grafting takes place via nucleophilic attack of the living branch at the bromomethyl group.

Using this procedure, narrow distributed comb structures can be obtained, this is illustrated in the SEC diagram in Fig. 2.24. It shows an example of a comb with a backbone molecular weight of 197 kg/mol and branches with a molecular weight of 42 kg/mol each. The molecular weight of the comb and the backbone was determined by SEC-MALLS. Low polydispersities (PDI $\leq$ 1.07) were achieved. The entanglement molecular weight (M_e) of PpMS is about 24400 g/mol section 3.1.4. The molecular weight of the fractionated comb (M_w = 765 kg/mol) results in average 13.5 branches per backbone. To control this result and to achieve a higher accuracy in the branching degree, the number of branches determined via SEC was compared with the number of bromomethyl groups, which were calculated by the comparison of the NMR integrals. The ratio of the peak integrals (238.35:1) gives a number of 14 branches per backbone (1 branch per 240 C-atoms) which compares favorably with the value calculated from the average molecular weights and prooves furthermore the high accuracy of the determination of the number of bromomethyl groups even at low amounts using NMR.

2.4.5   Polystyrene based combs

Although well defined combs of PpMS can be synthesized, still some disadvantages remain, which makes the development of other comb formation strategies desireable. The main disadvantage of using PpMS is the restricted usage of CCl_4, necessary for the bromination of the PpMS backbone. Chemical substitutes (e.g. chloroform, dichloromethane or cyclohexane) were not appropriate solvents to achieve low bromination degrees (< 1 mol-%). The usage of CMR- (carcinogenic, mutagenic, toxic for reproduction) or highly toxic substances, like CCl_4 as solvent in the case of the bromination of PpMS or chloromethyl
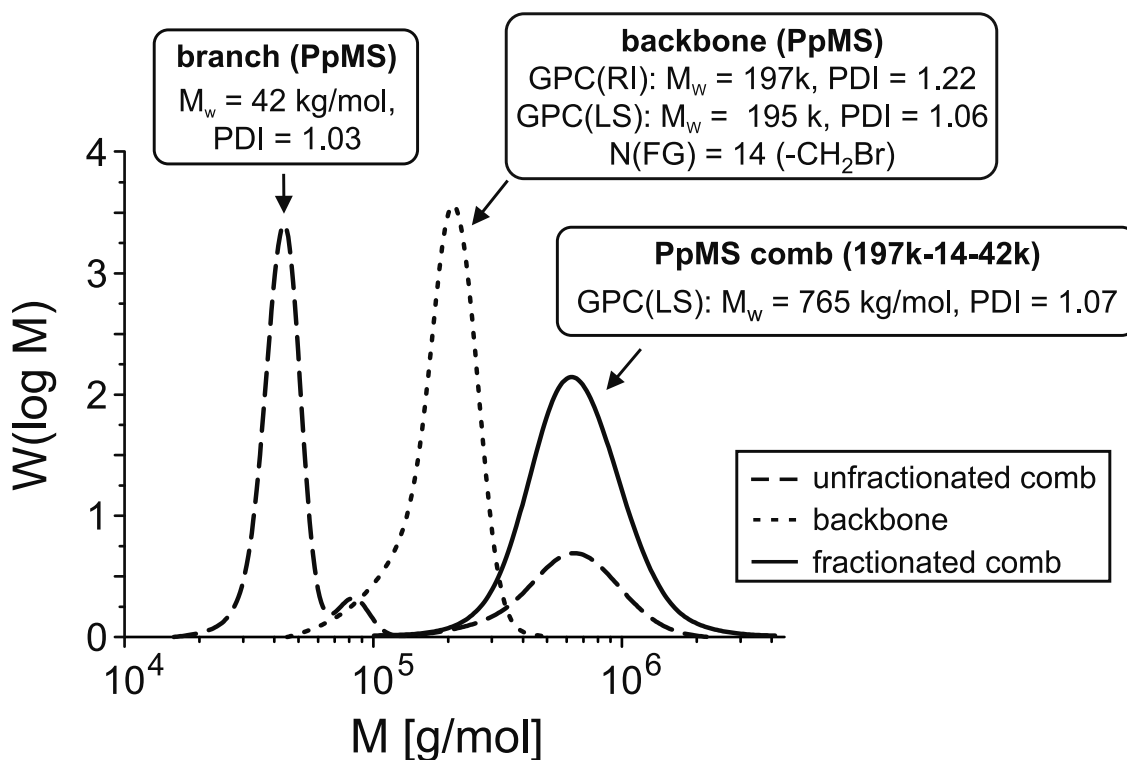
Figure 2.24: GPC of the PpMS comb (197k-14-42k), with M_w(backbone) = 197 kg/mol, average number of functional groups per main chain n(FG) = 14 and M_w(branch) = 42 kg/mol;

methyl ether in the case of the chloromethylation of polystyrene should be avoided. An upscaling of the bromination process to functionalize more than 5 g of PpMS backbone at once is problematic, due to crosslinking reactions. A minor problem for the synthesis in the laboratory, but much more important for an industrial usage is the higher price of p-methylstyrene, which is about ten times more expensive than styrene.

Polystyrene was choosen as the polymer basis for a further comb synthesis approach, since low polydispersities (< 1.1) even at high molecular weights (> 200 kg/mol) can be achieved, the benzyl ring is furthermore amenable to functionalization reactions to introduce branching points.

2.4.5.1 Introduction of acetyl-groups as branching points

To achieve a small number of branching points (< 1 mol-%), acetyl-groups were introduced via Friedel-Crafts-Acetylation at the PS backbone [Janata 02, Li 01], acetylchloride was used hereby as an acetylation agent, Fig. 2.25.

The electron withdrawing acetyl group deactivates the aromatic ring, which is then no longer amenable to further functionalization, leading to the introduction of only one acetyl group per monomer unit. As a result of the steric hinderance of the polymer back-
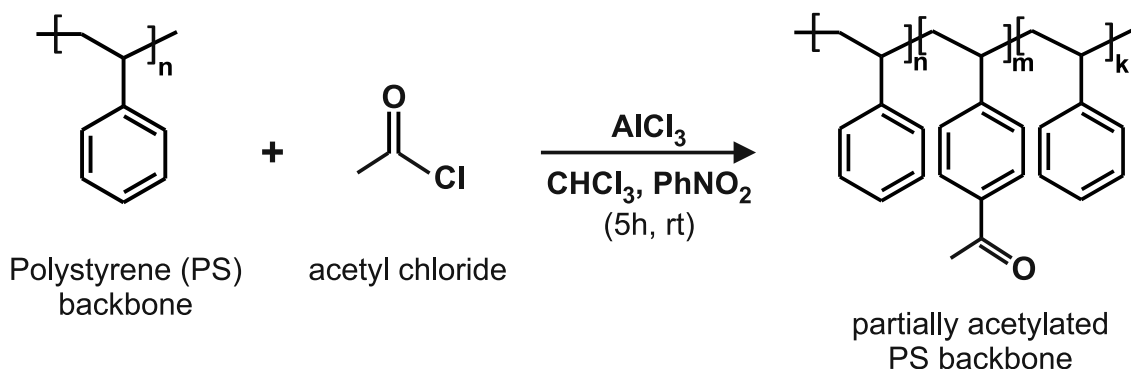
Figure 2.25: Introduction of acetyl groups at the PS backbone via Friedel-Crafts-Acetylation using acetylchloride as the acetylation agent.

bone, the acetylation takes place solely in para-position of the benzyl ring [Janata 02]. Thereby a controlled number of branching points can be introduced. The average number of acetyl groups was determined by high field ^{1}H-NMR, as in the case of the bromomethyl groups of PpMS. The number of acetyl groups was calculated with high accuracy by the ratio of the peak integrals of the CH_3 protons adjacent to the carbonyl group at $\delta = 2.51$ ppm and the five aromatic protons located between 6 and 7.5 ppm. The NMR spectrum of an acetylated PS backbone (M_w = 275 kg/mol, PD = 1.07) with in average seven branching points per backbone is shown in Fig. 2.26.

Using polystyrene (PS) as comb backbone the number of branching points can be well controlled via selective acetylation of the aromatic ring. Degrees of functionalization are in the range from 0.1 to 1.0 mol-% (which corresponds to a range for the number of branching in the synthesized combs from 1 to 10 branches per 2500 backbone C-atoms) can be achieved without detectable crosslinking in the SEC measurements. In comparison to the bromination of PpMS a ten times lower degree of functionalization can be realized by the acetylation of PS. Using this method a backbone with only two branches, which is the limit for the classification of a comb, was obtained.

2.4.5.2   Comb formation

The procedure for the formation of PS combs is similar to the PpMS procedure. To ensure a fast reaction, THF is choosen as a solvent. Low temperatures ($\approx$ - 70 °C) reduce possible ring-opening reactions of THF by the living PS branches. Therefore only a low amount of branches is terminated by the ring-opening of THF. This is necessary because the nucleophilicity of the living branches cannot be lowered by endcapping with DPE as in the case of the PpMS comb formation. The steric hinderance of the DPE-endcapped PS branches leads to very low grafting yields. For the grafting reaction the functionalized
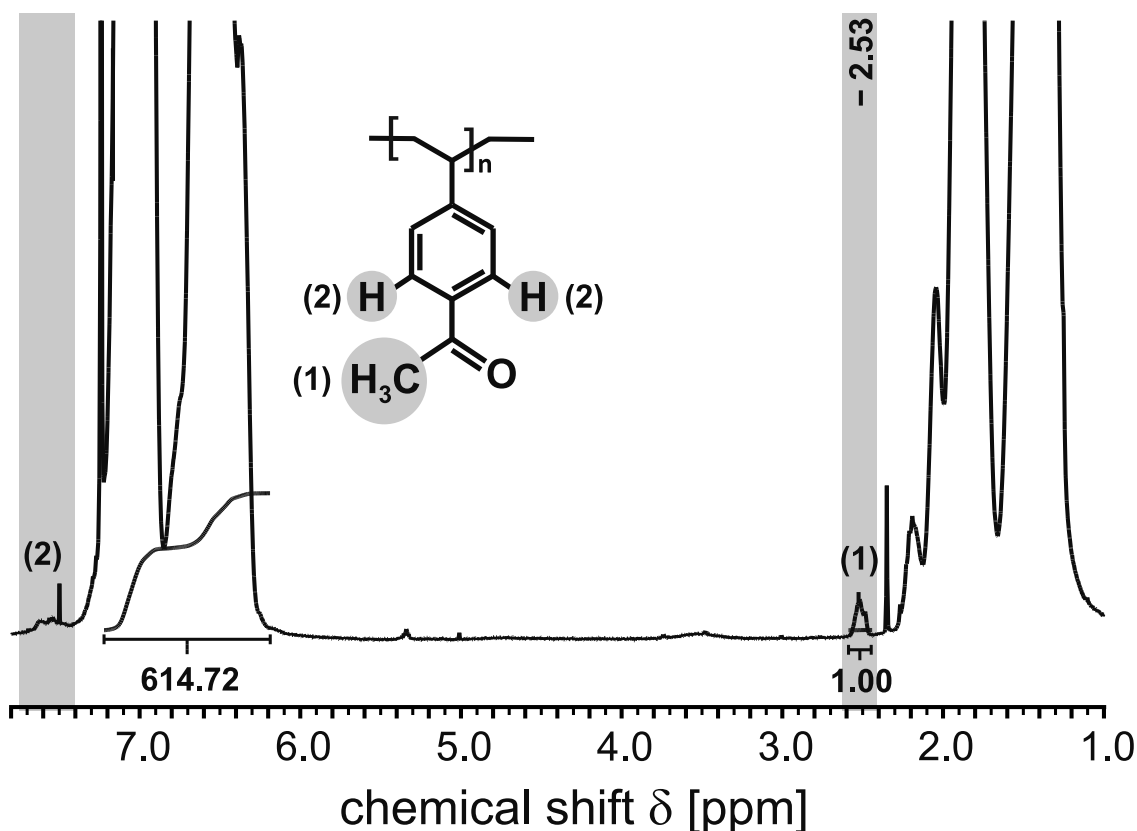
Figure 2.26: ^{1}H-NMR spectrum of partially acetylated polystyrene, M_w = 275 kg/mol, PDI = 1.07, average number of functional groups per main chain (FG) = 7 (1 FG per approx. 1000 C-atoms), measured in CDCl$_3$ at 500 MHz with 512 scans.

backbone has to be added diluted and slowly to an excess of living branches. Thereby it can be avoided, that the alkoxides formed by the nucleophilic attack of the living PS branches at the carbonyl carbon-atom can in turn act as nucleophilics and attack inter- or intramolecularly at other carbonyl groups, leading to crosslinking of the backbones. The grafting reaction for the formation of PS combs is illustrated in Fig. 2.27. The living PS branches attack nucleophilic at the carbonyl carbon-atom of the acetyl group, the formed alkoxides and residual living PS branches are protonated after complete addition of the backbone by the addition of degassed methanol.

The grafting reaction can also be performed in toluene at room temperature. Side reactions like ring-opening are avoided. In contrast to the reaction in THF, the grafting in toluene is slower. The Li-cation can only be stabilized unsufficiently by the aromatic system of the toluene, which leads to an aggregation of the living branches and the Li-cations. To accelerate the reaction N,N,N',N'-Tetramethylethylendiamin (TMEDA) is added, which complexes the Li-cation sufficiently. The grafting reaction in the case of the acetylated PS backbone with living PS branches did not proceed quantitatively for the backbone with
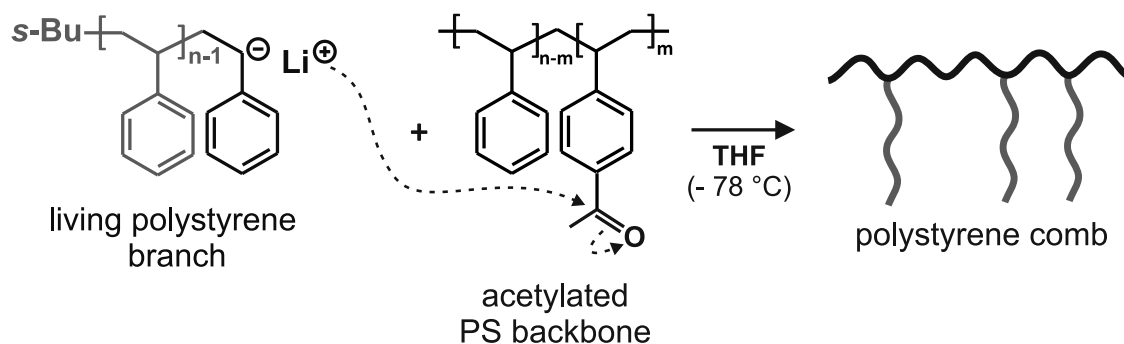
Figure 2.27: Schematic illustration of the PS comb formation reaction, living PS branches attack nucleophilic at the carbonyl carbon-atom of the acetyl group, the formed alkoxides and residual living PS branches are protonated after complete addition of the backbone by the addition of degassed methanol.

seven acetyl-groups. For the backbones with only two acetyl-groups the conversion was quantitative according to SEC-MALS measurements of the comb. It is supposed, that the reason for the low grafting yield is a result of the enolate formation, due to the protic methyl group adjacent to the carbonyl group, which leads to inactive branching points [Li 01]. Though the conversion is not quantitative, the method is still appropriate to synthesize model comb systems. A ten times lower branching degree can be accomplished in
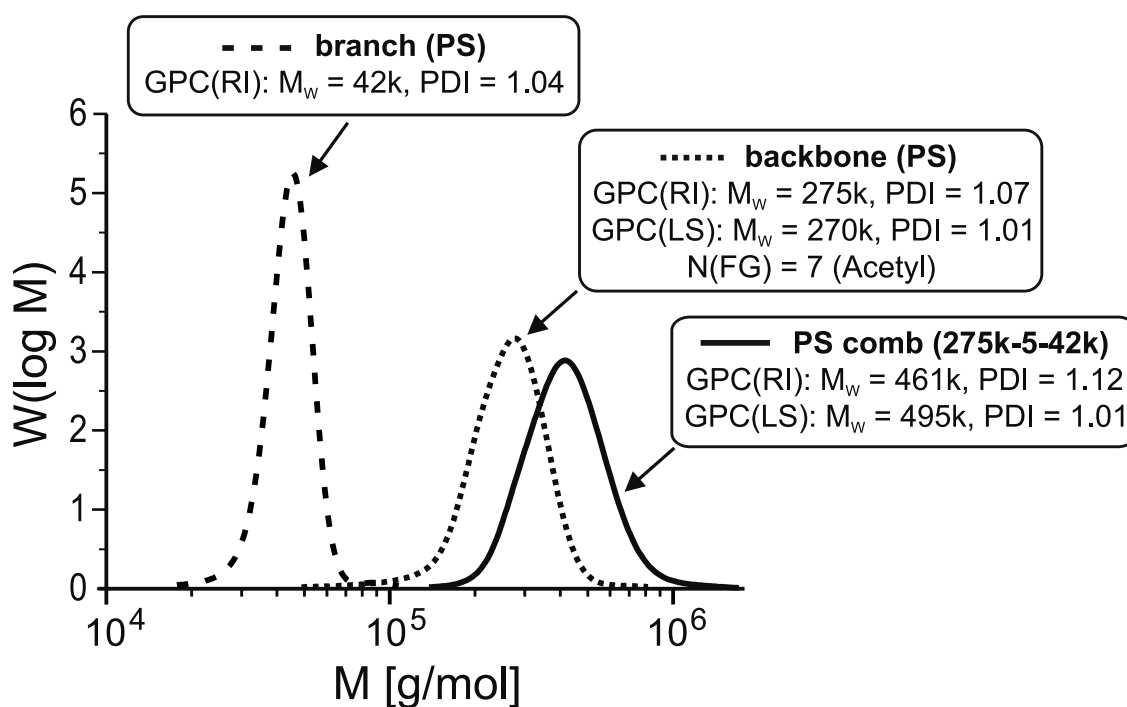
Figure 2.28: GPC of the PS comb (275k-5-42k), with M_w(backbone) = 275 kg/mol, average number of functional groups per main chain (FG) = 5 and M_w(branch) = 42 kg/mol.

comparison to the PpMS combs. Furthermore the number of branches can be calculated accurately using the total molecular weight, determined via SEC-MALLS, with the aid of the molecular weights of the backbone and the branches, which are known, Fig. 2.28

2.4.6 Side reactions

2.4.6.1 Ring-opening reaction of THF

The half-life time of butyllithium or polystyryllithium is only a few minutes at room temperature in THF, a ring-opening reaction with THF leads to termination of the initiator or the living polymer chain respectively, Fig. 2.29 [Glasse 83]. Lower temperatures increase the half-life time, which is advantageous for the comb formation process, where the living branches are present in excess.
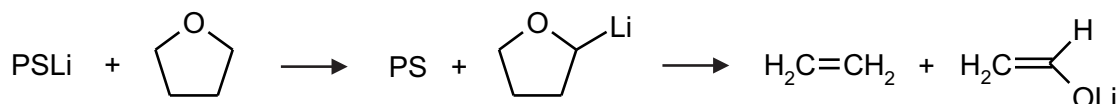
Figure 2.29: Schematic of the reaction of polystyryllithium with THF.

2.4.6.2 Lithium-halogen exchange

Another side reaction is the metal-halogen exchange. This leads to an exchange of the bromine at the backbone with the Li-cation at the living branch, Fig. 2.30. Though the branch is now terminated, the backbone is carrying the active species and can react inter- or intramolecularly with the methylbromine groups under nucleophilic substitution, leading to crosslinking [Hsieh 96]. A dimerization of branches can also take place. It is assumed that the dimerization of the branches is similar to a Wurtz-coupling [Hsieh 96], it

| brominated backbone | living side chain | lithiated backbone | brominated side chain |
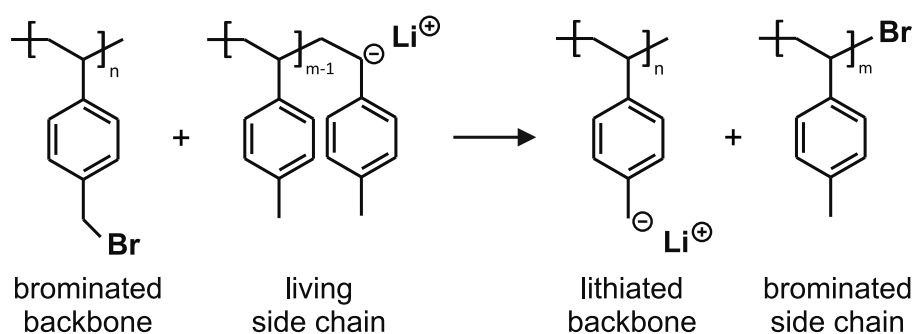
Figure 2.30: Lithium-bromide exchange reaction between the PpMS-Li branch and the brominated backbone.
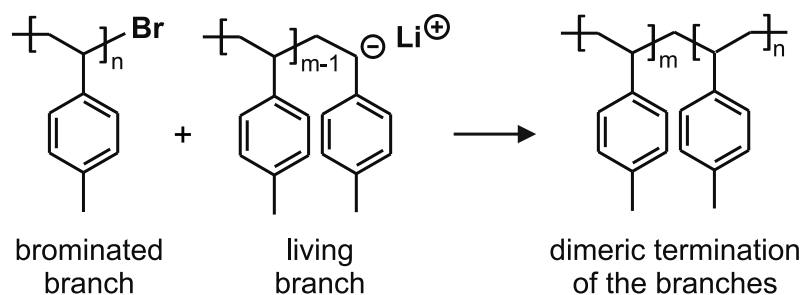
Figure 2.31: Dimerization reaction of two branches, as a result of the lithium-bromide exchange.

can be assumed that the dimerization takes place by the nucleophilic substitution reaction between a brominated and a living branch, Fig. 2.31. Takaki et al. [Takaki 79] discussed the possible side reactions involved, but a detailed investigation is still missing.

The addition of the backbone to an excess of living branches suppresses the lithium-halogen exchange, because the functional groups of the added backbone can instantly react with the living branches and the possibility of a backbone combination can be minimized.

2.4.7   Transformation of functional groups at the PS backbones

Since the grafting reaction at the acetylated polystyrene backbone is not quantitative for functionalization degrees higher than 0.1 mol-%, it is desired to introduce functional groups to make the polystyrene backbone amenable to a quantitative nucleophilic reaction via living polymers or to other coupling reactions. The major advantages of the Friedel-Crafts acetylation at the polystyrene backbone are the introduction of a low number of functional groups (0.1 - 1 mol-%) with high precision and without crosslinking involved as well as the accessability of the introduced carbonyl group to other functional groups. For the further conversion of the carbonyl group two different approaches were used, the Wittig-transformation to obtain an alkene and the conversion to a bromine.

2.4.7.1   Wittig-transformation

The Wittig-transformation can be used to introduce an alkene functionality, which can be further used in coupling reactions. The resulting isopropenyl group at the PS backbone could be used for the nucleophilic attack of living (carbanionic) species. However due to the residual charge, obtained after nucleophilic attack, this could lead to intra- or intermolecular reactions with unreacted isopropenyl groups, resulting in crosslinking. Another method of choice would be the introduction of chlorosilyl-groups via hydrosilylation, which would be amenable to nucleophilic attack by living (carbanionic) species.
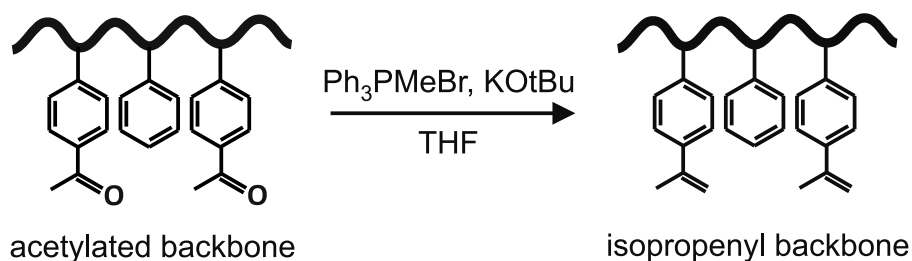
Figure 2.32: Schematic of the Wittig reaction

A further advantage is the absence of halogen-metal exchange during this reaction, so the living branches could be added via "titration" and an excess of residual chains could be avoided. Thiol-ene click-chemistry [Hoyle 10] could also be used in the case of an alkene functionalized backbone by the addition of branches with thiol-functionality, e.g. generated using RAFT-polymerization [Barner-Kowoll 08].

The conversion to the alkene could not be conducted quantitatively, as confirmed by ^{1}H-NMR, Fig. 2.33. Only 86 % of the in total 35 acetyl-groups were converted to isopropenyl
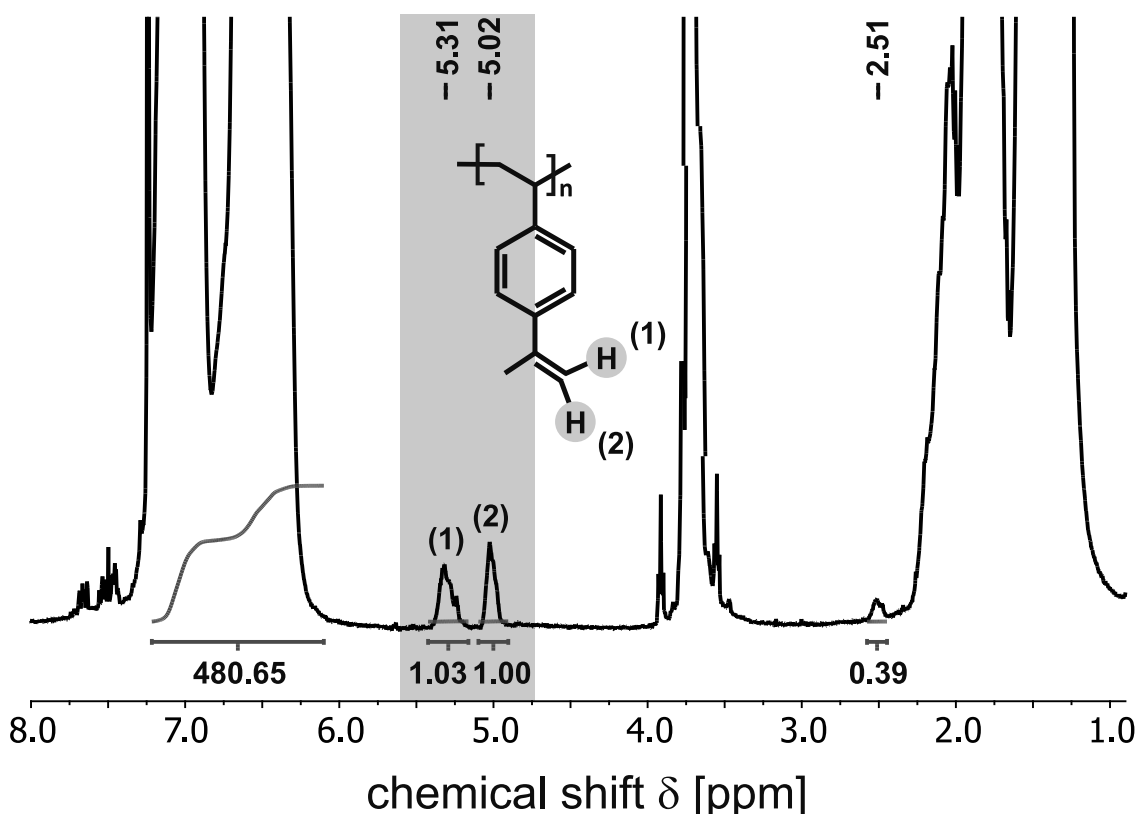
Figure 2.33: ^{1}H-NMR spectra of a Wittig transformed acetylated PS backbone with M_w = 286 kg/mol, PDI = 1.17, N(FG) = 35 (acetyl groups), measured in CDCl$_3$ at 400 MHz with 512 scans. 86 % of the acetyl-groups (30 acetyl groups) were converted to isopropenyl groups.
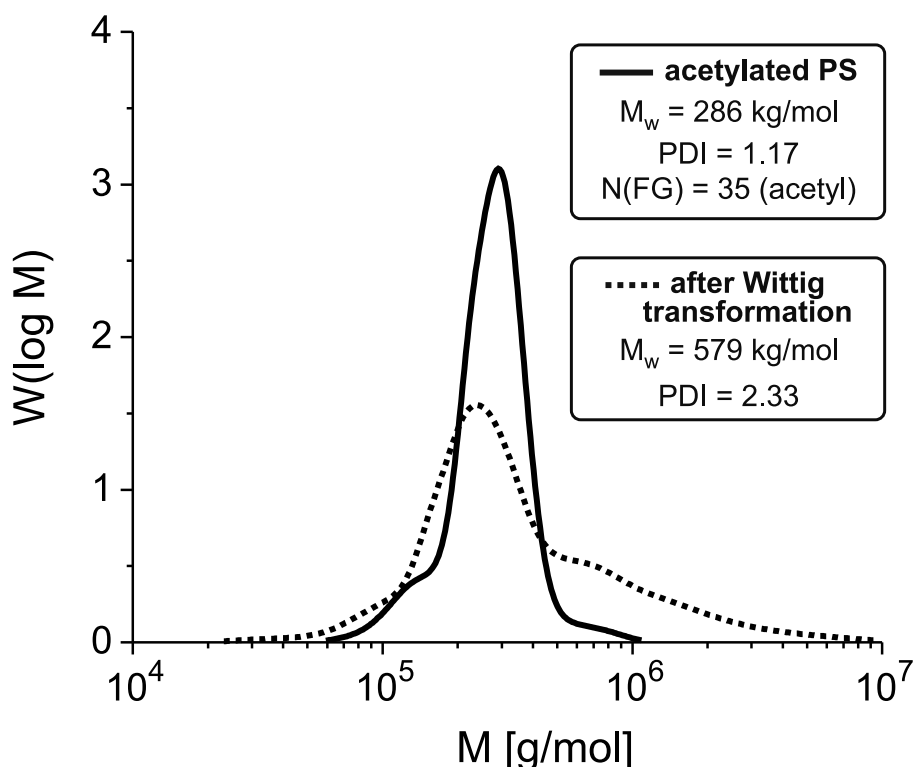
Figure 2.34: GPC of the Wittig transformed acetylated PS backbone with M_w = 286 kg/mol, PDI = 1.17, N(FG) = 35 (acetyl groups). Crosslinking occured during the Wittig reaction, leading to both, an increase of the molecular weight and polydispersity.

groups. A further negative effect is the crosslinking during the Wittig-Transformation reaction.

This can be observed by the high increase in polydispersity, which is almost doubled in comparison with the acetylated polystyrene, Fig. 2.34. The possibility for side reactions, like crosslinking increases with the number of functional groups. Studies with lower functionalization degrees revealed indeed lower polydispersities, but the result that crosslinking takes place stays the same. Though the conversion to an alkene would be an advantageous step, the resulting high polydispersity makes it unusable for the preparation of model polymers.

2.4.7.2   Conversion of the acetyl to a bromoethyl group

The introduction of a methylbromine functionality with bromine as a leaving group lead to quantitative grafting in the case of the synthesis of Poly(p-methylstyrene) comb polymers. Besides the nucleophilic substitution reaction using living (carbanionic) species, the Sonogashira coupling reaction or Click reactions [Binder 08] (after the exchange of the bromine by an azide) would be possible. Two major aspects have to be considered for
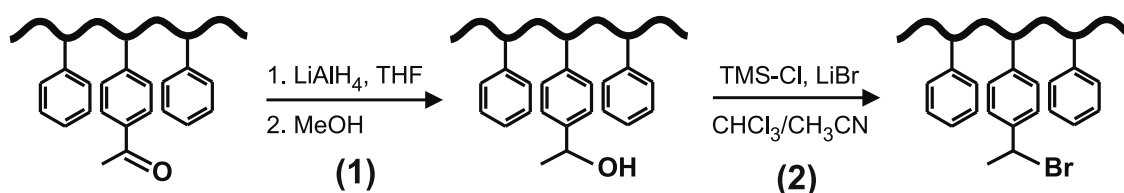
Figure 2.35: Schematic of the synthesis steps for the conversion of an acetyl to a bromoethyl-group. (1) reduction of an acetylated PS to an hydroxylated PS using Lithiumaluminium hydride as reducing agent, (2) conversion of the hydroxy- to a bromine group using chlorotrimethylsilane (Me$_3$SiCl) and lithium bromide (LiBr).

the conversion reaction to be choosen. The reaction should not involve crosslinking side-reactions to avoid an increase in polydispersity and a quantitative conversion is necessary to achieve a quantitative grafting reaction.

The conversion of the acetyl to the bromoethyl group is a two step synthesis procedure. The first step is the reduction of the carbonyl group to a hydroxy group, using Lithiuma-luminium hydride as a reducing agent [Janata 02], Fig. 2.35.

An almost quantitative conversion of $\approx$ 96% was achieved using chlorotrimethylsilane
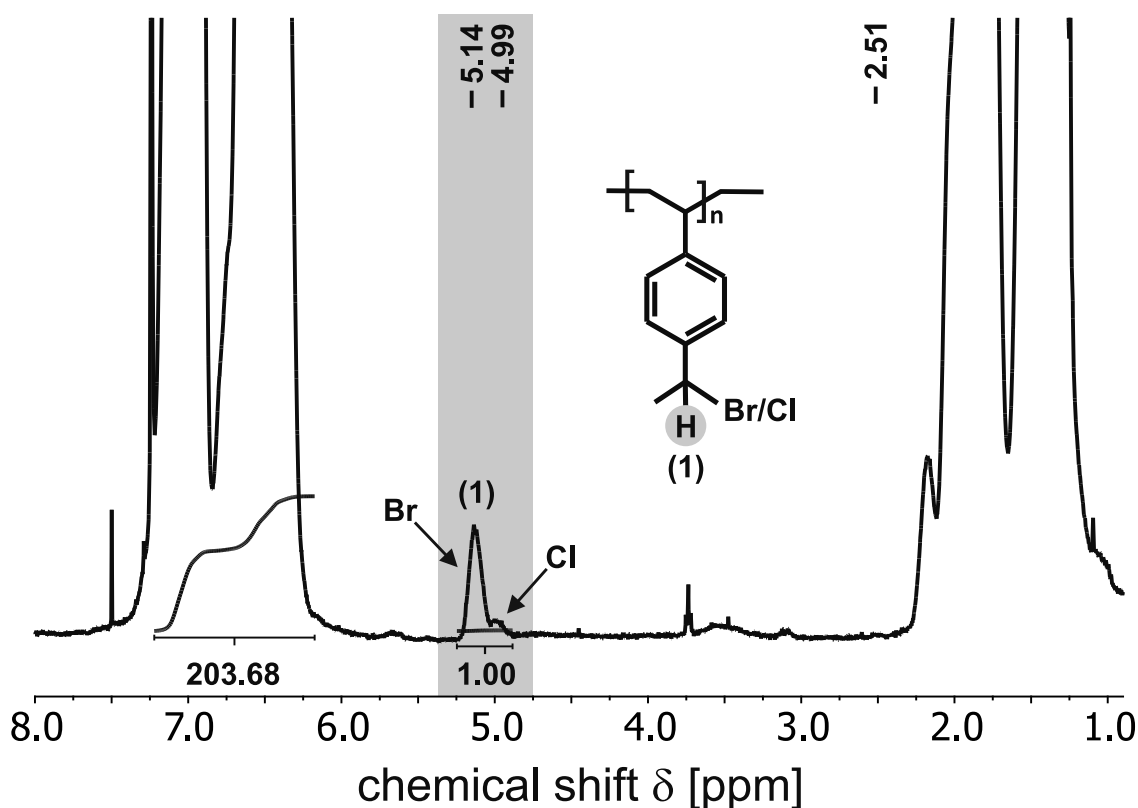
Figure 2.36: ^{1}H-NMR spectra of the brominated PS backbone with M$_w$ = 203 kg/mol, PDI = 1.15, N(FG) = 48 (bromine groups), measured in CDCl$_3$ at 400 MHz with 512 scans.
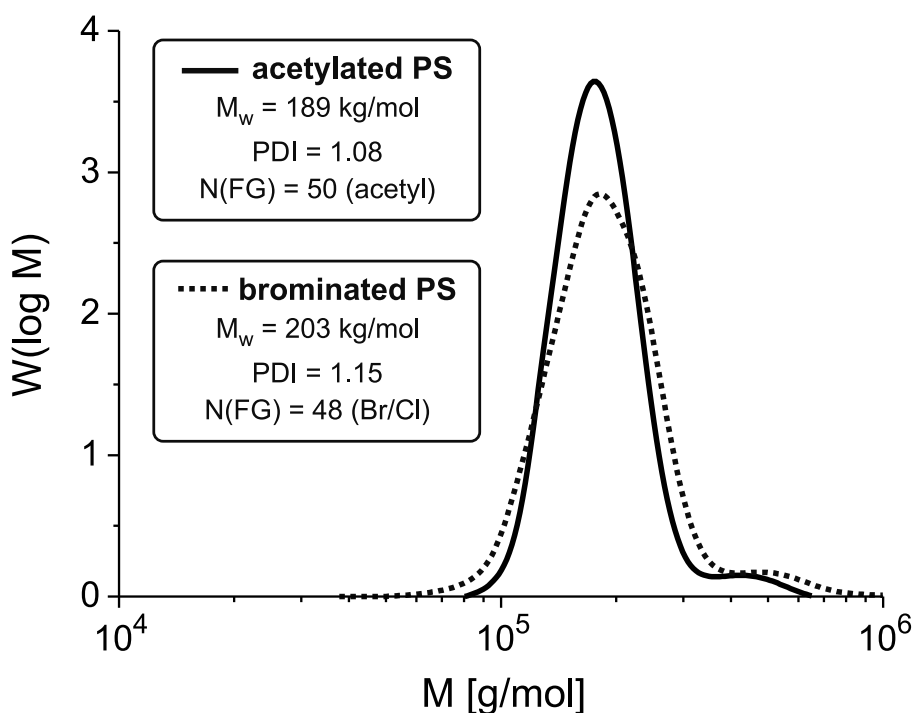
Figure 2.37: GPC of the brominated PS backbone with M_w = 203 kg/mol, PDI = 1.15, N(FG) = 48 (bromine groups), only a slight increase in molecular weight and polydispersity took place.

(Me_3SiCl) and lithium bromide (LiBr) as reaction agents [Olah 80, Hirao 09] for the conversion of the hydroxy-group to a bromine in the second reaction step, Fig. 2.35.

The degree of conversion was confirmed by means of ^{1}H-NMR of the polystyrene backbone after conversion, Fig. 2.36. The peak for the hydroxy-group at δ = 4.78 ppm vanished completely, while two new peaks for the bromine (δ = 5.14 ppm) and the chloro (δ = 4.99 ppm) functionality appear. The chloro functionality, which has a part of 10 % in total is a side product. Since it is also a good leaving group for the nucleophilic substitution reaction, it is an acceptable side product for the further grafting reaction. By comparison of the integrals of the proton adjacent to the bromo/chloro group (at δ = 5.14 and 4.99 ppm respectively) with the protons of the aromatic ring of the polystyrene backbone, 48 carbonyl groups were converted. The polydispersity as well as the molecular weight were slightly increased during the reaction, which can be seen in a slight tailing towards higher molecular weights in the SEC curve of the brominated product, Fig. 2.37.

For the model comb systems lower functionalization degrees (< 1%) are desired, so that an increase in polydispersity can be neglected for those systems, in case the polydispersity remains below a value of PDI < 1.1.

The bromo functionality can be achieved with high conversion and low increase in polydispersity. It is therefore, within the described and examined method, an ideal conversion

reaction for the acetylated polystyrene backbones to permit further grafting reactions.

2.5 Conclusion

The controlled introduction of a low number of branching points (< 1 mol-%) with branches of high molecular weight is a major problem in the synthesis of model combs. Using poly(p-methylstyrene) (PpMS) as comb backbone the number of branching points can be well controlled via selective bromination of the methyl group and degrees of functionalization of less than 1 mol-% can be achieved. Due to its similarity to styrene, p-methylstyrene allows the independent anionic polymerization of the backbone and the branches with well defined molecular weights and low polydispersities. Disadvantageous is the usage of CCl_4 as solvent for the bromination of the PpMS backbone, which is carcinogenic and therefore restricted in usage.

Alternatively polystyrene based model comb systems with lower polydispersities and functionalization degrees in comparison to PpMS can be synthesized. Functionalization degrees of 0.1-10 mol-% can be achieved without significant occurring crosslinking. The grafting yield in the case of the acetylated PS backbones is not quantitative. However, well-characterized PS model combs can be obtained, since the molecular weights of the branches, the backbone and the total molecular weight of comb are known, so that the number of branches can be accurately calculated. Furthermore the acetylated polystyrene backbone opens perspectives for the use with other coupling methods, due to its accessability to other functional groups.

Several model combs were synthesized using the PpMS and PS approach, with a controlled number of branches ranging from 2 to 29, backbone molecular weights from 200-300 kg/mol and branch molecular weights from 15-42 kg/mol.

As a conclusion, the PpMS approach is so far the best method for the synthesis of model comb polymers. However, PS based model comb polymers are superior to the PpMS combs, due to wider range of functionalization degrees and the accessability of a high amount (> 50 g) of functionalized backbone with the same average functionalization degree. The disadvantage of the PS based combs is the non-quantitative grafting yield, which has to be optimized by the conversion to another functional group.

Chapter 3

Shear rheology in the linear regime

In this chapter the fundamentals of the rheology in the linear regime are described. Starting from the basic principles of rheology and later passing on to the involved relaxation processes. In the experimental part the behavior of linear mastercurves are discussed in relation to the branching degree of model comb polymers. Whereas the afterwards introduced van Gurp-Palmen plot allows a better correlation between the measurements in the linear viscoelastic regime and the degree of branching.

3.1   Basics of rheology

Rheology is defined as the study of the deformation and flow of matter [Macosko 94, Barnes 98]. Whereby it distinguishes between three types of materials. Ideal solids are purely *elastic* and follow *Hooke's law*, while ideal fluids are purely *viscous* and follow *Newton's law*. However most materials are *viscoelastic,* which have a viscous as well as an elastic part.

3.1.1   Terminology

On the basis of a two-plate model Fig. 3.1 the fundamental rheological concepts are introduced, which are necessary for the application of further models.
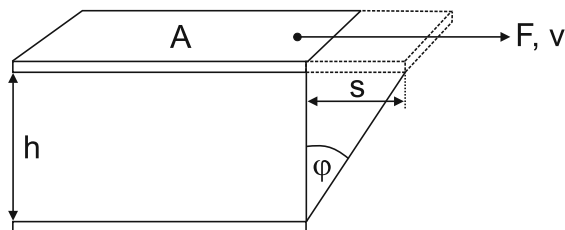
Figure 3.1: Schematic of the two plate-model for the illustration of shear experiments.

The upper plate (with area A) is laterally deflected by the value s with a force F. The lower plate is stationary (deflection $s = 0$). The sample is sheared between the two plates with the plate-to-plate distance h.

The *shear stress* σ [Pa] is defined by the ratio of the (shear) force F [N] and the (shear) area A [m^2].

$$\sigma = \frac{F}{A} \tag{3.1}$$

The *deformation* γ is defined by the ratio of the deflection s [m] and the plate-to-plate distance h [m].

$$\gamma = \frac{s}{h} \tag{3.2}$$

The shear rate $\dot{\gamma}$ [s^{-1}] is determined by the derivative of the time-dependent deformation with respect to time.

$$\dot{\gamma} = \frac{d\gamma}{dt} = \frac{v}{h} \tag{3.3}$$

with the velocity v [m/s] and the plate-to-plate distance h [m] [Mezger 06].

3.1.2 Phenomenological models

3.1.2.1 Ideal elastic deformation: Hooke's law

Ideal elastic matter is described by *Hooke's law*, Eq. 3.4, and its behavior is explained, for simplification for the one-dimensional case, on the basis of a spring model, Fig. 3.2.

$$\sigma = G \cdot \gamma \tag{3.4}$$
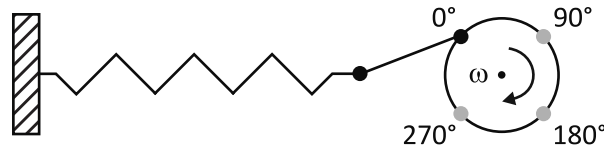
Figure 3.2: Schematic of the spring model for ideal elastic behavior.

The *shear modulus* G [Pa], Eq. 3.5, is a material constant for ideal elastic matter, which specifies the ratio between the shear stress σ and the deformation γ in the reversible deformation regime at constant temperature.

$$G = \frac{\sigma}{\gamma} \tag{3.5}$$

The spring is deflected under load, with the deflection proportional to the applied force. After removal of the load, the spring returns to its original state, without residual deformation. The deformation energy is stored in the elastic matter during deformation and is completely recovered after deformation.

A sinusoidal deformation is obtained for a spring, which is deformed and relaxed with an angular velocity ω_1 and a maximum deformation amplitude γ_0.

$$\gamma(t) = \gamma_0 \; sin(\omega_1 t) \tag{3.6}$$

The combination of Eq. 3.6 and Eq. 3.4 results in the shear stress σ:

$$\sigma(t) = G \cdot \gamma_0 \; sin(\omega_1 t) \tag{3.7}$$

In the linear regime $G = \sigma(t)/\gamma(t)$ = const., the $\sigma(t)$- and $\gamma(t)$ signals are both sinusoidal and in phase ($\delta = 0°$) [Mezger 06], Fig. 3.3.
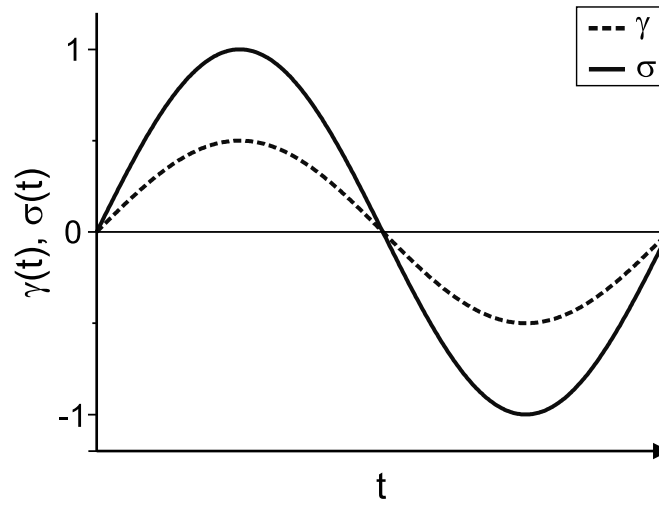
Figure 3.3: Time dependent deformation and shear stress for ideal-elastic behavior.

3.1.2.2 Ideal viscous flow of fluids: Newton's law

The ideal viscous flow of fluids is described by Newton's law:

$$\sigma = \eta \cdot \dot{\gamma} \tag{3.8}$$

The shear viscosity η [Pa·s] is a material constant for ideal viscous fluids, which is described by the ratio of the shear stress σ and the shear rate $\dot{\gamma}$ at a constant temperature.

$$\eta = \frac{\sigma}{\dot{\gamma}} \tag{3.9}$$

The behavior of an ideal viscous fluid can be illustrated using a dashpot model, Fig. 3.4.

Under constant load and deformation velocity, the deformation of the dashpot fluid increases continuously. The deformation is retained after removal of the load, the ideal viscous fluid remains in the deformed state. The applied deformation energy is dissipated
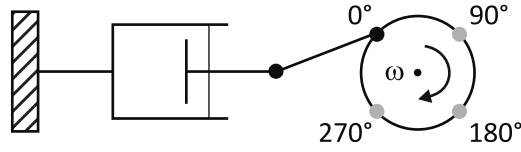
Figure 3.4: Schematic of the dashpot model for ideal viscous fluids.

completely. The shear stress σ and the shear rate $\dot{\gamma}$ are connected in a linear relationship, with the proportionality constant η, correspondig to the flow stress of the dashpot fluid. For a sinusoidal deformation, the shear rate $\dot{\gamma}$ is obtained from Eq. 3.6 by the derivative of the deformation with respect to time.

$$\dot{\gamma}(t) = \frac{d\gamma}{dt} = \gamma_0 \omega_1 \, cos(\omega_1 t) \tag{3.10}$$

In combination with Eq. 3.8 follows for the shear stress

$$\sigma(t) = \eta \, \gamma_0 \omega_1 \, cos(\omega_1 t) \tag{3.11}$$

In the linear regime $\eta = \sigma(t)/\dot{\gamma}(t) = $ const., the $\sigma(t)$ and $\dot{\gamma}(t)$ signals are both cosinusoidal. For ideal viscous behavior the $\sigma(t)$ and $\gamma(t)$ signals are phase shifted by $\delta = 90°$, Fig. 3.5 [Mezger 06].

The phase shift of 90°, can be shown by the conversion of Eq. 3.11.

$$\sigma = \eta \, \gamma_0 \omega_1 \, sin(\omega_1 t + 90°) \tag{3.12}$$
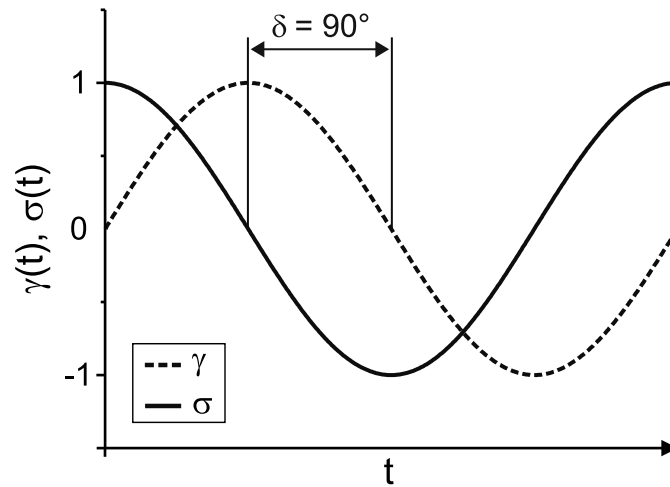
Figure 3.5: Schematic illustration of the relationship between deformation and shear stress as a function of time for ideal viscous behavior.

3.1.2.3 Viscoelastic materials

Materials with purely elastic and viscous properties can be described with the simple model of a spring or a dashpot, respectively. Materials, which combine these two behaviors are called viscoelastic. Those materials can be described by models, which combine the spring and dashpot. Simple onedimensional examples are the Kelvin-Voigt and the Maxwell model [Mezger 06].

a.) Kelvin-Voigt model

The Kelvin-Voigt model describes the behavior of a viscoelastic solid, it is mostly used for elastic solids with a low pronounced viscous part. Within this model the spring and the dashpot are connected in parallel, Fig. 3.6a.
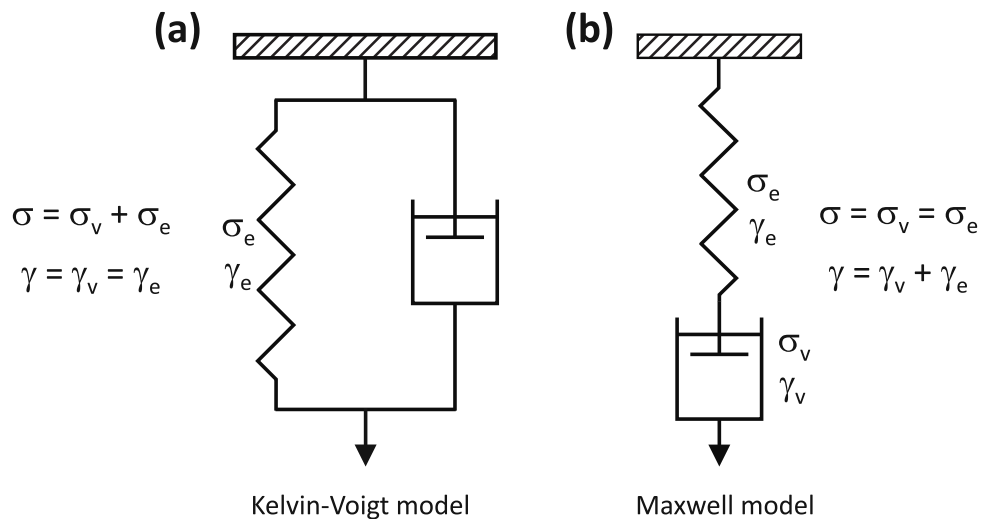
Figure 3.6: (a) Kelvin-Voigt model for elastic solids with a viscous part (b) Maxwell model for viscous fluids with an elastic part.

The viscoelastic solid shows a time-delayed, but complete relaxation after a load and unload cycle. The substance behaves like a solid with a small viscous part. Those solids are also called Kelvin-Voigt solids.

The total shear stress σ consists of the shear stress of the the spring σ_e (elastic part) and of the dashpot σ_v (viscous part).

$$\sigma = \sigma_e + \sigma_v \tag{3.13}$$

The deformation and the shear rate of both components are equal.

$$\gamma = \gamma_v = \gamma_e \quad \text{and} \quad \dot{\gamma} = \dot{\gamma}_v = \dot{\gamma}_e \tag{3.14}$$

The shear stress of the viscous part is obtained from Newton's law, Eq. 3.8.

$$\sigma_v = \eta \cdot \dot{\gamma}_v \tag{3.15}$$

The shear stress of the elastic part is obtained from Hooke's law, Eq. 3.4, respectively.

$$\sigma_e = G \cdot \gamma_e \tag{3.16}$$

The sum of both shear stresses leads to the differential equation of Kelvin-Voigt:

$$\sigma = \sigma_e + \sigma_v = \eta \cdot \dot{\gamma}_v + G \cdot \gamma_e = \eta \cdot \dot{\gamma} + G \cdot \gamma \tag{3.17}$$

b.) Maxwell model

The behavior of a viscoelastic fluid can be described by the Maxwell model. The spring and the dashpot are hereby connected in series, Fig. 3.6b.

A viscoelastic fluid remains partially deformed after a load and unload cycle, due to its dominating viscous part. The material behaves like a fluid with a small elastic part. Such materials are also called Maxwell fluids.

The total deformation γ is the sum of the viscous γ_v and the elastic γ_e deformation:

$$\gamma = \gamma_v + \gamma_e \tag{3.18}$$

which yields correspondingly a shear rate $\dot{\gamma}$ of:

$$\dot{\gamma} = \dot{\gamma}_v + \dot{\gamma}_e \tag{3.19}$$

the shear stress, taking effect on both components, is the same for each element:

$$\sigma = \sigma_v = \sigma_e \tag{3.20}$$

For the viscous part, the shear rate from Newton's law, Eq. 3.8 is

$$\dot{\gamma}_v = \frac{\sigma_v}{\eta} \tag{3.21}$$

and for the elastic part from Hooke's law, Eq. 3.4.

$$\dot{\gamma}_e = \frac{\dot{\sigma}_e}{G}. \tag{3.22}$$

The sum of the shear rates leads to the differential equation of Maxwell:

$$\dot{\gamma} = \dot{\gamma}_v + \dot{\gamma}_e = \frac{\sigma_v}{\eta} + \frac{\dot{\sigma}_e}{G} = \frac{\sigma}{\eta} + \frac{\dot{\sigma}}{G} \tag{3.23}$$

In combination with Eq. 3.10 follows:

$$\dot{\gamma} = \frac{\sigma}{\eta} + \frac{\dot{\sigma}}{G} = \gamma_0 \omega_1 \, cos(\omega_1 t) \tag{3.24}$$

The solution of this differential equation leads to:

$$\begin{aligned}
\sigma &= \gamma_0 \left(G_N^0 \cdot \frac{(\omega_1 \lambda)^2}{1 + (\omega_1 \lambda)^2} \, sin(\omega_1 t) + G_N^0 \cdot \frac{\omega_1 \lambda}{1 + (\omega_1 \lambda)^2} \, cos(\omega_1 t) \right) \quad (3.25) \\
&= \gamma_0 \left(G' \cdot sin(\omega_1 t) + G'' \cdot cos(\omega_1 t) \right)
\end{aligned}$$

with $\lambda = \eta/G$ the relaxation time of the system and G_N^0 the plateau value.

For low frequencies holds: G' $\propto \omega^2$ and G" $\propto \omega$. G' is called the storage modulus, it is a degree for the stored deformation energy in the substance during the shear process and describes the elastic part. G" is called the loss modulus and is a degree for the dissipated deformation energy of the substance during the shear process and describes therefore the viscous part.

The ratio between G" and G' is the loss factor $tan\ \delta$, which describes the relationship between the viscous and elastic part of the deformation behavior.

$$tan\ \delta = \frac{G''}{G'} \quad (3.26)$$

Ideal elastic behavior is reached for $\delta = 0°$ or $tan\ \delta = 0$, respectively and ideal viscous behavior for $\delta = 90°$ or $tan\ \delta = \infty$, respectively. Viscoelastic behavior results in a phase shift between shear stress and deformation of $0° < \delta < 90°$, $tan\ \delta$ is therefore in a the range $0 < tan\ \delta < \infty$.

The Maxwell model can be used as an approximation for polymer melts with a narrow molecular weight distribution at high temperatures or low frequencies, since those behave then like viscoelastic fluids [Mezger 06].

3.1.3 Time-Temperature Superposition (TTS)

With the time-temperature superposition (TTS) principle [Ferry 80, Dealy 06, Dealy 09] it is possible to obtain rheological data over a wide range of times or frequencies. The data obtained at several temperatures are therefore shifted to a common reference temperature (T_{ref}) and a mastercurve with a much wider frequency range can be achieved. This is possible since time and temperature have the same influences on the rheological properties. High temperatures or slow deformations lead to a high mobility of the polymer chains and thus to a decrease of the dynamic moduli. Low temperatures and fast deformations lead to a low mobility of the polymer chains and therefore to an increase in the dynamic moduli.

The frequency data obtained at different temperatures are horizontally shifted along the frequency axis, whereby the shifting factor a_T, is determined by the superposition of the data. The equation of Williams, Landel and Ferry (WLF equation) [Williams 55] gives

an estimation for the shift factor depending on the time-temperature superposition:

$$log\ a_T = \frac{-C_1\ (T - T_{\text{ref}})}{C_2 + T - T_{\text{ref}}} \tag{3.27}$$

The horizontal shift factor a_T is the ratio of the relaxation time at a temperature T and the relaxation time at a reference temperature T_{ref} with the two polymer-independent constants C_1 and C_2.

To compensate stress differences over the measured temperature range a vertical shift factor b_T is used, which is close to unity. The Bueche-Rouse theory assumes a proportionality between the stress magnitudes (e.g. the dynamic moduli G' and G") and the product of density ρ and Temperature T, which implies:

$$b_T = \frac{T_0 \rho_0}{T \rho} \tag{3.28}$$

The time-temperature superposition principle does only apply for thermo-rheological simple materials (linear, monodisperse homopolymers), where no structural change occurs in the investigated temperature range. For other materials the validity needs to be checked.

3.1.4   Entanglement $\mathbf{M}_e$ and critical $\mathbf{M}_c$ molecular weight

The motion of a polymer chain is significantly hindered by the topological interaction with surrounding chains. Segments of one polymer chain as well as polymer chains among each other cannot occupy the same space, i.e. polymer segments and chains cannot cross each other but overlap. Thus the Brownian motion of one polymer chain is highly constrained by the surrounded polymer chains. These constraints are referred to as entanglements. The entanglement concept is derived from the classical theory of rubber elasticity and is related to the plateau modulus. The polymer shows a rubber-like behavior when the applied deformation is faster than the disentanglement of the polymer chains. For entangled and monodisperse polymers a plateau can be observed over a certain frequency range, which is referred to as the rubber plateau with the plateau modulus G_N^0. This plateau region increases in the frequency range with increasing molecular weight, leading to longer relaxation times. This can be observed by a decrease in the frequency ω_1 (at the specific point, where G' and G" intersect) with increasing molecular weight. The reciprocal of the frequency ω_1 is approximately the terminal relaxation time of the polymer λ. Since the terminal relaxation time is proportional to the zero-shear viscosity, the viscosity increases with increasing molecular weight by $\eta_0 \propto M^{3.4}$. Whereas this relation was found for $M > M_c$, with M_c as the critical molecular weight, which is about two to three times the entanglement molecular weight. For $M < M_c$ the relation $\eta_0 \propto M$ is found [Dealy 06].

The molecular weight between entanglements M_e is defined as:

$$M_e = \frac{\rho RT}{G_N^0} \qquad (3.29)$$

Due to the Rouse relaxation a part of about 1/5 of the imposed tension along the chain is relaxed before entanglement sets in. The actual measured plateau modulus is reduced of about 4/5 of the calculated value in Eq. 3.29: [Graessley 80, Fetters 94].

$$M_e = \frac{4}{5} \frac{\rho RT}{G_N^0} \qquad (3.30)$$

The M_e decreases with increasing chain stiffness [Heymans 00]. For PS, typical literature values of the entanglement molecular weight range from M_e = 13.3 kg/mol to 18.1 kg/mol [Ferry 80, Fetters 94, Fetters 99].

3.2   Dynamics of polymer systems - Fundamentals

The motion or relaxation processes of a branched polymer are restricted by the presence of long-chain branching. This is examplarily illustrated in Fig. 3.7 for a three-arm star, which is the simplest case of a long-chain branched topology. The star can only move by reptation, if one of the arms is dragged into the tube, which is occupied by the other two arms. Consequently the relaxation of a branched polymer is slowed down is most cases, when compared to a linear polymer with the same molecular weight [Dealy 06]. For a highly branched archictecture, e.g. a comb polymer, the relaxation motion is more complex. The motion of a comb polymer is further complicated by the backbone segments between two branching points, which restrain the backbone segment from relaxation.

For the better understanding of the relationship between the dynamics and the underlying molecular structure various concepts have been developed to describe the dynamics of polymer systems, which are introduced in the following.
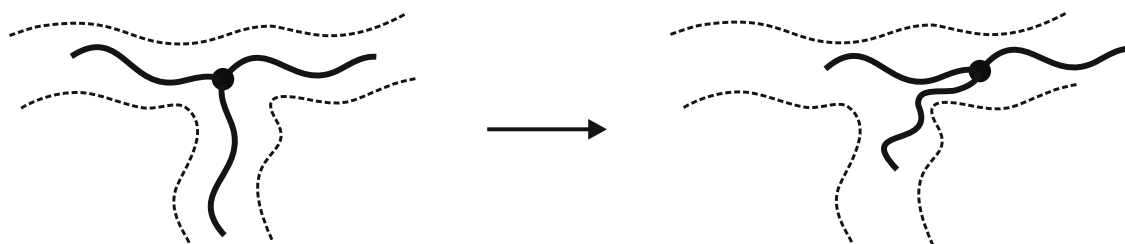
Figure 3.7: Illustration of the movement of a three-arm star via reptation. The star can only reptate out of its tube, by dragging one of the arms into the tube of the other two.

3.2.1 Tube Model

The tube model, first applied to polymer melts by Doi and Edwards [Doi 86], can be used to predict the slowing down of the relaxation process of a branched polymer. To simplify the many body problem, the tube model is restricted to the examination of a single chain. The chain and its movement is confined to a mean-field tube, which is affected by the constraints (entanglements) with the surrounding chains describing the external field, Fig. 3.8a [McLeish 02].
The polymer is restricted to the movement in the tube, which is defined by the tube diameter a and the length of the tube L_{tube} (also called primitive path or contour length). The diameter and length a of a tube segment is related to the entanglement spacing by

$$a^2 = \frac{4}{5} \frac{\rho R T b^2}{M_0 G_N^0} \tag{3.31}$$

with b as the random-walk parameter derived by $b = R/\sqrt{N}$, where R $= <$R$^2>_0$ is the root-mean-square end-to-end length of the tube. The tube length can be calculated using

$$L_{tube} = a \cdot Z = a \cdot \frac{M}{M_e} \tag{3.32}$$

with a as the tube segment length, Z the random-walk steps each of length a (number of entanglements), M the chain molecular weight and M_e the entanglement molecular weight. The length scales in the tube model are illustrated in Fig. 3.8b.
In the case of the deformation of a polymer melt, the streching of the polymer chains leads consequently to a stretch and orientation of the tubes. The polymer chains can relax from the generated stress, originated by the applied deformation, by escaping the stretched tube. The relaxation processes, by which the chain can escape the stretched tube and form a new undeformed tube are reptation, primitive path fluctuations and constraint
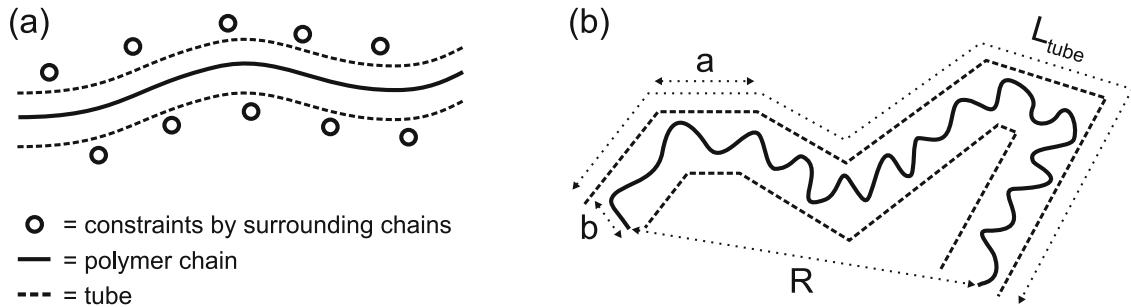
Figure 3.8: (a) Polymer tube arising from the topological constraints of neighboring polymer chains; (b) Definition of length scales in the tube model, with a as the tube diameter, b as the random walk step length, R as the root-mean-square end-to-end distance and L_{tube} as the length of the tube. Adapted from Dealy and Larson [Dealy 06].

release, which are briefly introduced in the following. Furthermore, the dynamic dilution and hierarchical relaxation processes are explained, to give a complete overview of the most important relaxation processes involved.

3.2.2 Reptation

The reptation process was introduced by de Gennes [Gennes 71]. It is a random diffusive process, where the polymer chain escapes from its tube by a snake-like displacement along the tube contour, which is restricted due to the constraints of the other chains. The parts of the polymer chain, which can escape the original tube can take a random confirmation, Fig. 3.9. Although the polymer is able to escape the tube, a new tube will be formed again by the re-entanglement with other polymer chains.

Due to the diffusive process, the time required for the polymer chain to escape its tube is proportional to the square of the contour length, from Eq. 3.32, devided by the diffusion coefficient of the chain, which is the diffusion coefficient of the Rouse model:[Larson 99]

$$\tau_d = \frac{L_{tube}^2}{D_c \pi^2} \tag{3.33}$$
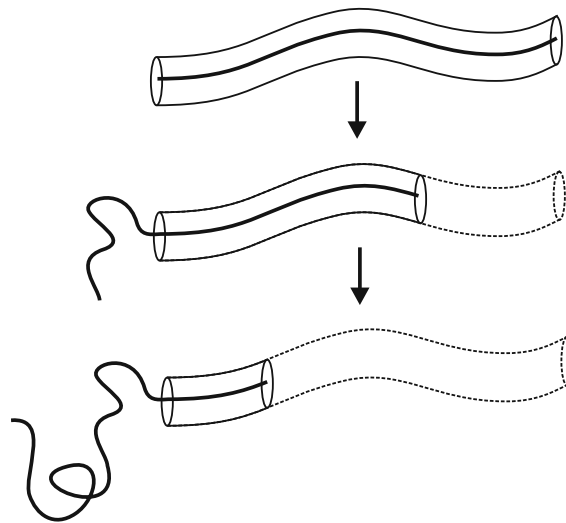
Figure 3.9: Schematic illustration of the reptation process. The polymer chain escapes its tube by a snake-like diffusion process. The escaped parts of the polymer chain are rearranged in a new tube by the constraints of the surrounding polymer chains.

3.2.3 Primitive Path Fluctuations

In the case of branched polymers, the branches are connected at one end to the polymer backbone. Therefore the branches cannot diffuse as a whole along the tube, which makes
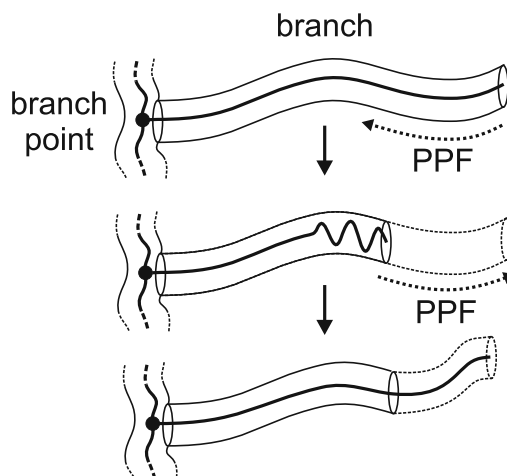
Figure 3.10: Schematic illustration of primitive path fluctuations of a branched polymer. The chain end diffuses inside the tube, the former occupied part of the tube gets lost and the chain end can relax inside the tube. When the chain end diffuses out, a new tube is created.

reptation impossible. The branch end is still able to relax and can wrinkle-up via Brownian motion inside the tube, since the tube diameter is much wider than the diameter of the chain. By pulling the chain end inside the tube, the previously occupied tube vanishes and as soon as the chain end is pushed out, a new tube is created for the chain end, Fig. 3.10. The primitive path fluctuation (PPF), also called contour length fluctuation (CLF), was proposed by de Gennes [Gennes 75] and Doi and Kuzuu [Doi 80].

Thereby the stress associated to the prior chain end is lost. The chain ends can relax very fast in contrast to the inner segments. Because for a full relaxation the chain ends would have to diffuse to the branch point, which is entropically unfavorable. The time for the relaxation process increases therefore exponentially with the distance of the chain end to the branching point. A precise model for the determination of the relaxation time related to primitive path fluctuations was proposed by Milner and McLeish [Milner 98]. For the relaxation by primitive path fluctuations Rouse motions are responsible, which can occur at the chain end as well as in the interior of the tube [Likhtman 02]. Experimentally the PPF has an influence on the zero shear viscosity η_0. Since η_0 scales with the longest relaxation time, η_0 increases exponentially (and not as $\eta \propto M^{3.4}$) with the molecular weight of the branches. This was confirmed by Pearson and Helfand [Pearson 84] for star polymers.

3.2.4 Constraint Release

While reptation and primitive path fluctuation is considered for the chain motion of a chosen single chain (the test chain), the surrounding chains are undergoing similar motions.
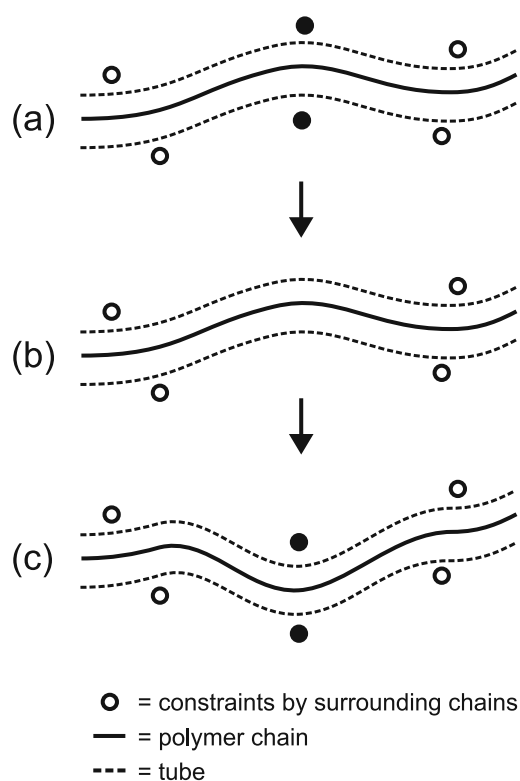
Figure 3.11: Schematic illustration of the constraint release (CR) effect. (a) The tube is confined by the constraints of the surrounding chains. By the motion of a surrounding chain (filled black spheres) the entanglements are released (b) and the tube can take a new conformation, which will be entangled by new neighboring chains (c).

Thereby constraints via entanglements on the test chain are released by the movement of surrounding chains and vice versa, Fig. 3.11. This effect is called constraint release (CR) and is especially important for branched or polydisperse linear polymers. Because short chains can release constraints much faster via diffusion than long chains via reptation [Larson 99]. A simple description of constraint release, called double reptation was proposed by Tuminello [Tuminello 86] and des Cloizeaux [Cloizeaux 88].

3.2.5 Dynamic Dilution

Dynamic dilution can be considered for polymer systems with different relaxation time scales, e.g. polydisperse linear or branched polymers. In the case of polydisperse linear polymers, the smaller chains can relax much faster than the time scale for the motion of the longer chains. The contraints induced by the smaller chains are released so frequently relative to the motion of the long chains that the motion of the longer chain is hardly effected. The short chains can consequently be regarded as diluent for the longer chains. This phenomenon is called dynamic dilution [Ball 89] or tube enlargement [Marrucci 85].
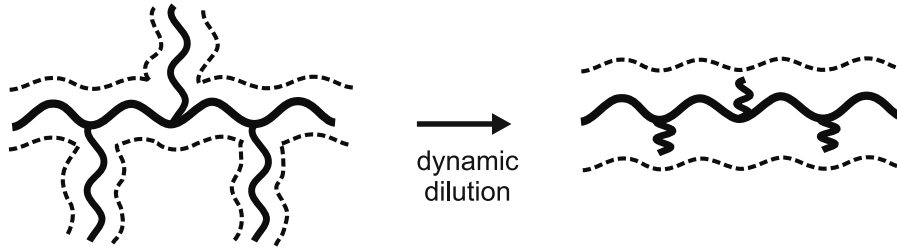
Figure 3.12: Schematic illustration of the dynamic dilution effect. The branches of the comb polymer relax and are retracted to the backbone, leading to an increase of the tube of the backbone chain, due to the generated free volume, previously occupied by the branches.

In the case of branched polymers an exponential difference exists in the relaxation times along the branches. As a result, tube segments at the end of the branch relax exponentially faster than the segments close to the branch point or even the backbone segments. The fast relaxation of the branches leads to a dynamic dilution and an enlargement of the backbone tube, due to the generated free volume, previously occupied by the branch segments, Fig. 3.12. Due to the dynamic dilution, the ability of the backbone to entangle is reduced, which leads to a decrease in the plateau modulus G_N^0 and to an increase in the tube diameter a, according to Eq. 3.31.

In the general case of a polymer solution, the G_N^0 decreases with decreasing polymer concentration Φ_P. It has been suggested that $G_N^0 \propto \Phi_P^{1+\alpha}$, with $1 \leq \alpha \leq 4/3$ [Ferry 80, Colby 90, Watanabe 99]. For branched polymers the polymer concentration can be correlated to the backbone volume fraction, in the case where the branches can be assumed to be fully relaxed and acting as a solvent. The dynamic dilution concept has been applied successfully by Milner and McLeish et al., e.g. to monodisperse linear polymers [Milner 98], monodisperse stars [Milner 97] and combs [Daniels 01].

3.2.6 Hierarchical Relaxation

The hierarchical relaxation describes the relaxation sequence of chains in a branched polymer. A comb architecture consists of two different chain types, the branches and the backbone ends as well as the backbone segments between two branching points. The motion of the backbone segments between the branching points depends on the motion of the branches. As soon as the branches have relaxed the backbone can relax too, Fig. 3.13. Due to the dynamic dilution, induced by the branch relaxation, the backbone relaxes like a linear chain in a solution, with entanglements between the backbones only. The relaxation of the backbone occurs by reptation, but it is retarded due to the drag exerted by the relaxed arms along the backbone [Larson 01, Park 04].
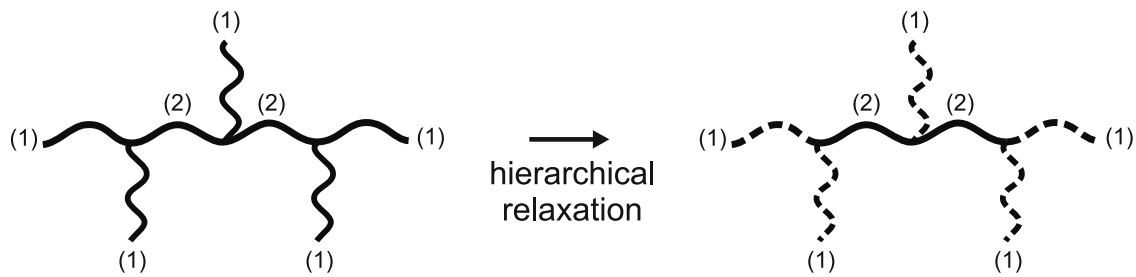
Figure 3.13: Schematic illustration of the hierarchical relaxation of a comb polymer. The branches and the backbone ends (1) relax first before the relaxation of the inner backbone segments (2) starts.

The hierarchical relaxation process can be investigated experimentally, Fig. 3.14. In the case of a linear polymer, only one relaxation process can be observed for the reptation of the chain. While in the case of a branched polymer two relaxation processes, related to branch and backbone relaxation, can be observed. At higher frequencies the relaxation process of the branches (by primitive path fluctuations) can be observed. After the relaxation of the branches, the backbone relaxation process (via reptation) can proceed, which occurs at lower frequencies. The retraction of the branches leads to dynamic dilution and to reduced entanglements of the backbone chains, this can be observed by a decrease of
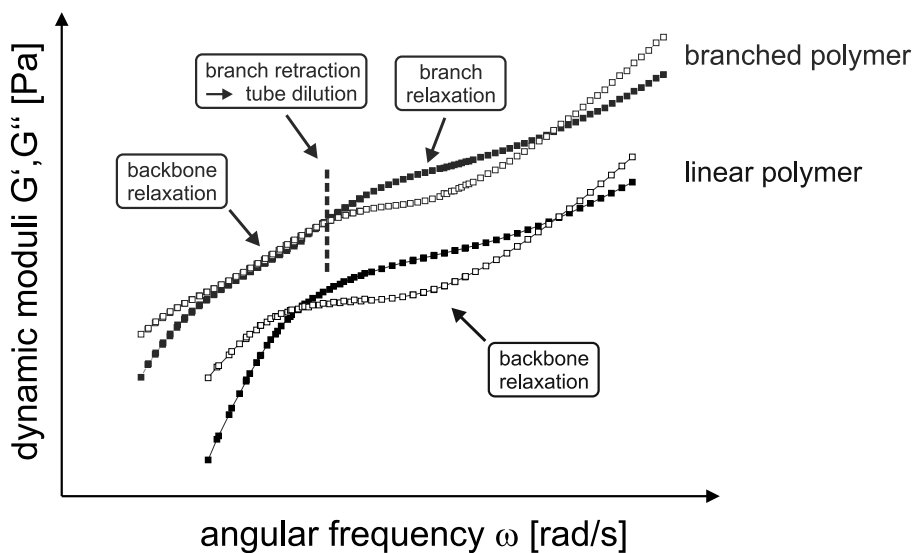
Figure 3.14: Hierarchical relaxation process of a comb polymer in comparison to the single relaxation process of a linear chain. At higher frequencies the relaxation of the branches occurs. After retraction of the branches, the backbone relaxation process takes place. Due to the dynamic dilution and associated decrease of backbone entanglements, the plateau value decreases. For better visualization, the dynamic moduli of the branched polymer curve were multiplied by a constant factor, thus the decrease of the plateau value is not evident from the figure.

the plateau modulus ($G_N^0 \propto \Phi_{bb}^{\alpha+1}$, with Φ_{bb} as the backbone volume fraction and $\alpha = 1$ or 4/3) in contrast to the linear chain [Watanabe 99, Dealy 06].

3.3   Experimental part

3.3.1   Influences of branching on linear viscoelastic data

The investigated comb polymers range from slightly to well entangled branches, while the backbone is highly entangled in all cases. The dimensionless number of entanglements is defined as $s_{br} = M_{w,br}/M_e$ for the number of branch entanglements and as $s_{bb} = M_{w,bb}/M_e$ for the number of backbone entanglements. The values for the number of entanglements s_{br} and s_{bb}, as well as the entanglement molecular weights for the different polymers used, can be found in Table 3.1.

Table 3.1: Comb polymer structural and rheological parameter

sample #	sample name	$\Phi_{br}^{(a)}$	$s_{bb}^{(b)}$	$s_{br}^{(b)}$	$C_1^{(c)}$ [-]	$C_2^{(c)}$ [K]
LK95	195k	-	9.9	-	6.4	112.8
CK106	197k-14-42k	0.75	9.9	2.1	6.1	97.7
CK123	275k-5-42k	0.43	16.2	2.5	6.7	131.4
CK128	197k-14-15k	0.52	9.9	0.8	6.7	111.7
CK132	197k-29-15k	0.69	9.9	0.8	7.3	123.9
CK158	262k-2-17k	0.11	15.4	1.0	5.6	115.2
CK159	262k-2-37k	0.22	15.4	2.2	5.8	123.4
C632	275k-25-26k	0.70	16.2	1.5	4.9	105.1
C642	275k-29-47k	0.83	16.2	2.8	5.4	106.3

$^{(a)}$: volume fraction of the branches

$^{(b)}$: M_e(PS) = 17.3 kg/mol [Ferry 80]

$^{(c)}$: T_{ref} = 170 °C (PS: $T_{ref} \approx T_g$ + 80 °C; PpMS: $T_{ref} \approx T_g$ + 70 °C)

The linear viscoelastic data for a series of linear and comb homopolymer melts of PS and PpMS is presented in Fig. 3.15. The polymer LK195 is shown to demonstrate the behavior of a monodisperse linear polymer in contrast to monodisperse comb polymers. It shows only one rubbery plateau, due to the entanglement of the polymer chains. In the case of comb polymers, two rubbery plateaus can be observed. Those correspond to
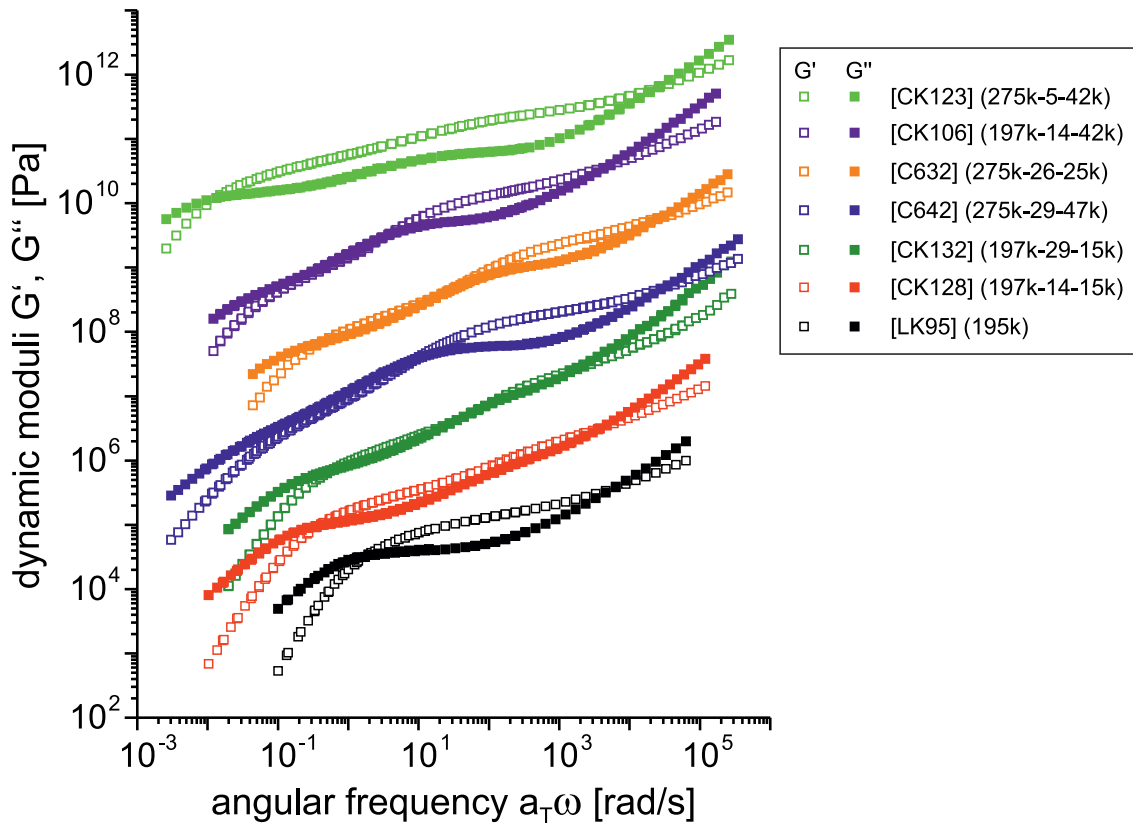
Figure 3.15: Linear viscoelastic data: mastercurves of PS and PpMS combs

the relaxation of the branches at higher frequencies and of the diluted backbone (as a result of the dynamic dilution by the relaxed branches) at lower frequencies, respectively [Daniels 01]. Comb polymers with similar branch lengths are compared with each other with decreasing branching degree. CK132 (197k-29-15k) and CK128 (197k-14-15k) are an example for combs, where the branch molecular weight (15 kg/mol) is slightly below the entanglement molecular weight ($M_e \approx 20.3$ kg/mol) and the number of branches (14 and 29 branches) differs by a factor of two. While the combs CK106 (197k-14-42k), C642 (275k-29-47k) and CK123 (275k-5-42k) with a branch molecular weight of above 42 kg/mol are well entangled and the number of branches (5, 14 and 29 branches) are separated by a factor of three and two.

In contrast to the other combs, CK158 (262k-2-17k) and CK159 (262k-2-37k) have both the same branching degree of two, with different molecular weight of the branches from slightly (17 kg/mol) to well entangled (37 kg/mol). Those two combs do not show two rubbery plateaus like the other combs, but only the rubbery plateau of the backbone, Fig. 3.16. A slight increase in the terminal relaxation time can be observed for the two combs in contrast to the linear backbone. Though this is a result of the delayed backbone relaxation influenced by the branches, the terminal relaxation time is not a useful criteria
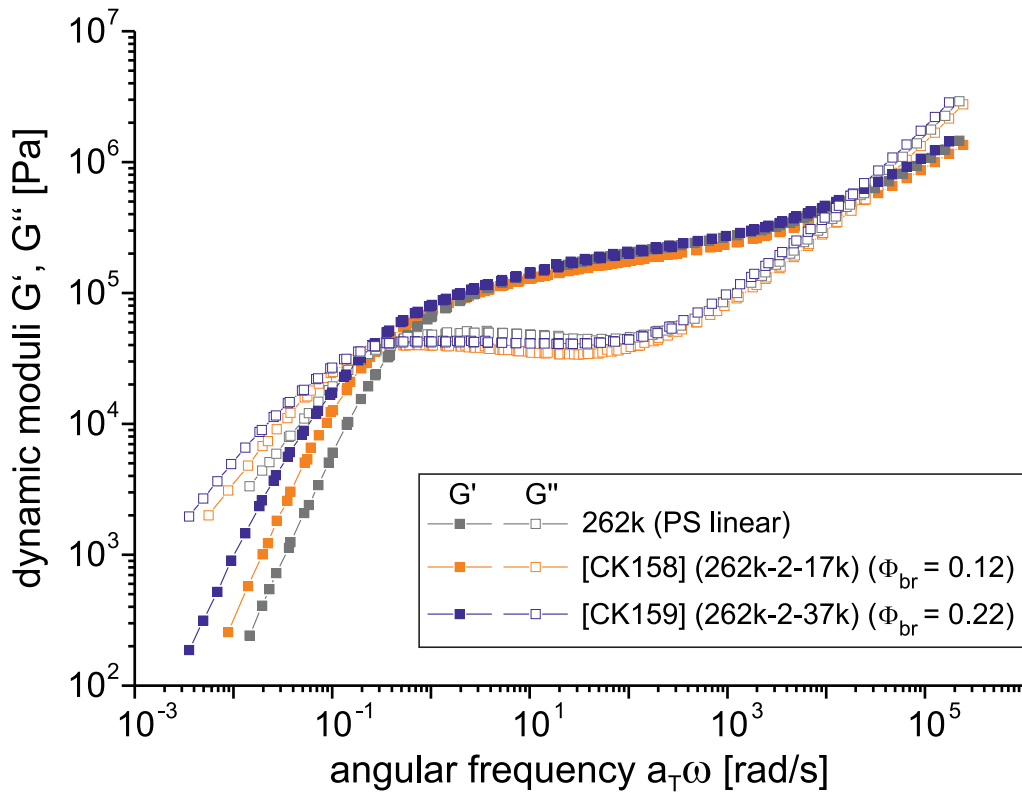
Figure 3.16: Linear viscoelastic data: $tan\ \delta$ vs. angular frequency ω plots of PS and PpMS combs

for the destinction between linear and slightly branched polymers. Whereas an increase of the relaxation could also be attributed to an increase of the molecular weight of a linear polymer. Hepperle et al. [Hepperle 05] investigated polystyrene combs with 0.5 to 4 branches per backbone with slightly to well entangled branches. A second rubbery plateau could not be found for less than four branches. The number of branches and the molecular weight of the branches is in this case not high enough to achieve a significant entanglement of the branches, thus a branch rubbery plateau could not be observed. A certain minimum limit of the number of branches should exist, from which on an effective entanglement can occur. The limit should lie in the range from 3 to 4 branches, since with five branches (CK123, 275k-5-42k) two rubbery plateaus can already be well distinguished.

In contrast to this, the samples CK106 (197k-14-42k) and C642 (275k-29-47k), with a higher number of branches, show a power law dependence of the moduli (G', G" $\propto \omega^n$) with n = 0.5 in the frequency region where the backbone relaxation takes place (an exponent of n = 0.5 is predicted by the Rouse theory for unentangled polymers). In the terminal region the classical behavior G' $\propto\ \omega^2$ and G" $\propto\ \omega$ is observed. Kapnistos et al. [Kapnistos 05] used the dynamic dilution concept [McLeish 88, Milner 98, McLeish 99,

McLeish 02] to explain this behavior. Depending on the volume fraction of the branches the dynamic dilution effect leads to a decrease in entanglements up to only a few or virtually no entanglements (behavior of a Rouse-chain) in the case of high volume fractions. This behavior can be observed for $\Phi_{br} > 0.75$ (CK106, 197k-14-42k), while for Φ_{br} of 0.69 (for sample CK132, 197k-29-15k) this is not the case. The limit for the volume fraction of branches, when Rouse-like behavior for the backbone chains starts, must be in the range of $0.70 > \Phi_{br} > 0.75$. This behavior bears resemblance to a crosslinking system at its gel point, which was proposed by Winter et al. [Winter 86]. This behavior was also observed by García-Franco et al. [García-Fran 01] for polyethylene with low levels (0.3-0.8 LCB per 10000 carbon atoms) of long chain branching.

Using $tan\ \delta$ vs. frequency plots Figs. 3.17 and 3.18 the effect of the dilution of the backbone can be better illustrated. The relaxation of the backbone is associated with the minimum in $tan\ \delta$ at low frequencies and of the branches at high frequencies, respectively. The $tan\ \delta$ value of the minimum at low frequencies is dependend on the volume fraction of the branches Φ_{br}. The lower Φ_{br} the lower is the value of $tan\ \delta$. This can be found for example in Fig. 3.18 by the comparison of CK132 (197k-29-15k, $\Phi_{br} = 0.69$) and CK128 (197k-14-15k, $\Phi_{br} = 0.52$). This is also the case for CK106 (197k-14-42k, $\Phi_{br} = 0.75$) and CK123 (275k-5-42k, $\Phi_{br} = 0.52$) in Fig. 3.17, where
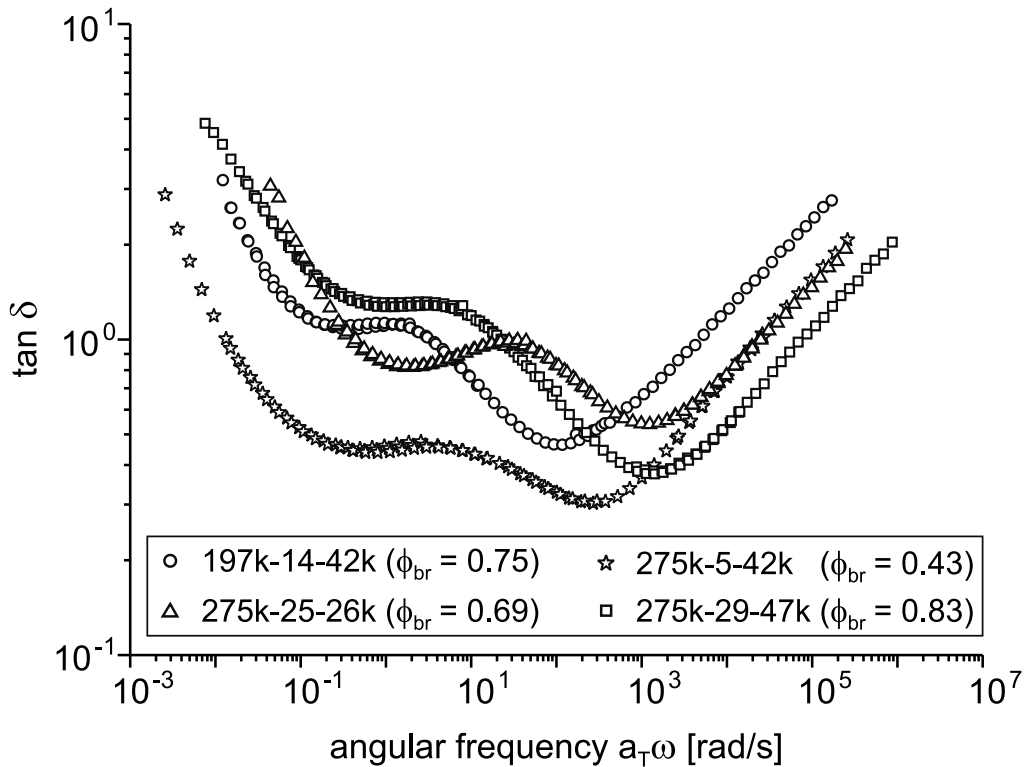
Figure 3.17: Linear viscoelastic data: $tan\ \delta$ vs. angular frequency ω plots of PS and PpMS combs.
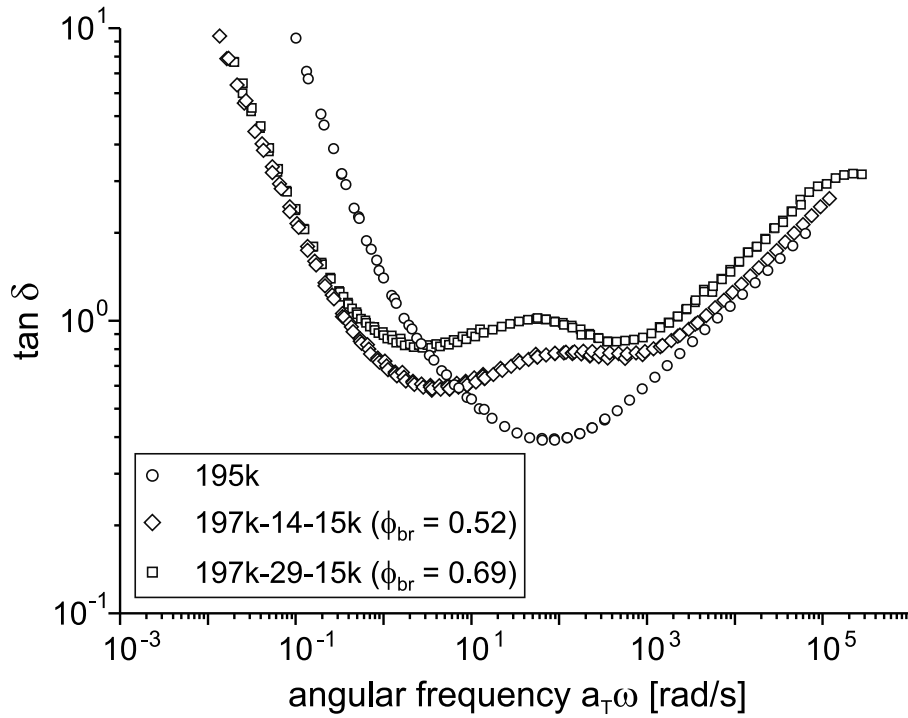
Figure 3.18: Linear viscoelastic data: $tan\ \delta$ vs. angular frequency ω plots of PS and PpMS combs.

the $tan\ \delta$ value of CK123 is much lower than the one of CK106 (197k-14-42k). But the dependency between $tan\ \delta$ and Φ_{br} is limited to a certain range, because at high Φ_{br}, where Rouse-like behavior of the backbone occurs, an upper limit is reached, where $tan\ \delta$ has a value of 1. This can be observed in Fig. 3.17 for the samples CK106 (197k-14-42k) and C642 (275k-29-47k), where $tan\ \delta$ is around 1 for both samples. Their difference in Φ_{br} cannot be distinguished anymore solely by the difference in $tan\ \delta$. The $tan\ \delta$ plot can be used to draw a qualitative picture of the volume fraction effect, but it is not sufficient to achieve a quantitative conclusion.

As already mentioned in section 3.2.5 the plateau modulus of a polymer in solution decreases with decreasing polymer concentration. It is assumed, that $G_N^0 \propto \Phi_P^{1+\alpha}$ with Φ_P as the polymer volume fraction and with $1 \leq \alpha \leq 4/3$ [Watanabe 99, Dealy 06]. To proove whether this assumption holds also for the investigated comb polymers and to determine the most appropriate dilution exponent α, the plateau values of the diluted backbones were compared with the plateau values of the undiluted backbone and plotted versus the volume fraction of the backbone Φ_{bb}, Fig. 3.19. The plateau moduli of the diluted backbone $G(\Phi)$ and the undiluted backbone G_N were determined using the G' value corresponding to the minimum in $tan\ \delta$, section B.1. Using the volume fraction of the backbone Φ_{bb} as actual polymer concentration, assumes that the branches have fully
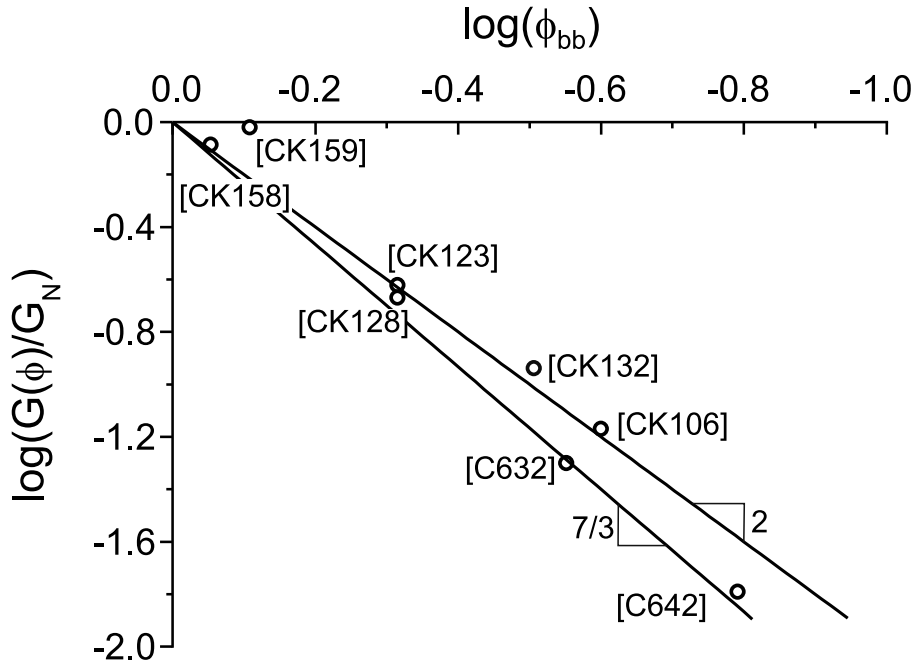
Figure 3.19: Ratio $G(\Phi)/G(_N)$ of the diluted backbone $G(\Phi)$ over the plateau modulus of the undiluted backbone G_N against the volume fraction of the backbone (Φ_{bb}) in the comb. Experimental data is shown for PS and PpMS combs. The theoretical behavior is indicated by the two straight lines with slopes of 2 and 7/3, corresponding to a dilution exponent of α = 1 or 4/3 respectively. The experimental data shows good aggrement for an dilution exponent α = 1.

relaxed and act as solvent. The theoretical assumptions for the dilution exponent are also included and indicated as straight lines in the plot (a line with a slope of 2 for α = 1 and slope of 7/3 for α = 4/3 respectively, using $\Phi_{bb}^{1+\alpha}$). The experimental data for the synthesized PS and PpMS polymers shows good agreement with a dilution exponent α = 1, while the data for the combs of the Roovers series are in good agreement with a dilution exponent α = 4/3. It can be assumed, that the higher branching degree of the combs C632 (275k-25-26k) and C642 (275k-29-47k) leads to a dilution of the backbone to a higher extent and results in a lower diluted plateau modulus $G(\Phi)$ than in the case of combs with a lower branching degree.

3.3.2   The reduced van Gurp-Palmen-Plot

The comparison of polymers with different architectures and as in this case with different chemistry is difficult, due to different relaxation times of the samples. To circumvent this issue the reduced van Gurp-Palmen Plot can be used (red-vGP-plot) [Gurp 98, Trinkle 01, Trinkle 02], where the complex modulus is normalized to the plateau modulus. The reduced van Gurp-Palmen Plot contains the same information of

conventional mastercurves, but due to the temperature and time invariance of the plot, temperature differences between experiments and changes in relaxation times are tolerated [Schulze 05]. In contrast to the mastercurve data in the previous section, the different polymers and architectures are directly comparable and differences in the branching degree and branch molecular weight can be elucidated. Like in the $tan\ \delta$ vs. frequency plot in Fig. 3.17, the first minimum at low reduced complex modulus G_{red} corresponds to the backbone relaxation and the minimum at $G_{red}\ \approx 1$ to the branch relaxation process. The advantage of the comparability in the reduced van Gurp-Palmen plot is accompanied by complexity, if many different plots are to be compared. So it is appropriate to reduce the amount of data to two characteristic points, which correspond to the two minima in the plot. Those characteristic points are obtained by the intersection of two tangent lines through the inflection points enclosing the minimum, for clarity only one example for the determination of the characteristic points is shown in Fig. 3.20. The two characteristic points are described by the two values P_1 and P_2 which correspond to the value of the phase angle at the first and second minimum and the two values G_1 and G_2 for the re-
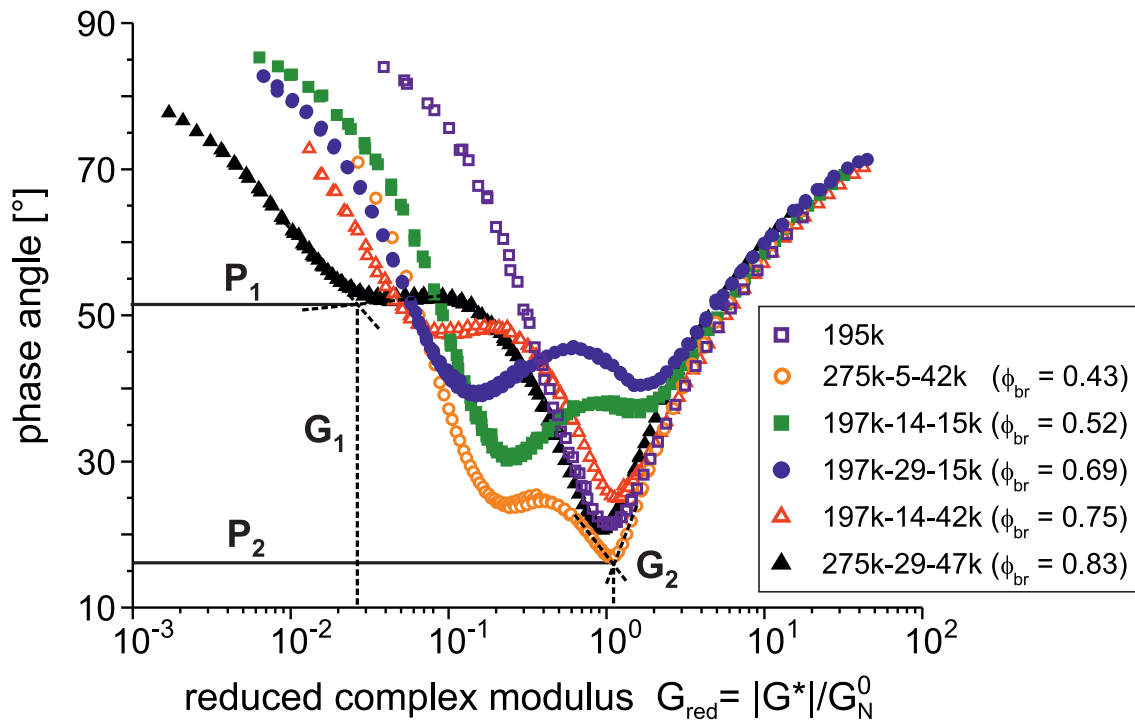
Figure 3.20: Reduced van Gurp-Palmen plot of PS and PpMS combs. The data of the curves is reduced to two characteristic points, which correspond to the two minima in the plot. The two characteristic points are described by the two values P_1 and P_2 which correspond to the value of the phase angle at the first and second minimum and the two values G_1 and G_2 for the reduced complex modulus at the first and second minimum.

duced complex modulus at the first and second minimum, respectively. In the previous section an indication for the correlation between the first minimum of $tan\ \delta$ and the volume fraction of the branches Φ_{br} was found. The absolute values of $tan\ \delta$ or the phase angle (P_1) in the case of the reduced van Gurp-Palmen Plot give only indications for the influence of Φ_{br}, if combs with similar backbone and branch molecular weight, but different branching degree are compared. Instead of using P_1, the comparison of the second corresponding value (G_1, the reduced complex modulus of the first minimum) with Φ_{br} leads to a linear relationship between the two values Fig. 3.21, where the volume fraction of the branches Φ_{br} is linearly decreasing with increasing G_1 . This can be explained
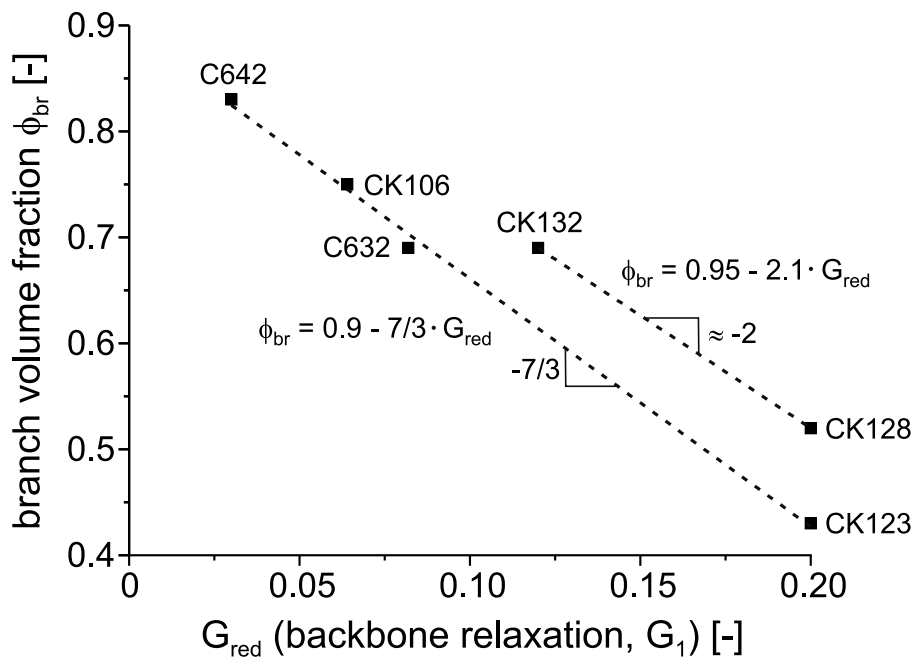
Figure 3.21: Linear dependence of the branch volume fraction Φ_{br} with the reduced complex modulus G_{red} of the backbone relaxation G_1 (which corresponds to the value of the first minimum). The combs CK132 and CK128 with slightly entangled branches correlate with the dilution exponent of 2, while the combs with entangled branches show a dependence of 7/3.

by the dynamic dilution concept, the higher Φ_{br} the higher is the dilution effect and the number of entanglements is reduced. $|G^*|$ and therefore G_1 decreases, since G_N^0 which is used for the normalization, can be assumed as constant for the same linear polymer type. Those findings are similar to the dependence, which was illustrated in Fig. 3.19. However, the combs with well entangled branches show now a linear dependence with a slope of about -7/3 and the combs with slightly entangled branches a slope of about -2. Those values correspond well with the theoretical values for the dilution exponent. It can be concluded that the dilution exponent of 2 is valid for branched structures, which

behave like a linear polymer, due to their slightly entangled branches. While the dilution exponent 7/3 holds for branched structures with well entangled branches. The reduced van Gurp-Palmen plot can be therefore used to determine the dilution factor α for a certain structure for the further use in simulations. The volume fraction of the branches can be also determined using the following equations, for the case of branched structures with well-entangled branches:

$$\Phi_{br} = 0.9 - 7/3 \cdot G_{red} \tag{3.34}$$

and for the case of slightly entangled branches:

$$\Phi_{br} = 0.95 - 2.1 \cdot G_{red}. \tag{3.35}$$

Furthermore it can be observed that the value of P_1 increases with the number of branches. There is a significant increase from CK123 (275k-5-42k, 5 branches) to CK106 (197k-14-42k, 14 branches), but the increase from CK106 (197k-14-42k, 14 branches) to C642 (275k-29-47k, 29 branches) is much lower, though the number of branches was doubled in each case.
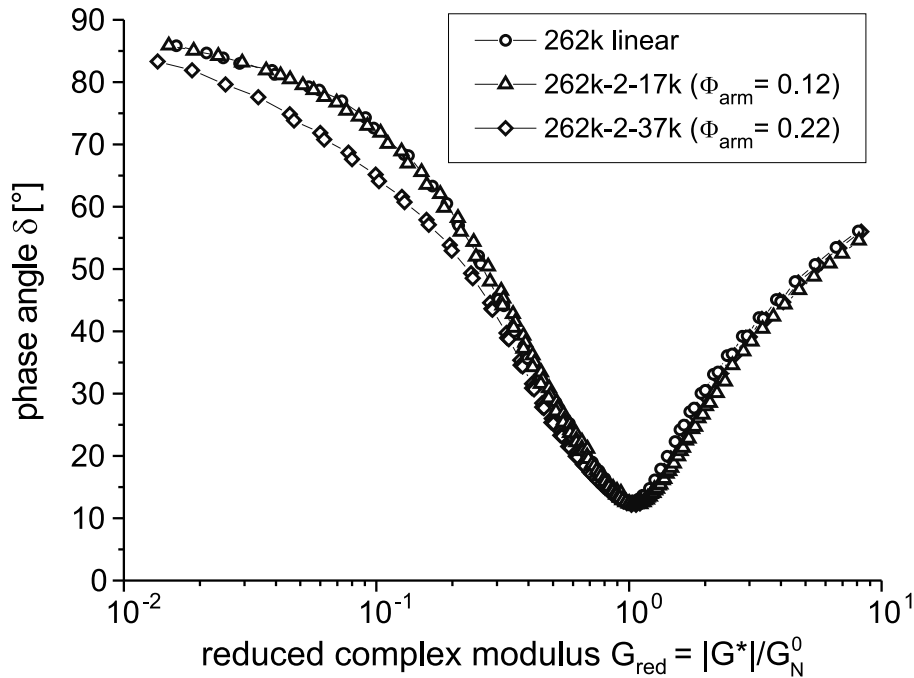
Figure 3.22: Reduced van Gurp-Palmen plot for two combs with two branches each (CK158: $M_{w,br}$ = 17 kg/mol and CK159: $M_{w,br}$ = 37 kg/mol) in comparison with the linear backbone. Only the comb CK159 (262k-2-37k) with well entangled branches shows a deviation from the behavior of the backbone. This is a result of the dynamic dilution of the backbone, leading to a decrease in phase angle at low G_{red} values.

The reduced van Gurp-Palmen plot was also used to compare the combs with only two branches with the linear backbone, Fig. 3.22. The comb CK158 (262k-2-17k) with slightly entangled branches shows the same behavior as the linear backbone. In contrast, the phase angle value decreases at low reduced complex modulus in the case of the comb CK159 (262k-2-37k) with well-entangled branches. This is an indication for the occurence of a second relaxation process, due to the branch relaxation. The reduced van Gurp-Palmen plot can therefore be a useful tool to distinguish between branched and linear topologies even for very low branching degrees, in contrast to the conventionally used mastercurve.

3.4 Conclusion

Using the reduced van Gurp-Palmen plot a linear correlation of the volume fraction of the branches with the value of the reduced modulus at the minimum, corresponding to the backbone relaxation, as well as an increase of the phase angle with increasing number of branches could be found. Even for low branching degrees (five branches) a second minimum can be observed, while for the case of only two branches only a slight deviation from the linear behavior for well entangled branches was found. Due to the lack of experimental data only a semi-quantitative picture on the influence of branching on the linear rheological properties could be drawn. To improve and to validate the findings, the comparison with simulated linear data, obtained by the BoB (branch on branch) [Das 06] or hierarchical [Wang 10] model, would be helpful.

Chapter 4

Extensional rheology

Extensional rheology is an important and reliable method for the determination of branching in homopolymer melts. Extensional flow properties of the polymer can be determined, which is not possible using shear flow measurements. The extensional flow properties are of special interest for polymer processing, where extensional flows play a significant role (e.g. in film blowing, thermoforming, etc.).

4.1 Fundamentals

Extensional rheology measurements can be conducted in various extensional deformations (e.g. in uniaxial, biaxial or planar extension) [Macosko 94]. Since the measurement in uniaxial deformation is the most commonly used method due to its simplicity the basic theory is restricted to this case.

In an uniaxial experiment the sample is elongated at both ends with a constant velocity v in the direction of deformation x to generate a steady uniaxial extension, Fig. 4.1. The velocity v_x of the two ends along the deformation direction x is related to a constant Hencky strain rate $\dot{\epsilon}_H$:

$$v_x = \dot{\epsilon}_H \cdot x \qquad (4.1)$$

In a constant rate experiment the center of the rod has a velocity of zero and the velocity of both sample ends v_{end} increases with the distance from the center

$$v_{end} = \dot{\epsilon}_H \frac{L}{2} \qquad (4.2)$$

or

$$\frac{dx}{dt} = \dot{\epsilon}_H \cdot x \qquad (4.3)$$
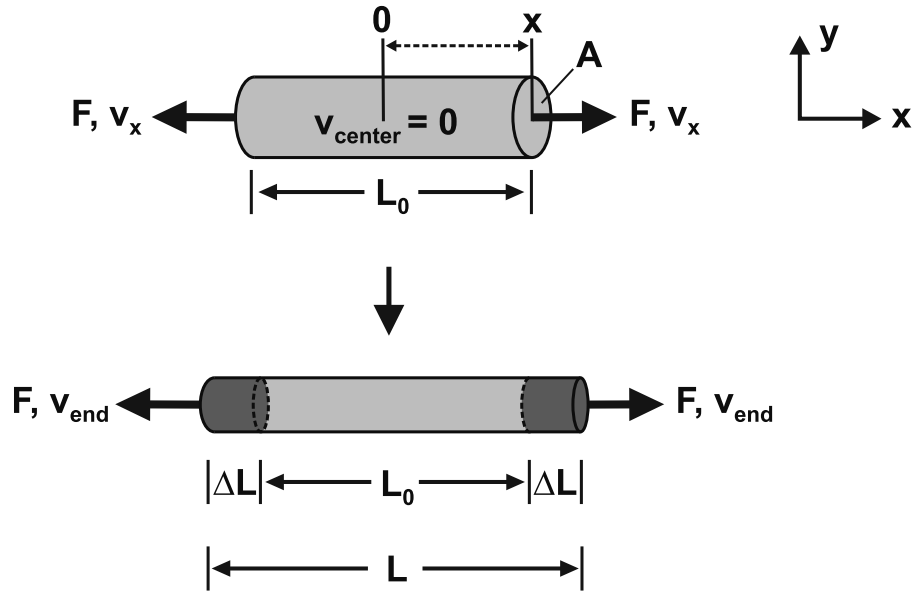
Figure 4.1: Schematic illustration of the extension of a rod in the deformation direction x.

By integration from L_0 to L follows:

$$\dot{\epsilon}_H \cdot t = \epsilon_H = \int_{L_0}^{L} \frac{1}{x} dx = ln\left(\frac{L}{L_0}\right) \Leftrightarrow L = L_0 \exp(\dot{\epsilon}_H t) \tag{4.4}$$

with the so-called Hencky strain ϵ_H [Macosko 94]. The combination of the Eqs. (4.2) and (4.4) results in:

$$v_{end} = \frac{1}{2} \dot{\epsilon}_H L_0 \exp(\dot{\epsilon}_H t) \tag{4.5}$$

To achieve a constant extension rate during the extension of the sample, the endpoint velocity v_{end} has to increase exponentially.

A tensile stress σ_x is applied in the deformation direction to elongate the sample, while the surface of the sample is under an uniform normal stress σ_y, Fig. 4.2. The extensional stress σ_{ext} is the force F per unit area A acting on the end of the sample and is defined as the difference between the applied axial stress σ_x and the stress acting on the free surface
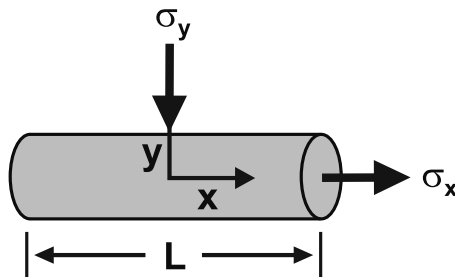
Figure 4.2: Components of the extensional stress σ_{ext} acting on the sample during extension.

σ_y [Macosko 94].

$$\sigma_{ext} = \sigma_x - \sigma_y = \frac{F}{A} \tag{4.6}$$

In the case of an incompressible material, the volume of the sample before the extensional deformation is identical with its volume after the deformation (at time t):

$$\pi R_0^2 L_0 = \pi R^2(t) L(t) \quad \rightarrow \quad \pi R_0^2 L_0 = A(t) L(t) \tag{4.7}$$

in combination with Eq. 4.4 can be seen, that the sample area decreases exponentially during the experiment:

$$A(t) = \pi R_0^2 L \cdot \exp(-\dot{\epsilon}_H t) = A_0 \cdot \exp(-\dot{\epsilon}_H t). \tag{4.8}$$

The extensional stress becomes then

$$\sigma_{ext} = \sigma_x - \sigma_y = \frac{F \cdot \exp(\dot{\epsilon}_H t)}{A_0}. \tag{4.9}$$

A commonly used material function is the tensile stress growth coefficient or also called transient extensional viscosity $\eta_E^+(t, \dot{\epsilon}_H)$, which is defined as

$$\eta_E^+(t, \dot{\epsilon}_H) = \frac{\sigma_{ext}(t, \dot{\epsilon}_H)}{\dot{\epsilon}_H}. \tag{4.10}$$
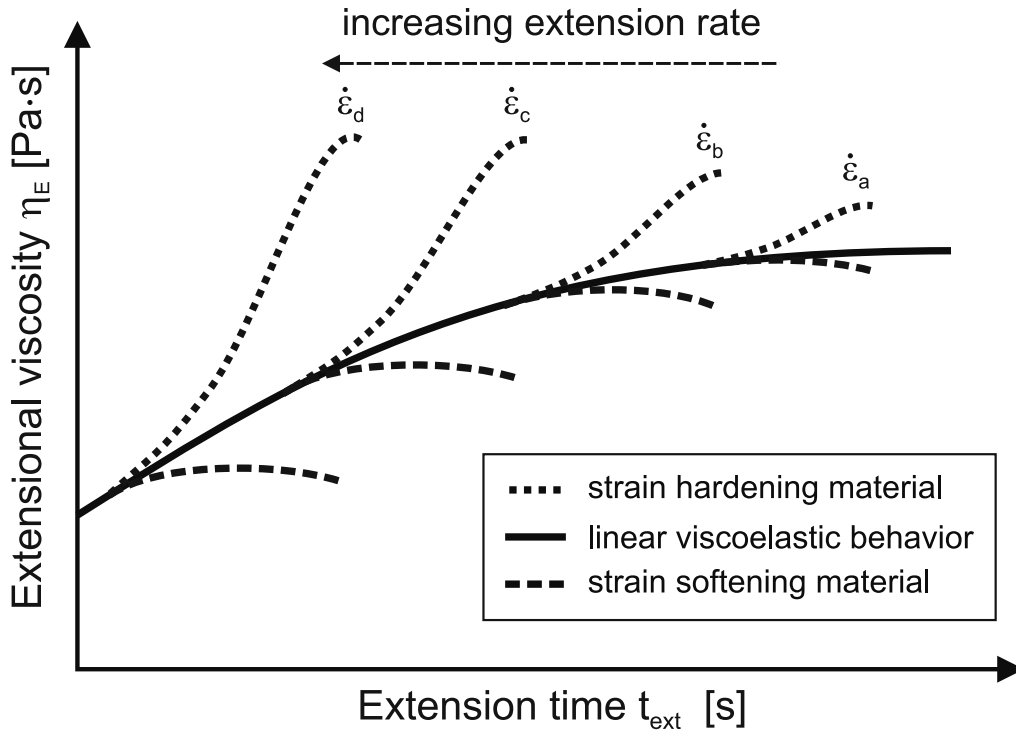
Figure 4.3: Schematic illustration of the extensional rheology of materials with linear viscoelastic, strain softening and strain hardening behavior at different extension rates.

To verify the accuracy of the extensional measurement, $\eta_E^+(t, \dot{\epsilon}_H)$ is compared with the linear viscoelastic (LVE) behavior, derived by the Boltzmann superposition principle given by

$$\eta_E^+(t) = 3 \int\limits_0^t G(t) \; dt = 3\eta^+(t). \tag{4.11}$$

At low extension rates or small times, the transient shear viscosity $\eta^+(t)$ differs from the transient extensional viscosity $\eta_E^+(t)$ only by a factor of 3. This dependence is also called the *Trouton ratio* [Trouton 06]. The departure from the linear viscoelastic (LVE) behavior can give an information about the extensional flow behavior. In case the $\eta_E^+(t, \dot{\epsilon}_H)$ exceeds the LVE curve the material is said to be strain hardening, in case it falls below, it is said to be strain softening. If the extensional viscosity increases with strain rate, the material is said to be extension thickening, in case it decreases, it is extension thinning.[Dealy 06] Strain softening is observed for linear polymers. Strain hardening occurs for branched, polydisperse as well as for linear polymers with a small amount of a high-molecular weight component Fig. 4.3 [Münstedt 80, Münstedt 79]. The standard tube model prediction for the extensional viscosity in uniaxial extension is shown
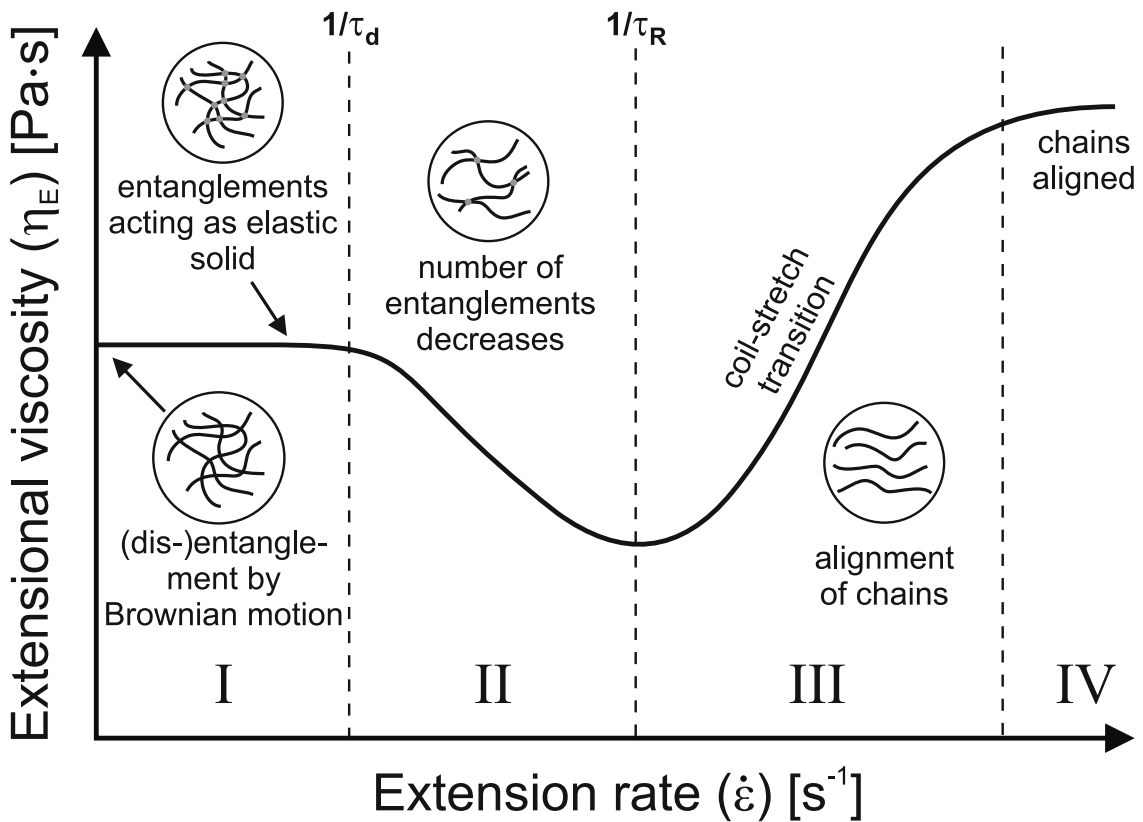
Figure 4.4: Steady-state extensional viscosity as a function of the extension rate, as predicted by standard molecular theories of entangled polymers [Marrucci 04]

in Fig. 4.4 for a linear and monodisperse polymer. At small extension rates $\dot{\epsilon}$, below the inverse reptation time τ_d^{-1} (zone I), the polymer chains are in the equilibrium of (dis-) entanglement dominated by Brownian motion. As the extension rate increases the entanglements between the polymer chains act as an elastic solid, leading to an increase in the extensional viscosity. In zone I the viscosity is constant and conform with the *Trouton value* $\eta_E = 3\eta_0$.

For higher extension rates $(1/\tau_d^{-1} < \dot{\epsilon} < 1/\tau_R^{-1})$ (zone II) the number of entanglements decreases and the tubes orient parallel to the extensional direction. The polymer chains are not yet stretched and the stress saturates with the tube orientation. Due to the constant stress the extensional viscosity decreases with a slope of -1, which is in accordance with the definition of the extensional viscosity ($\eta_E = \sigma_{ext}/\dot{\epsilon} \rightarrow \eta_E \propto \dot{\epsilon}^{-1}$ with $\sigma_{ext} =$ const.). Experimentally a slope of -1/2 was found, which can be explained by the contribution of interchain pressure effects [Marrucci 04]. For extension rates exceeding the inverse Rouse time ($\dot{\epsilon} > 1/\tau_R^{-1}$)) (zone III) chain stretch occurs until the chains are fully stretched and aligned (zone IV). The phenomena of the increase of the extensional viscosity η_E in zone III is the so-called *coil-stretch transition* [Marrucci 04, Dealy 06].

4.2   Instrumentation: Extensional Viscosity Fixture (EVF)

Recent improvements on extensional rheometry, including the Sentmanat Extensional Rheometer (SER) from Xpansion Instruments [Sentmanat 04, Sentmanat 05], as well as its related Extensional Viscosity Fixture (EVF) [Franck a, Franck b] developed by TA Instruments have widened and simplified the possibility of performing uniaxial extensional viscosity measurements on polymer melts using conventional rotational rheometers. The advantages of such systems are their simplicity, the low amount of sample needed, and the reliability when compared with previous dedicated instruments (e.g. the Rheometrics-Melt Extensiometer (RME) [Meissner 94] or the Münstedt-type [Münstedt 75, Münstedt 79] extensional rheometer).

The rotational extensional rheometers, mentioned above, combine the advantage of constant extensional velocity. Since the sample length L_0 remains constant during the extension, the velocity of the sample end v_{end} is also constant. In contrast to extensional stretch rheometers, the extensional velocity does not have to be increased exponentialy to maintain a constant extension rate. Rotational extensional rheometers are therefore in contrast to extensional stretch rheometers small in size. Furthermore the sample can be easier supported and a uniform deformation and temperature throughout the experiment can be maintained. A major advantage is the use of rotational extensional tools
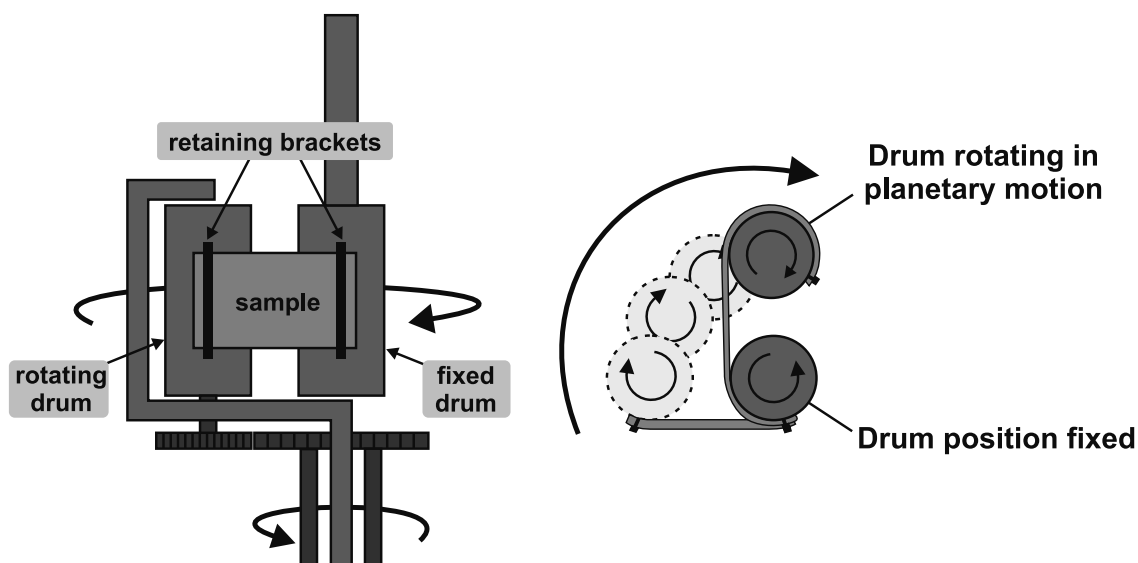
Figure 4.5: Schematic of the Extensional Viscosity Fixture (EVF).

(e.g. EVF or SER) in combination with commercial rotational rheometers. For the extensional measurements the Extensional Viscosity Fixture (EVF) from TA Instruments was used, Fig. 4.5. The major part of the EVF consists of two cylinders, where the sample is attached to. One of the cylinders is rotating and the other one is fixed and is measuring the force. To elongate the sample equally in both directions, the rotating cylinder moves in a planetary motion around the other one, while rotating at the same time around its own axis. Due to this type of motion no gear friction, like in the case of the SER occurs, leading to a material response which is not affected by friction.

The EVF as well as the SER are both restricted to Hencky strains between 3 and 4, to avoid contact of the retaining brackets or of the sample with the stretched sample, which would result in a filament rupture or in a sudden increase in the extensional viscosity.

4.3   Extensional rheology of comb polymers

Uniaxial extensional experiments were performed on polystyrene and poly(p-methylstyrene) comb structures with different number q and molecular weight $M_{w,br}$ of the branches. Of particular interest is the resulting strain hardening behavior and its dependence on the molecular structure of the combs. A quantification of the influences on the strain hardening can be obtained by a strain hardening factor (SHF), which is defined as the ratio of the steady state extensional viscosity of the experimental data $\eta_E(t, \dot{\epsilon})$ and the extensional viscosity derived by the Doi-Edwards (DE) prediction $\eta_E^+(DE)$ (which

reflects the behavior of a linear polymer chain):

$$SHF = \frac{\eta_E(t, \dot\epsilon)}{\eta_E^+(DE)} \qquad (4.12)$$

Wagner et al. [Wagner 00] proposed that the Doi-Edwards prediction should be taken as the basis for defining strain hardening. The accuracy of the extensional measurements was assured by the conformance of the experimental data with the linear viscoelastic (LVE) prediction (which is indicated by the dashed line in Figs. 4.6 to 4.8 in the linear viscoelastic range for all extension rates). The LVE and DE predictions were obtained from dynamic-mechanical data using home-written Matlab programs. The discrete relaxation spectra with partial moduli G_i and relaxation times τ_i were obtained by the IRIS program [Winter 08] from the linear mastercurves.

4.3.1 Influence of the number of branches

The influence of the average number of grafted branches on the strain hardening behavior is investigated on a series of combs with similar molecular weight of the branches and the backbone, but with a variation in the number of branches q from 5 to 29. The number of branches between the combs differs by a factor two to three, Fig. 4.6. By the comparison of the absolute values of the steady state extensional viscosity η_E at the highest Hencky strain rate ($\dot\epsilon_H = 3$ s^{-1}), the values for the two polystyrene combs CK123 (275k-5-42k) and C642 (275k-29-47k) are almost identical $\eta_E(\text{CK123}, \dot\epsilon_H = 3 \ s^{-1}) = 648 \ kPa \cdot s$ and $\eta_E(\text{C642}, \dot\epsilon_H = 3 \ s^{-1}) = 656 \ kPa \cdot s$, though the number of branches differs by a number of about six. The comb with 14 branches (CK106) has a slightly higher value $\eta_E (\text{CK106}, \dot\epsilon_H = 3 \ s^{-1}) = 725 \ kPa \cdot s$, but is still in the range of the other two combs, and so far comparable. By decreasing the Hencky strain rate $\dot\epsilon_H$ the steady state extensional viscosity η_E increases for the combs with comparable values. When comparing the three comb structures it can be observed, that the comb with the lowest amount of branches CK123 (275k-5-42k, 5 branches) shows the lowest amount of strain hardening (SHF $\approx$ 4). When the number of branches is increased by a factor of about three CK106 (197k-14-42k, 14 branches) the amount of strain hardening increases also by a factor of three (SHF $\approx$ 12). By the further increase of the number of branches C642 (275k-29-47k, 29 branches), by a factor of two, the difference in strain hardening in contrast to the comb with only 14 branches is low and reaches for high Hencky strain rates ($\dot\epsilon_H = 3$ s^{-1}) comparable values (SHF $\approx$ 12-13). The difference between the amount of strain hardening for C642 (275k-29-47k) and CK106 (197k-14-42k) increases with decreasing Hencky strain rate. In the case of only slightly entangled branches ($M_{w,br} \approx 15$ kg/mol), the absolute steady state extensional viscosity values increase also in the case of 14 branches (CK128, 197k-
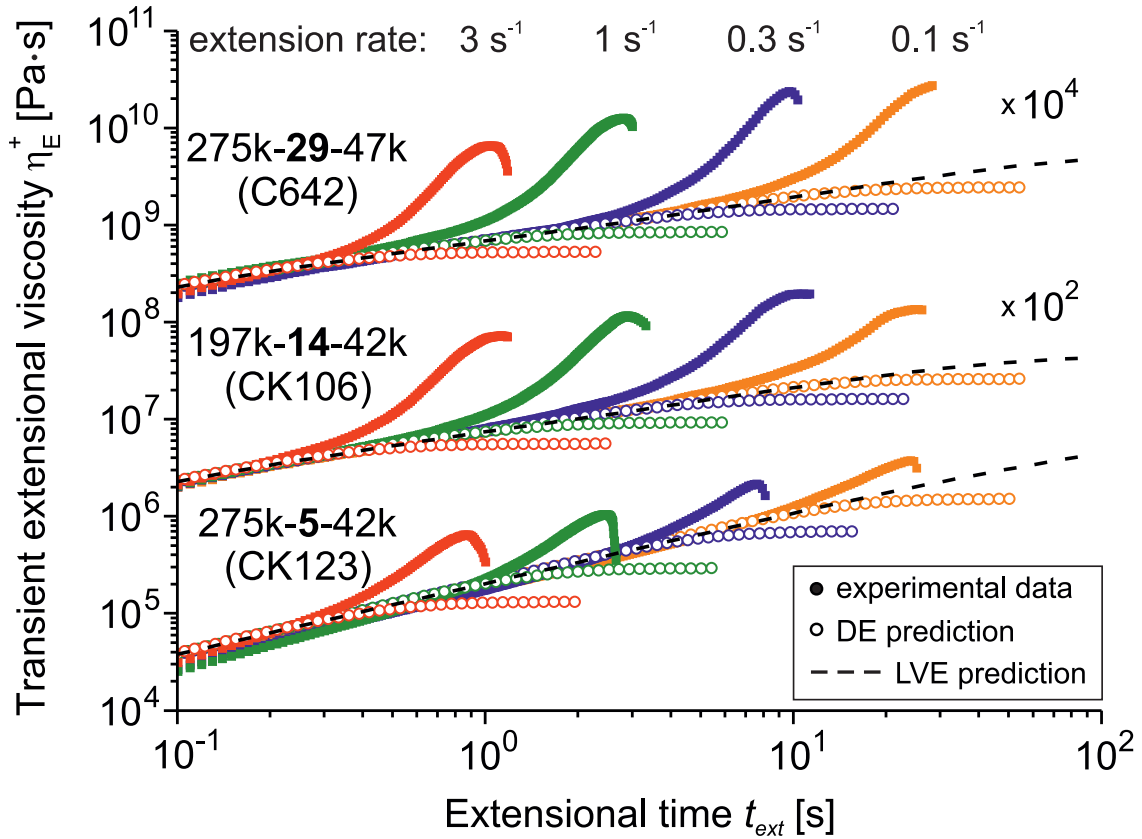
Figure 4.6: Extensional rheology measurements of combs with different number of branches. The number of branches is varied (q = 5, 14, 29), the number of branches between the combs differs by a factor of two to three. The molecular weight of the branches $M_{w,br}$ is almost identical. The filled spheres stand for the experimental data, the unfilled spheres for the Doi-Edwards (DE) prediction and the dashed line for the linear viscoelastic (LVE) prediction.

14-15k), but are far lower. However in the case of 29 branches (CK132, 197k-29-15k) the values for η_E decrease with decreasing extension rate, also at the highest extension rate of 3 s^{-1} the highest SHF (SHF = 19.6) for the compared combs could be observed. Out of the above results it can be concluded that the increase of the number of branches does not have an influence on the absolute steady state extensional viscosity, but on the amount of strain hardening, which can be increased up to a critical number of branches. When this limit is reached, the increase in strain hardening is then only small and the influence of the number of branches reaches a limit. This was observed for the two combs C642 (275k-29-47k) and CK106 (197k-14-42k), so it can be concluded that the limiting number is the range of 14 to 29 branches.

4.3.2 Influence of the branch molecular weight

The influence on the molecular weight of the branches is investigated by the comparison of two combs with similar molecular weight of the backbone and the same number of branches, with molecular weights of the branches of 15 kg/mol (slightly below the entanglement molecular weight) and 42 kg/mol (entangled branches), Fig. 4.7. The absolute viscosities of the comb with lower molecular weight of the branches CK128 (197k-14-15k) do not reach the level of CK106 (197k-14-42k). Also the values for the SHF factor are lower and they are decreasing with decreasing extension rate. The molecular weight of
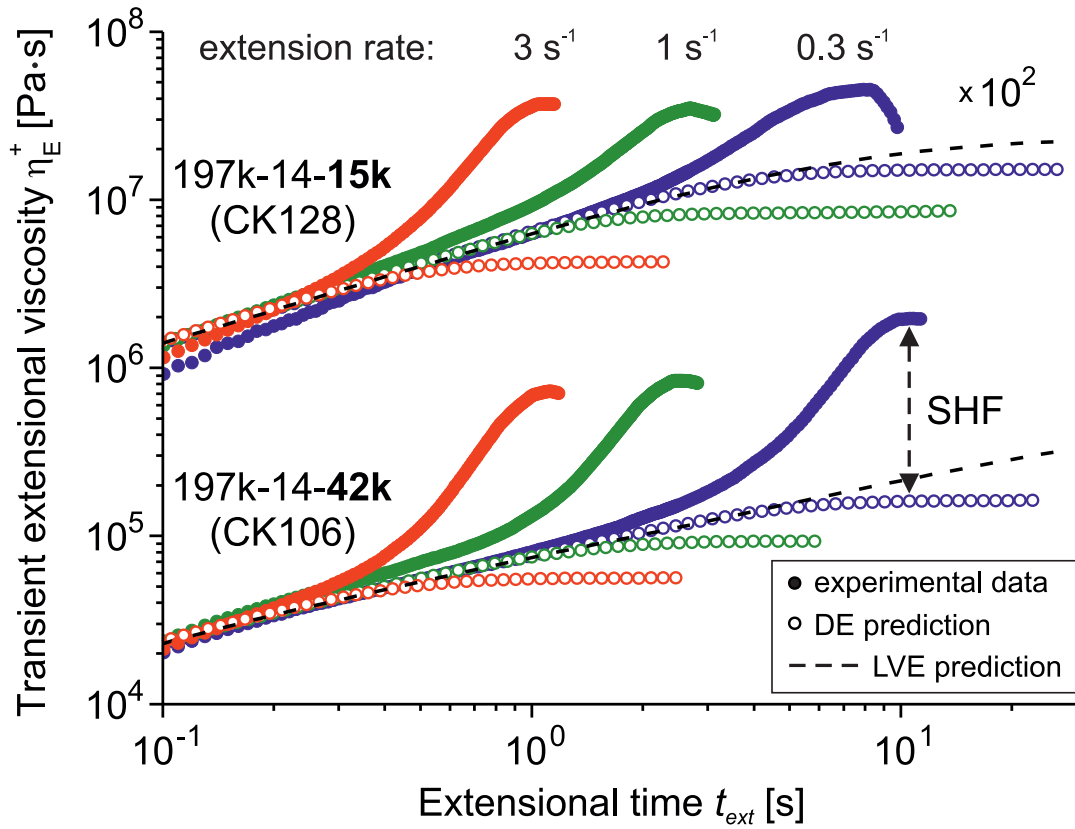
Figure 4.7: Extensional rheology measurements of combs with different molecular weight of the branches. The backbone molecular weight ($M_{w,bb}$ = 197 kg/mol) and the number of branches (q = 14) is identical for both combs, only the molecular weight of the branches ranges from slightly entangled ($M_{w,br}$ = 15 kg/mol) to well entangled ($M_{w,br}$ = 42 kg/mol). The filled spheres stand for the experimental data, the unfilled spheres for the Doi-Edwards (DE) prediction and the dashed line for the linear viscoelastic (LVE) prediction.

the branches $M_{w,br}$ of sample CK128 (197k-14-15k) is below the critical molecular weight M_c and slightly below the entanglement molecular weight M_e. A reduced contribution of entanglements can be the reason for a decreased strain hardening and viscosity values in contrast to the sample CK106 (197k-14-42k), where $M_{w,br} > M_c$.

4.3.3   Lower limit for the number of branches

By the comparison of the influence of the branching number, Fig. 4.6, it was observed, that there exists an upper limit for the increase in strain hardening. A lower limit for the number of branches might also exist, when strain hardening cannot be observed anymore. The lowest number of branches that could be introduced was in average two branches per backbone, Fig. 4.8. The molecular weight was choosen as in the other samples from slightly entangled (17 kg/mol) to entangled (37 kg/mol). In contrast to the other combs, only for the highest extension rate of 3 s^{-1} the transient extensional viscosity exceeded the DE-prediction and a slight strain hardening behavior (SHF $\approx$ 1.4) could be observed. The reason for the slight increase in strain hardening could be the underlying molecular topologies, with a mixture of asymmetric stars, H-polymers and combs. For stars, strain hardening cannot be observed due to the lack of backbone chain stretch. The number
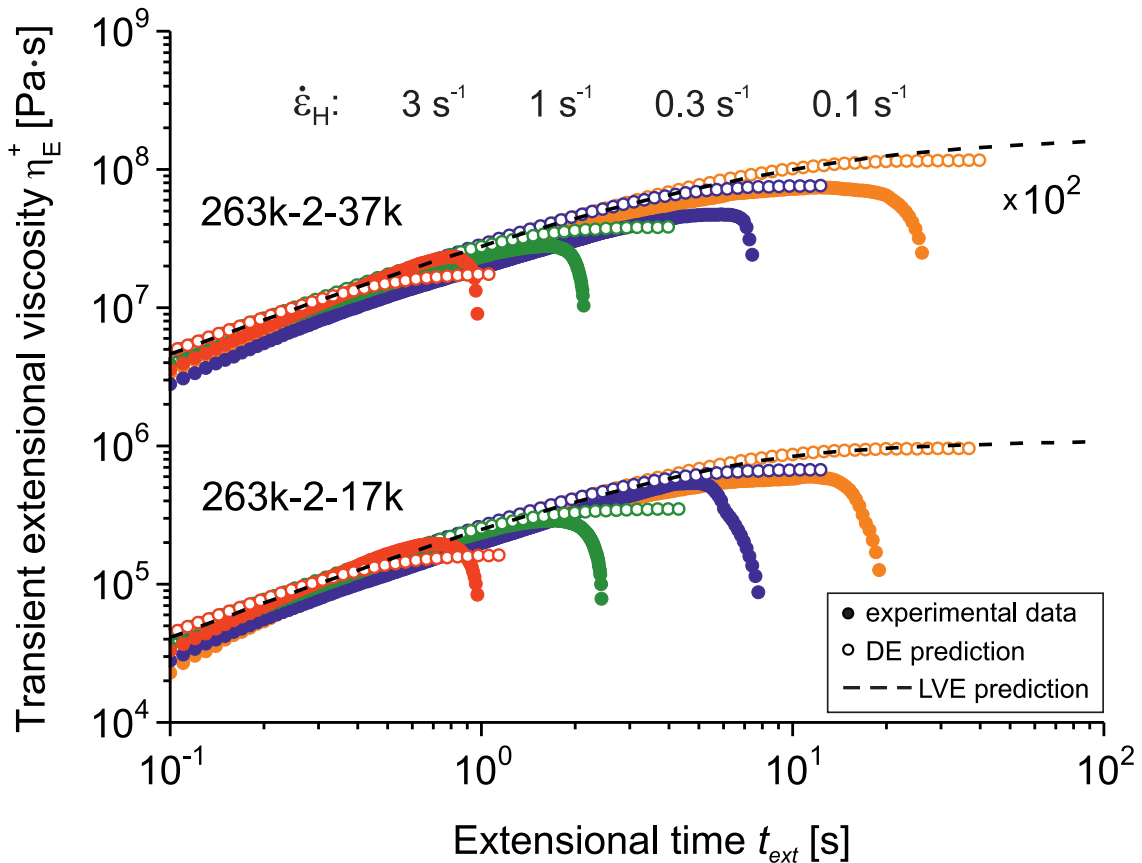
Figure 4.8: Extensional rheology measurements of combs with only two branches and different molecular weight of the branches. The filled spheres stand for the experimental data, the unfilled spheres for the Doi-Edwards (DE) prediction and the dashed line for the linear viscoelastic (LVE) prediction.

of branches could also be too low to reach a sufficient number of entanglements and an efficient backbone chain stretch.

4.3.4 Strain hardening behavior

In Fig. 4.9 the strain hardening factors for combs with slightly entangled branches CK128 (197k-14-15k) and CK132 (197k-29-15k) and for the combs with low number of branches CK158 (262k-2-17k) and CK159 (262k-2-37k) at different Hencky strain rates $\dot{\epsilon}_H$ are presented. Those combs show a linear increase of the SHF with increasing Hencky strain rate $\dot{\epsilon}_H$ and increasing number of branches.

The combs with entangled branches CK106 (197k-14-42k), C642 (275k-29-47k) and CK123 (275k-5-42k) show also an increase in SHF with increasing number of branches, for $\dot{\epsilon}_H < 0.3\ \mathrm{s}^{-1}$, Fig. 4.10. But in contrast to the combs with slightly entangled branches, the SHF decreases or is almost constant, when a Hencky strain rate $\dot{\epsilon}_H$ of about $0.3\ \mathrm{s}^{-1}$ is exceeded. This can be explained by the relaxation process related to the corresponding $\dot{\epsilon}_H$. For $\dot{\epsilon}_H > 0.3\ \mathrm{s}^{-1}$ the extension rate is close to or higher than the inverse Rouse time τ_R^{-1} of the backbone, branch relaxation comes now into the picture, leading to a reduced chain stretch. The transient extensional viscosity η_E^+ and subsequently the strain harden-
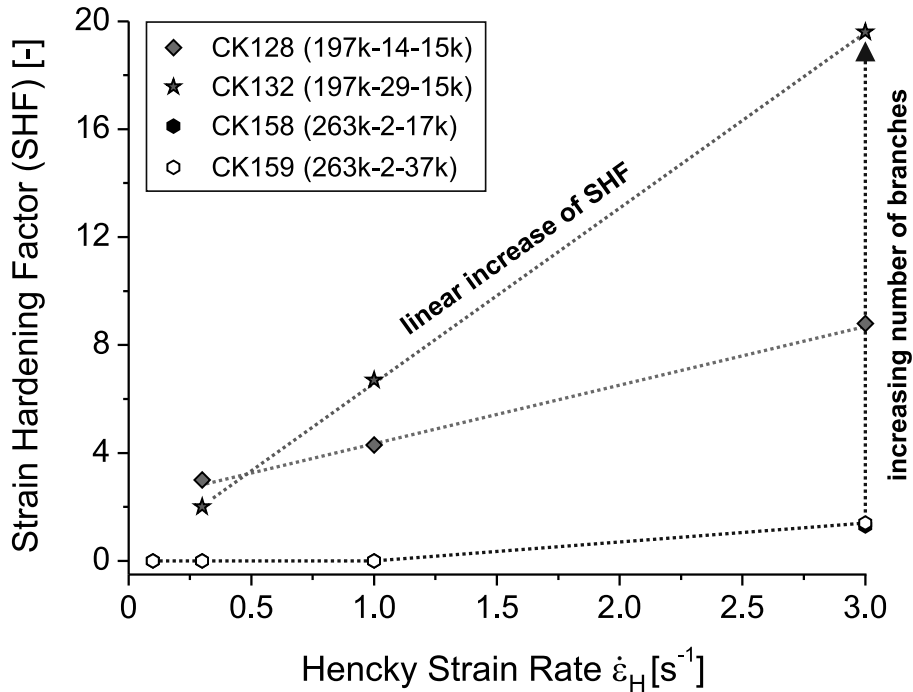
Figure 4.9: Behavior of the strain hardening factor (SHF) depending on the Hencky Strain Rate $\dot{\epsilon}_H$ for combs with slightly entangled branches. The SHF increases with $\dot{\epsilon}_H$ and the number of branches (T = 180 °C).
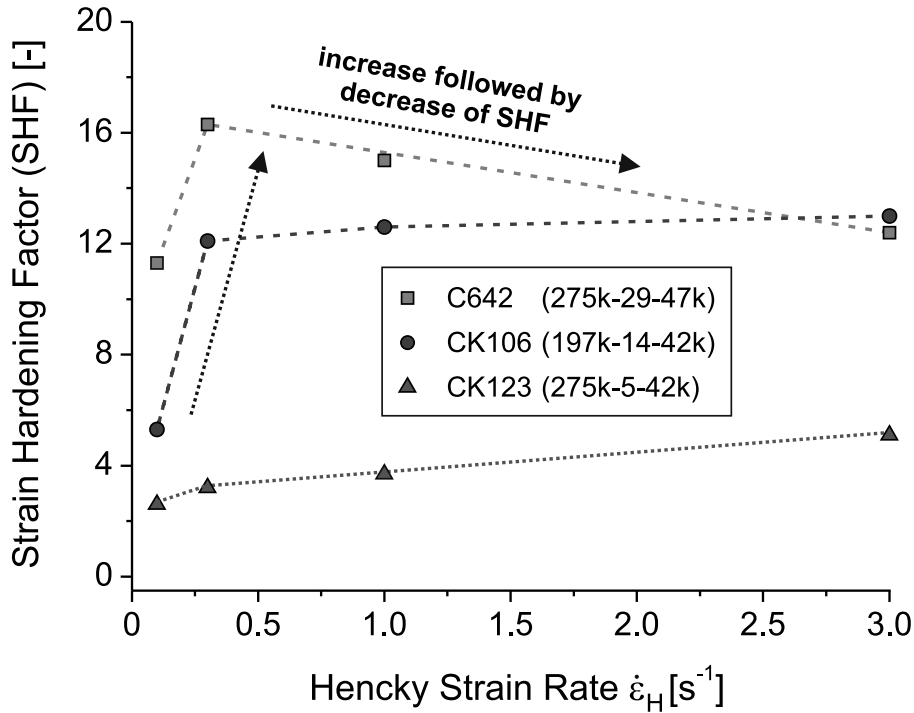
Figure 4.10: Behavior of the strain hardening factor (SHF) depending on the Hencky Strain Rate $\dot\epsilon_H$ for combs with well entangled branches. An increase of the SHF with the branching degree can be observed for $\dot\epsilon_H < 0.3$ s^{-1}. While for $\dot\epsilon_H > 0.3$ s^{-1}, the corresponding Rouse time of the backbone $\tau_{R,bb}$ is exceeded, which leads to branch relaxation. A decrease or constant value of the SHF is observed in this case (T = 180 °C).

ing decreases therefore at higher $\dot\epsilon_H$. This can also explain the occurance of a pronounced maximum of strain hardening with subsequent downturn of the transient extensional viscosity η_E^+ for high $\dot\epsilon_H$, where the extension time is closer to the backbone Rouse time $\tau_{R,bb}$ and the branch relaxation takes place. While for lower $\dot\epsilon_H$ a plateau at steady state or even no maximum is reached. A decrease of the SHF can be observed at higher Hencky strain rates presumably due to branch point withdrawal. The influences of the different relaxation processes on the SHF are reconsidered in the FT-Rheology section 5.2 using the intrinsic non-linear mastercurve. This phenomenon was already observed for pom-pom molecules measured by Nielsen et al. [Nielsen 06]. Similar maxima were reported for LDPE melts by Wagner et al. [Wagner 79] and Rasmussen [Rasmussen 05].

Wagner et al. [Wagner 08] explained the observed downturn after reaching the maximum in η_E^+ for a pom-pom molecule by the hypothesis, that after retraction of the branches into the tube of the backbone, the pom-pom behaves like a linear polymer, due to the loss of entangled branches. By the consideration of the branch point withdrawal in the MSF model the predictions corresponded well with the experimental data. The origin of the

occurrence of a maximum in η_E^+ is still under discussion. Recent findings of Burghelea et al. [Burghelea 11] give indications, that the maximum in η_E^+ is related to inhomogeneities of the deformation states and not to the rheological properties of the material.

Wagner et al. [Wagner 08] also noted that a high level of strain hardening can be achieved with a high number of branches, even if the branches are too short to be entangled. This corresponds to the findings for the comb polymers with slightly entangled branches CK128 (197k-14-15k) and CK132 (197k-29-15k), where the strain hardening increases with increasing number of branches with the same molecular weight. So it can be concluded that the introduction of a high number of slightly entangled branches can result in a higher strain hardening behavior than in the case of a low number of long-chain branching.

In the case of the combs with slightly entangled branches CK128 (197k-14-15k) and CK132 (197k-29-15k), the extension takes place in the terminal regime below the reptation time τ_d at low $\dot{\epsilon}_H < 0.3$ s^{-1}. Though it should be assumed that for $\dot{\epsilon}_H < \tau_d^{-1}$ the extension rate is too low to significantly affect the chain configuration, and the uniaxial extensional viscosity should consequently correspond to the linear viscoelastic behavior, this is not the case and strain hardening occurs.

From previous results it can be concluded that by an increase of the number of branches the amount of strain hardening increases until an upper limit for the number of branches is reached, Fig. 4.11. This is the case for the combs with well entangled branches, where
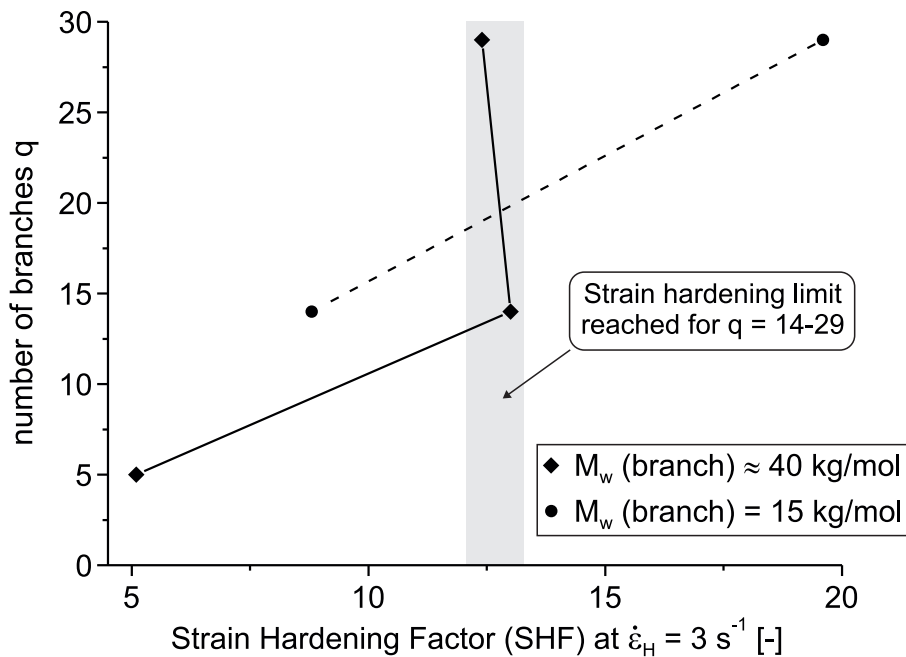
Figure 4.11: Dependence of the SHF factor

the limit of SHF is reached for a number of branches in the range from 14 to 29. For
the combs with slightly entangled branches a limit in SHF could not be observed for the
range from 14 to 29 branches. By lowering the number of branches a lower limit for
strain hardening can be reached, where strain hardening cannot be observed anymore.
The branches need to be at least slightly entangled ($\approx M_e$) to contribute to the strain
hardening, which increases with molecular weight of the branches, which corresponds to
findings of Hepperle and Münstedt [Hepperle 06].

The strain hardening behavior is caused by the restricted stretching of the backbone be-
tween the branch points connecting the branches [Inkson 99]. So it can be assumed that
for only two branches the stretching of the backbone is not effective enough to result in
strain hardening, while the molecular weight of the intersection between two branches
plays a role. In the case where the intersection molecular weight is too high, it cannot
be effectively stretched, while high molecular weight chain ends will also overlay a linear
behavior. For the two arm comb a slight emerging of strain hardening could already be
observed at high extension rates, while already with five branches a pronounced strain
hardening occurs. The number of branches, when the transition from linear to strain
hardening behavior takes place must be in the range between three and four branches.

4.3.5   Effects on the steady state extensional viscosity

Bach et al. [Bach 03] observed for the extensional measurements of two linear, well-
entangled and monodisperse polystyrene melts that for extension rates higher than the
inverse reptation time ($\dot{\epsilon}_H > \tau_d^{-1}$) the steady state extensional viscosity decreased with
the extension rate by a power-law of about -0.5. The steady state extensional viscosity,
at a given extension rate, was also proportional to the molecular weight. For extension
rates below the inverse reptation time, the steady state extensional viscosity followed the
Trouton rule $3\eta_0$.

This behavior could also be observed for the extensional viscosities of the comb structures,
Fig. 4.12. For the combs with entangled branches, the steady state extensional viscosity
is constant with the Hencky strain rate $\dot{\epsilon}_H$ and follows the Trouton rule as long as $\dot{\epsilon}_H <
\tau_d^{-1}$. When the Hencky strain rate is higher than the inverse reptation time, a decrease
of the steady state extensional viscosity with a power-law of -0.5 can be found. This
power law dependence was explained by Marrucci and Ianniruberto [Marrucci 04] by the
contribution of the interchain tube pressure effect to the classic tube theory. The decrease
of the steady state extensional viscosity η_E with $\dot{\epsilon}_H^{-1/2}$ is also valid for branched polymers.
It can be assumed, that the explanation for the decrease of the SHF is also valid for the
decrease of the steady state extensional viscosity. For extension rates below the inverse of
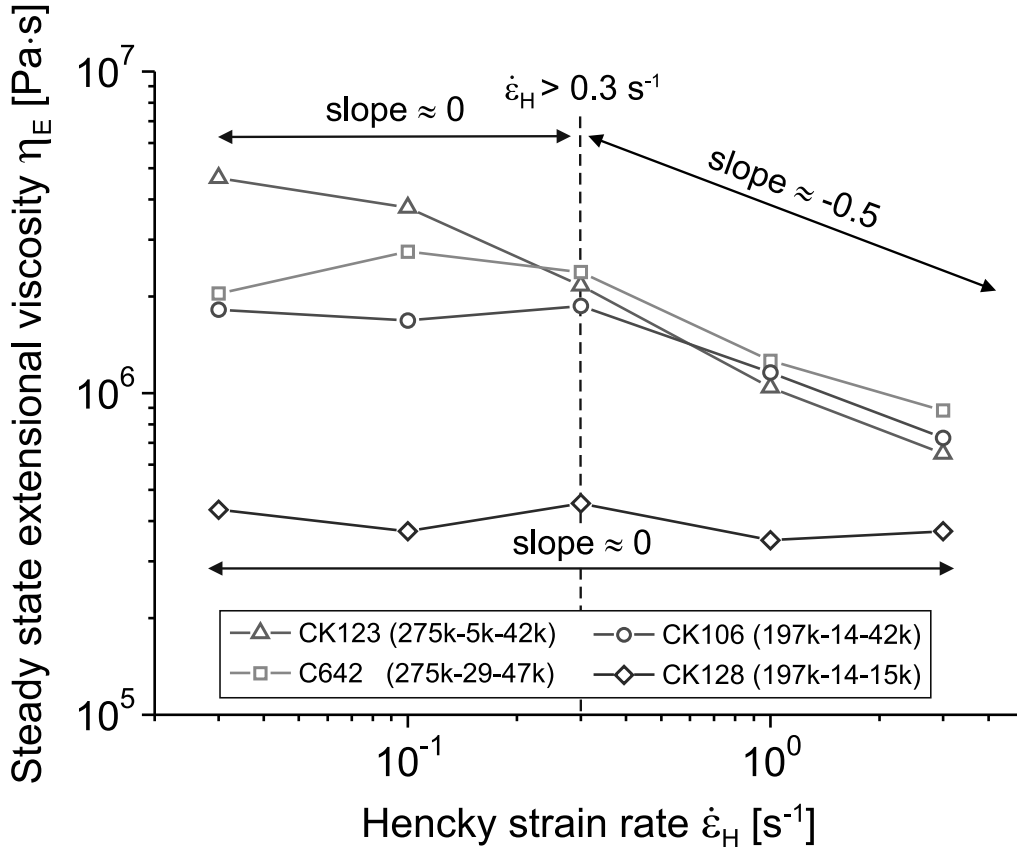
Figure 4.12: Steady state extensional viscosity as a function of the Hencky strain rate for combs with slightly (CK128) and well entangled (CK106, CK123 and C642) branches. For the combs with well entangled branches a decrease in the steady state extensional viscosity can be observed for $\dot{\epsilon}_H > 0.3 s^{-1}$. This is a result of the loss of entangled branches due to the branch relaxation, leading to the behavior of a linear polymer.

the reptation time τ_d^{-1}, the combs with similar branch molecular weight (CK123, C642, CK106, with $M_{w,br} \approx 40$ kg/mol) show a similar behavior and follow the Trouton rule. But the data for the combs overlays well for $\dot{\epsilon}_H > 0.3\ s^{-1}$ though the number of branches of the combs is very different. This can be explained by the retraction of the branches into the tube of the backbone, the combs behave consequently like a linear polymer, due to the loss of entangled branches. Since the molecular weights of the comb backbones are quite similar, it explains their overlay during the decrease. The decrease of the comb CK123 (275k-5-42k) starts already earlier than the other two combs, presumably due to the faster retraction of the branches, which is related to their low number of branches. The comb CK128 (197k-14-15k) with slightly entangled branches shows in contrast to the comb CK123 (275k-5-42k) a lower steady state extensional viscosity η_E. A decrease is not observed even for the highest Hencky strain rate.

4.4   Conclusion

From the above results it can be concluded that the number and the molecular weight of the branches have a pronounced influence on the extensional rheology of comb polymers. The strain hardening factor increases with increasing number of branches. However at a certain number of branches a maximum is reached, where the number of branches has only a low influence on strain hardening. By lowering the number of branches a lower limit for strain hardening can be reached, this is the case for a comb with only two branches, where slight strain hardening can only be observed for the highest extension rate applied. The number of branches, when the transition from no observable to extensive strain hardening takes place must be in the range between two to five branches per backbone, with two branches showing only slight, but with five branches a pronounced strain hardening occurs. Although the number of branches has an influence on the strain hardening behavior, the steady state extensional viscosity is not influenced by the number of branches. Similar values of the steady state extensional viscosity were found for combs with branching degrees varying from 5 to 29 branches.

The molecular weight of the branches needs to be at least slightly entangled to contribute to the strain hardening, which increases with molecular weight of the branches. The comb polymers with slightly entangled branches showed a linear increase of the strain hardening behavior with the extension rate, while no decrease was observed for the extension rates applied. In contrast to this, combs with well entangled branches show a decrease of strain hardening with extension rates exceeding the inverse Rouse time of the backbone due to branch relaxation. This result is important for industrial processes, where extensional flows play a major role and intense strain hardening even at high extension rates is desired. Branched polymers with a high number of slightly entangled branches could be therefore superior to polymers with a low number of long-chain branches.

Chapter 5

Shear rheology in the non-linear regime

The linear viscoelastic regime (LVE) is only valid for very small and slow deformations. In the case of large and rapid deformations, the response of the deformed polymer is non-linear. Further effects have to be incorporated into the tube model for the case of non-linear deformations. These effects are the retraction of chain segments within the tube and convective constraint release (CCR). For the investigation of the non-linear regime, large amplitude oscillatory shear (LAOS) in combination with FT-Rheology was used as a measurement technique within this work. The non-linear Q-parameter derived from a square-scaling of the non-linearity from FT-Rheology is used to create instrinsic non-linear mastercurves. The understanding of the non-linear behavior is fundamental for polymer processing, where large and rapid deformations take place.

5.1   Fundamentals

5.1.1   Relaxation processes in the non-linear regime

5.1.1.1   Retraction

When a deformation is applied, the test chain and the surrounding chains are stretched. This leads to a displacement of the entanglements and therefore to a deformation of the test chain tube, which is induced by the entanglements of the surrounding chains. The resulting tension on the test chain can be relieved via retraction within the deformed tube, Fig. 5.1. Retraction occurs in a Rouse-like motion of the test chain along the deformed tube, until the contour path occupied by the retracted chain equals the equilibrium length of the primitive path. Which equals the primitive path before the deformation. In contrast

87

to primitive path fluctuations, section 3.2.3, the retraction process does not take unlikely conformations, since the primitive path is longer than the equilibrium length. The retraction process is therefore much faster than primitive path fluctuations [Dealy 06].
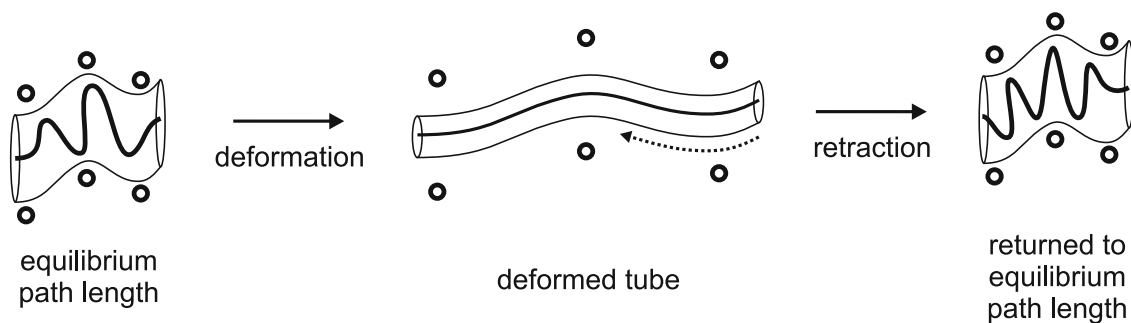
Figure 5.1: Schematic illustration of the retraction process. By the applied deformation the orignal tube, with the equilibrium path length, is deformed. By retraction of the chain, the equilibrium primitive path length is restored.

5.1.1.2   Convective Constraint Release

The surrounding chains of the test chain do also undergo retraction, which leads consequently to constraint release. Marrucci [Marrucci 96] called this process convective constraint release (CCR), due to the release of entanglements by the convection of the surrounding chains in a flow field.

5.1.2   Large Amplitude Oscillatory Shear (LAOS)

In a dynamic oscillatory shear experiment a sinusoidal deformation is applied to the polymer sample and the resulting mechanical response is measured as a function of time. For small deformations (small amplitude oscillatory shear, SAOS) a linear viscoelastic response is obtained. In case the amplitude is increased, resulting in large deformations (large amplitude oscillatory shear, LAOS), the response is non-linear [Giacomin 98].

The transition from the linear to the non-linear regime is illustrated for an oscillatory amplitude sweep experiment in Fig. 5.2. In the linear regime, the dynamic moduli (G' and G") are independent of the strain amplitude. For increasing strain amplitude, the dynamic moduli (G' and G") are decreasing. This phenomenon is called *strain thinning* and is a result of the orientation of the polymer chains along the flow field. Other effects, that can occur by the transition to the non-linear regime are strain-hardening and strain overshoot. The maximum strain amplitude, which is still within the linear regime, is in most cases determined by the transition point, just before the dynamic moduli (G' and
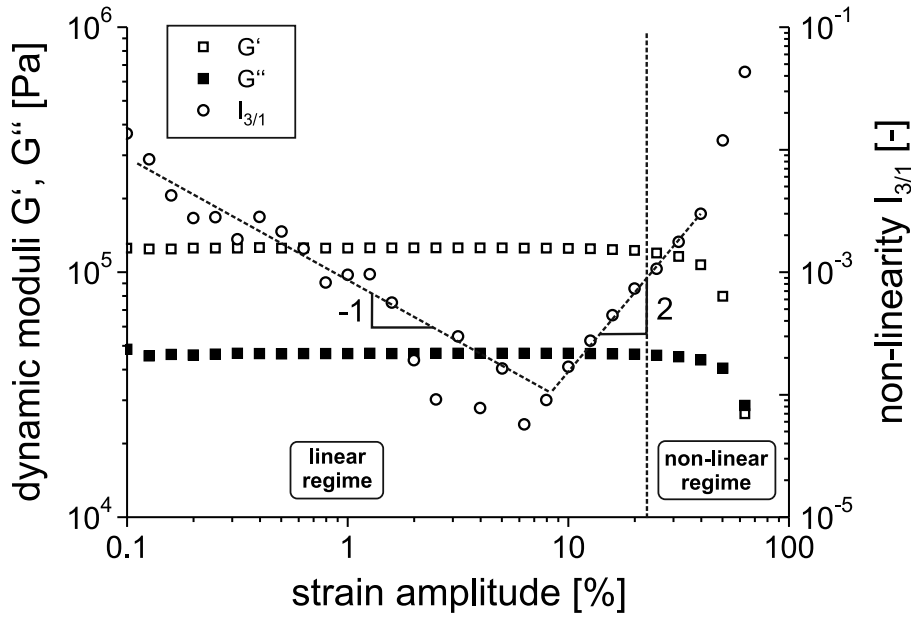
Figure 5.2: Oscillatory amplitude sweep experiment of polystyrene (M_w = 262 kg/mol, PDI = 1.18) ($\omega_1/2\pi$ = 1 Hz, γ_0 = 0.1-100 %, T = 170 °C). The transition from the linear to the non-linear regime can be determined for values of $I_{3/1}$ > 0.1%.

G") are decreasing. While already non-linear contributions appear, when the dynamic moduli (G' and G") seem to be still independent of the strain amplitude. The transition point can be better distinguished, using the non-linearity value $I_{3/1}$ from FT-Rheology, section 5.1.3. In the linear regime $I_{3/1} \propto \gamma_0^{-1}$, changing to $I_{3/1} \propto \gamma_0^2$ in the non-linear regime. The beginning of the non-linear regime can be determined for values of $I_{3/1}$ > 0.1% [Hyun 11]. In the linear regime, the dynamic moduli are independent of the strain amplitude, the mechanical (stress) response is in this case sinusoidal, Fig. 5.3a. In the non-linear regime, the dynamic moduli are a function of the strain amplitude, the resulting stress response deviates from the sinusoidal behavior, Fig. 5.3b. The distortion of the sinusoidal response becomes apparent at larger strain amplitudes, therefore non-linear dynamic experiments are referred to as large amplitude oscillatory shear (LAOS) experiments. A sinusoidal-like behavior can still be appearant in the non-linear regime, a clear differentation from the sinusoidal behavior can only be observed at large strain amplitudes. Other methods are therefore necessary to quantify the non-linear response under LAOS deformation [Hyun 11]. A highly sensitive method for the quantification of the non-linear response is FT-Rheology, which will be introduced in section 5.1.3. LAOS tests can be applied to a wide range of complex fluids and materials. The major advantage is the independent variation of the strain amplitude and frequency allowing a broad spectrum of conditions to be attained.
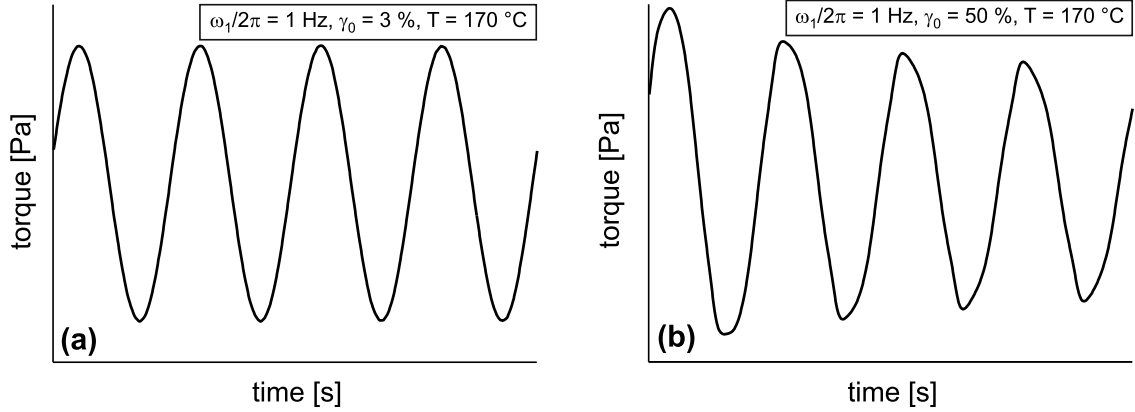
Figure 5.3: Stress response of polystyrene (M_w = 262 kg/mol, PDI = 1.18) measured by a time sweep experiment (a) in the linear regime, the stress response is sinusoidal ($\omega_1/2\pi$ = 1 Hz, γ_0 = 3 %, T = 170 °C), (b) in the non-linear regime, the sinusoidal stress response is distorted ($\omega_1/2\pi$ = 1 Hz, γ_0 = 50 %, T = 170 °C).

5.1.3 Fourier-Transformation Rheology (FT-Rheology)

For the analysis of the non-linear stress signal, obtained in a LAOS experiment, the concept of Fourier-Transformation [Butz 06] can be applied. Thereby a magnitude and phase spetrum, with higher harmonics with respect to the excitation frequency ω_1 are obtained. The underlying principles have already been used for rheological measurements [Krieger 73], but due to technical issues and experimental limitations, the application of this concept was not successful. The high sensitivity Fourier Transformation Rheology (FT-Rheology) concept was developed by Wilhelm [Wilhelm 98, Wilhelm 02] to circumvent those issues and to establish this concept to the analysis of non-linear rheological data.

In the following, the aspects of FT-Rheology are introduced using the example of dynamic oscillatory shear. In the case of a sinusoidal excitation with frequency $\omega_1/2\pi$, which is applied to a system with mass m, viscosity η and elastic modulus G, the force balance is described by a differential equation of the following type:

$$m\ddot{\gamma} + \eta\dot{\gamma} + G\gamma = A_0 \exp(i\omega_1 t). \tag{5.1}$$

The solution of this equation for the deformation γ, at constant η and G is given by a single harmonic function:

$$\gamma(t) = \gamma_0 \exp(i(\omega_1 t + \delta)) \tag{5.2}$$

with the excitation frequency $\omega_1/2\pi$ and the characteristic phase shift δ. In the case of a Newtonian fluid, the viscosity is independent of time and shear rate. In contrast, the viscosity of non-Newtonian fluids shows a shear rate and time dependence, $\eta = \eta(\dot{\gamma}, t)$,

in the non-linear regime. For steady shear under periodic conditions, the viscosity is only a function of the shear rate and independent of the shear direction, $\eta = \eta(\dot{\gamma}) = \eta(-\dot{\gamma})$. As a result, the viscosity can be approximated via a Taylor expansion with respect to the shear rate:

$$\eta(\dot{\gamma}) = \eta_0 + a \cdot \dot{\gamma}^2 + b \cdot \dot{\gamma}^4 + \dots \tag{5.3}$$

η_0, a and b are complex. For the case of oscillatory shear, the deformation γ is given by:

$$\gamma = \gamma_0 \cdot e^{i\omega_1 t} \tag{5.4}$$

and the shear rate respectively by:

$$\dot{\gamma} = i\omega_1\gamma_0 \cdot e^{i\omega_1 t} \tag{5.5}$$

By the introduction of Eqs. (5.3) and (5.5) into Newton's law Eq. 3.8, the shear stress is given by:

$$
\begin{aligned}
\sigma &= (\eta_0 + a\, i^2\omega_1^2\gamma_0^2 e^{i2\omega_1 t} + b\, i^4\omega_1^4\gamma_0^4 e^{i4\omega_1 t} + \dots)i\omega_1\gamma_0 e^{i\omega_1 t} \\
&= \underbrace{\eta_0 \cdot i\omega_1\gamma_0 e^{i\omega_1 t}}_{I_1} + \underbrace{a \cdot i^3\omega_1^3\gamma_0^3 e^{i3\omega_1 t}}_{I_3} + \underbrace{b \cdot i^5\omega_1^5\gamma_0^5 e^{i5\omega_1 t}}_{I_5} + \dots
\end{aligned}
\tag{5.6}
$$

with $I_1 \propto \gamma_0^1\omega_1^1$, $I_3 \propto \gamma_0^3\omega_1^3$, $I_5 \propto \gamma_0^5\omega_1^5$, etc..

By the Fourier transformation of a stress response signal, a frequency spectrum with the first harmonic as the excitation frequency ($\omega_1/2\pi$) and additionally for the case of a non-linear response further odd harmonics are obtained, Fig. 5.4.

The non-linearity can be quantified using the ratio $I_{n/1} = I(n\omega_1)/I_{\omega_1}$, with $I_n = I(n\omega_1)$ as the magnitude of the nth harmonic and $I_1 = I(\omega_1)$ as the fundamental frequency. The major advantage of the relative intensity $I_{n/1}$ over the absolute value of I$_n$ is the high reproducibility, thus errors originating from experimental variations can be compensated using normalization.

In the linear regime the I$_3$ value consists of a constant noise level, so that only the I$_1$ magnitude is obtained. This results then in $I_{3/1} \propto \gamma_0^{-1}$, which is indicated by the slope of -1 for the non-linearity in Fig. 5.2. As soon as the non-linear regime is reached, the I$_3$ magnitude is above the noise level, leading to $I_{3/1} = I_3/I_1 \propto \gamma_0^2$ (with $I_3 \propto \gamma_0^3$ and $I_1 \propto \gamma_0$), which results in a slope of 2 for the non-linearity.

5.1.4 Q-parameter

Large Amplitude Oscillatory Shear (LAOS) [Hyun 11] was applied for the measurements in the non-linear regime, the strain amplitude (γ_0) and the frequency ($\omega_1/2\pi$)
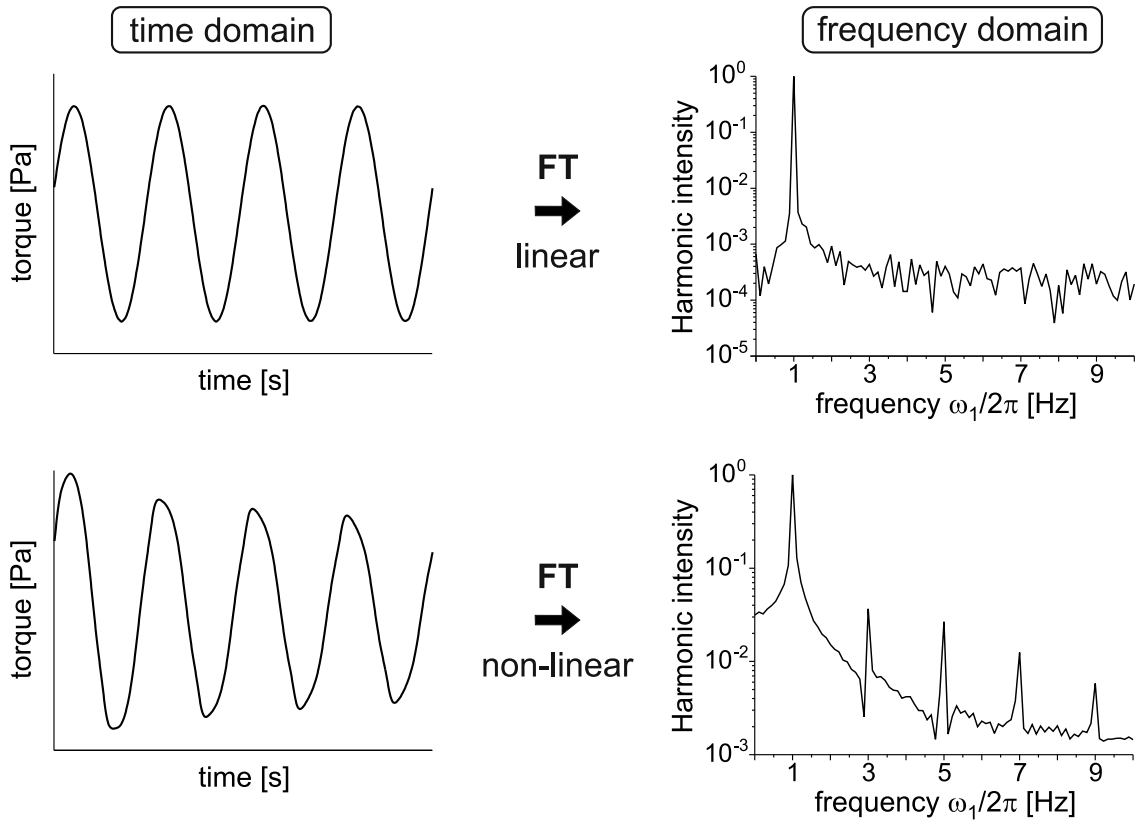
Figure 5.4: Fourier transformation of (a) a sinusoidal stress signal obtained in the linear regime, resulting in only one signal in the frequency spectrum, which corresponds to the excitation frequency (PS, M_w = 262 kg/mol, PDI = 1.18, $\omega_1/2\pi$ = 1 Hz, γ_0 = 3 %, T = 170 °C), (b) of a distorted sinusoidal stress signal obtained in the non-linear regime, resulting in the corresponding excitation frequency signal and further odd harmonics (PS, M_w = 262 kg/mol, PDI = 1.18, $\omega_1/2\pi$ = 1 Hz, γ_0 = 50 %, T = 170 °C).

were varied independently. The results from the LAOS measurements were analyzed using FT-Rheology [Wilhelm 02], in which the relative intensity of the third harmonic $I_{3/1} = I(3\omega_1)/I(\omega_1)$ (with $\omega_1/2\pi$ being the excitation frequency) was used to quantify the non-linearity.

In the non-linear regime $I_{3/1}$ increases with increasing strain amplitude. In the region of small to medium strain amplitudes, $I_{3/1}$ shows a quadratic scaling relationship as a function of strain amplitude, which is also called the region of medium amplitude oscillatory shear (MAOS) [Hyun 09].

$$I_3/I_1 \equiv I_{3/1} \propto \gamma_0^2 \tag{5.7}$$

$I_{3/1}$ was investigated as a function of strain amplitude γ_0 at different frequencies (from 0.5 to 20 rad/s). In Fig. 5.5a the dependency of the non-linearity $I_{3/1}$ on the strain amplitude is illustrated. In the MAOS region $I_{3/1}$ follows the quadratic strain dependence,

while at higher strain amplitudes the slope is reduced and $I_{3/1}$ turns into a plateau. The quadratic dependency is valid for various frequencies in the MAOS regime, as shown in Fig. 5.5b, where the non-linearity $I_{3/1}$ was measured for the PS comb CK106 (197k-14-42k) at various frequencies (from 0.5 to 5 rad/s). The quadratic strain dependence can be concluded to the non-linear coefficient Q, which is defined as

$$Q = I_{3/1}/\gamma_0^2. \tag{5.8}$$

At low strain amplitudes a constant non-linear zero strain value Q_0 can be achieved, which is also called the intrinsic non-linearity [Hyun 09].

$$\lim_{\gamma_0 \to 0} Q \equiv Q_0 \tag{5.9}$$

The intrinsic non-linearity Q_0 is frequency and temperature dependent, so that time-temperature superposition (TTS), with the shifting factors obtained from the linear mastercurve, can be applied to generate a new intrinsic non-linear mastercurve Fig. 5.6.
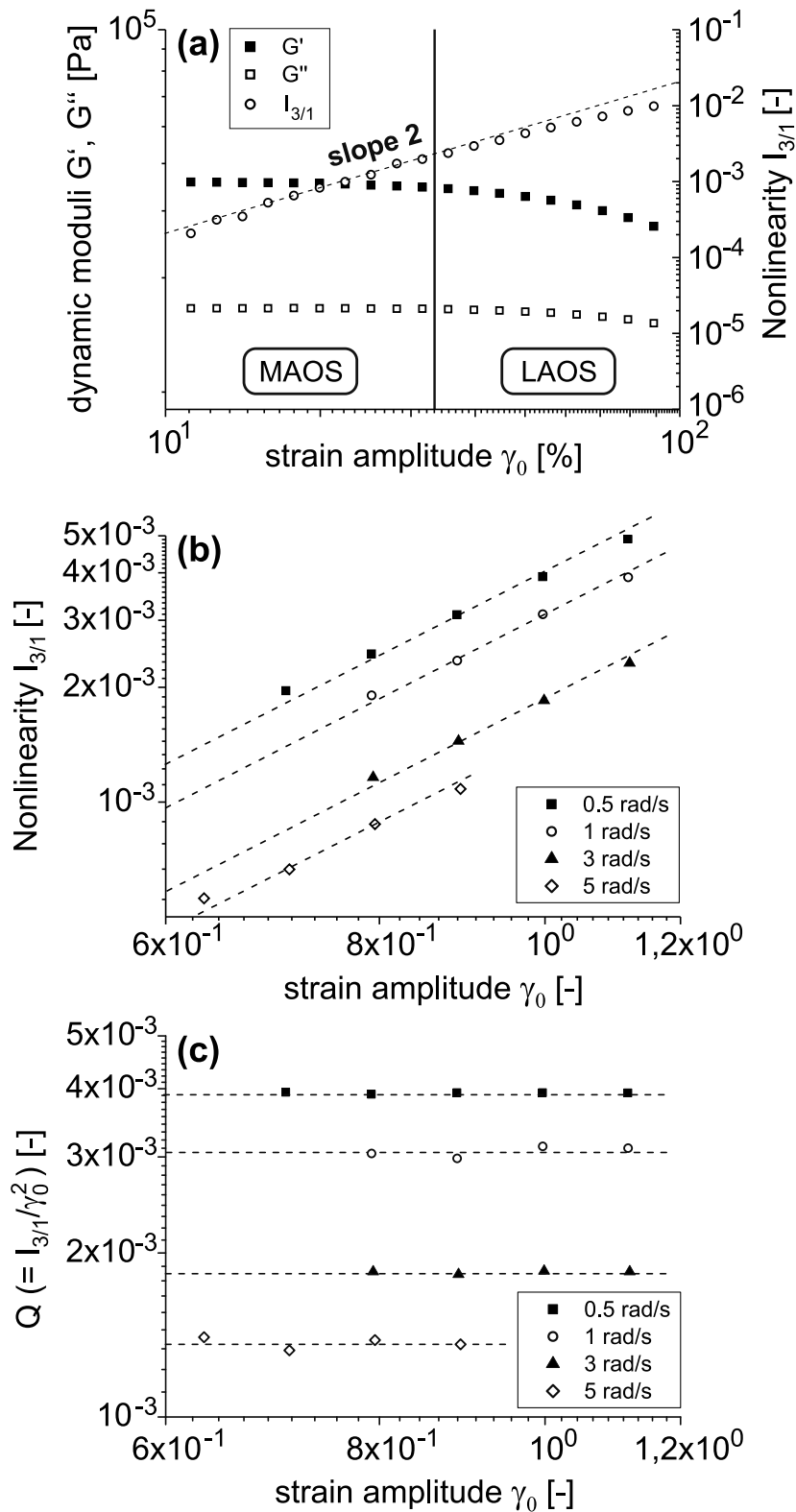
Figure 5.5: Non-linearity $I_{3/1}$ and Q-parameter as a function of the strain amplitude for a PpMS comb CK106 (197k-14-42k) at T = 190 °C): (a) strain dependence in the MAOS and LAOS region, quadratic dependence $I_{3/1} \propto \gamma_0^2$ only fulfilled in the MAOS region; (b) quadratic strain amplitude dependence at various frequencies from 0.5 to 5 rad/s; (c) Q-parameter ($Q = I_{3/1}/\gamma_0^2$) obtained from the non-linearity data.

5.2 Non-linear mastercurves of comb polymers

The generated intrinsic non-linear mastercurves show in contrast to linear mastercurves two maxima and one minimum. The two maxima refer to the backbone relaxation ($Q_{max,bb}$) and the branch relaxation ($Q_{max,br}$) respectively. The minimum corresponds to the transition region between the backbone and branch relaxation.

The instrinsic non-linear mastercurves of combs with unentangled branches or linear polymers show only one maximum $Q_{max,bb}$, due to the backbone relaxation. When the molecular weight of the branches exceeds the entanglement molecular weight, a second maximum $Q_{max,br}$ appears at higher frequencies, Fig. 5.6. With increasing molecular weight of the branches, $Q_{max,bb}$ decreases, as it is shown in Fig. 5.6, where CK106 (197k-14-42k) and C642 (275k-29-47k) have the same absolute $Q_{max,bb}$ value and C632 (275k-25-26k) with a lower branch molecular weight, a higher absolute value of $Q_{max,bb}$ is observed. But although the comb CK123 (275k-5-42k), Fig. 5.7, has the same molecular weight of the branches, the absolute value of $Q_{max,bb}$ is about one decade higher than measured for CK106 (197k-14-42k) or C642 (275k-29-47k). The absolute value of $Q_{max,bb}$ gives an indication for the molecular weight of the branches. It seems to be also dependent on the
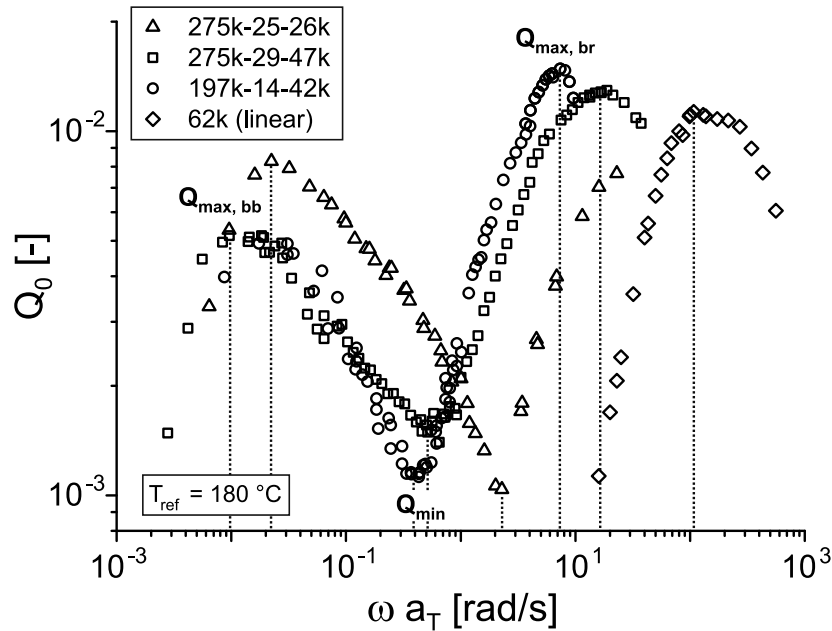
Figure 5.6: The intrinsic non-linearity Q_0 of the combs C642 (275k-29-47k), C632 (275k-25-26k) and CK106 (197k-14-42k) with entangled branches and a linear polymer (62k). The combs show two maxima $Q_{max,bb}$ and $Q_{max,br}$, due to backbone and branch relaxation respectively, while the linear polymer shows only one maximum due to the backbone relaxation. For increasing molecular weight of the branches, $Q_{max,bb}$ is decreasing and shifted to lower frequencies ($T_{ref} = 180\ °C$).
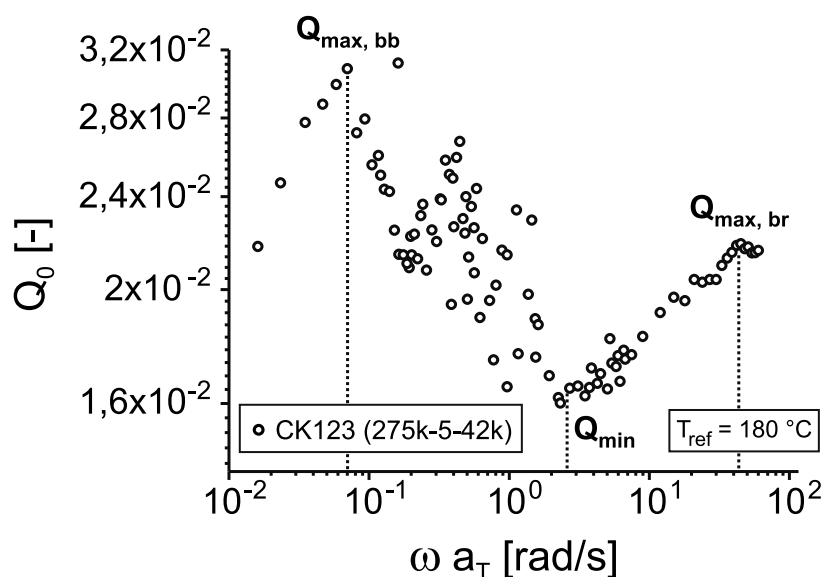
Figure 5.7: The intrinsic non-linearity Q_0 of a comb with a low number of branches CK123 (275k-5-42k, 5 branches). The ratio between the maxima and the minimum is decreasing significantly, which is a result of the reduced backbone chain stretch and reduced dilution of the backbone ($T_{ref} = 180\ °C$).

number of branches, since the value changes significantly, when the amount of branches is lowered (from 14 to 5). Combs with a low amount of branches seem to behave like linear polymers, as the example of the comb CK123 (275k-5-42k), with five branches, Fig. 5.7. Only a slight minimum can be observed, in contrast to the well pronounced minimum for higher number of branches. This can also be seen by the small differences between the maxima and the minimum in Fig. 5.7, resulting in a scattered curve.

To investigate the influences of the molecular structure on Q_0, only the maxima and minima values are used for further correlations. A difference of the ratio between $Q_{max,br}$ and Q_{min} can be observed in Fig. 5.8 for the three different combs. In case the number of branches is tripled, when comparing CK123 (275k-5-42k) and CK106 (197k-14-42k), the ratio $RQ_{12} = Q_{max,br}/Q_{min}$ is doubled (RQ_{12}(CK123) = 1.9 and RQ_{12}(CK106) = 4.4). For the comb C632 (275k-25-26k) the ratio RQ_{12} differs by a factor of 4 when compared to CK123 (275k-5-42k) and by a factor of 2 compared to CK106 (197k-14-42k). A linear dependency of the number of branches on the ratio RQ_{12} can be found, which is shown in 5.8. It can be concluded, that the smaller the number of branches, the smaller is the difference in the absolute values of $Q_{max,bb}$ and Q_{min}. This is due to the reduced backbone chain stretch and reduced dilution of the backbone in combs with low amount of branches. The value for the comb C642 (275k-29-47k) deviates from the linear behavior, since the Q_{min} cannot be exactly evaluated, due to the scattered data
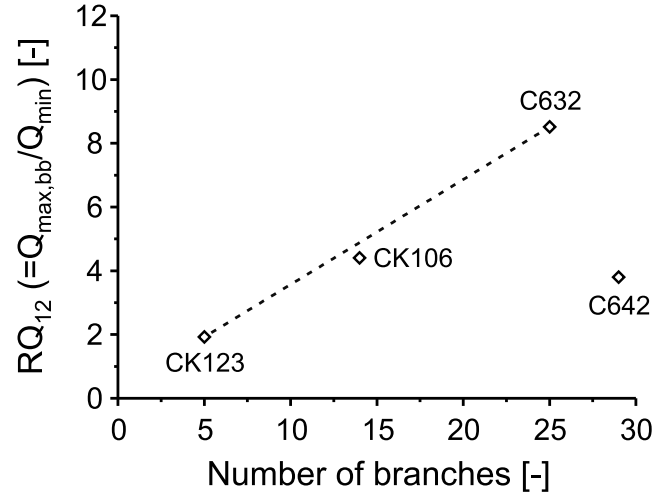
Figure 5.8: Dependencies derived from the comparison of the minima/maxima of the instrinsic non-linear mastercurves of the combs CK106 (197k-14-42k), CK123 (275k-5-42k), C632 (275k-25-26k) and C642 (275k-29-47k). The ratio between the maximum $Q_{max,bb}$ and the minimum Q_{min} shows a linear correlation with the number of branches.

around the minimum. For the combs C642 (275k-29-47k) and CK106 (197k-14-42k) with similar molecular weight of the branches ($M_{w,br}$ = 42-47 kg/mol) Q_{min} is in the same frequency region Fig. 5.6, while for C632 with a lower branch molecular weight ($M_{w,br}$ = 26 kg/mol) Q_{min} is shifted to higher frequencies.

A major advantage of the instrinsic non-linear mastercurve is the direct access to relaxation times and processes, which cannot be obtained directly from the linear mastercurve. In Fig. 5.9 the linear (Fig. 5.9a) and the non-linear (Fig. 5.9b) mastercurve of CK106 (197k-14-42k), (T_{ref} = 180 °C) are compared with each other. The maxima and minima of the instrinsic non-linear mastercurve correspond to observable transitions in the linear mastercurve. The first maximum at low angular frequencies (A) corresponds to the reptation time τ_d, which is in agreement with the findings of Pom-Pom model simulations, where a maximum at the reptation frequency $1/\tau_d$ was found, section 6.2.3. This is important for an accurate determination of the reptation time for polymers with complex architecture or high polydispersity, where the reptation frequency does not correspond to the crossover point of G' and G". Using the instrinsic non-linear mastercurve, the reptation time can be therefore evaluated for more complex architectures (e.g. for LDPE). The minimum (B) corresponds to the Rouse time of the backbone $\tau_{R,bb}$ and is good agreement with the minimum of tan δ for the determination of the plateau modulus G_N^0. The second maximum (C) is assumed to correspond with the branch relaxation time τ_{br} and indicates the transition zone between the branch and backbone relaxation process. It is likely, that also a second minimum exists, which corresponds to the branch relaxation
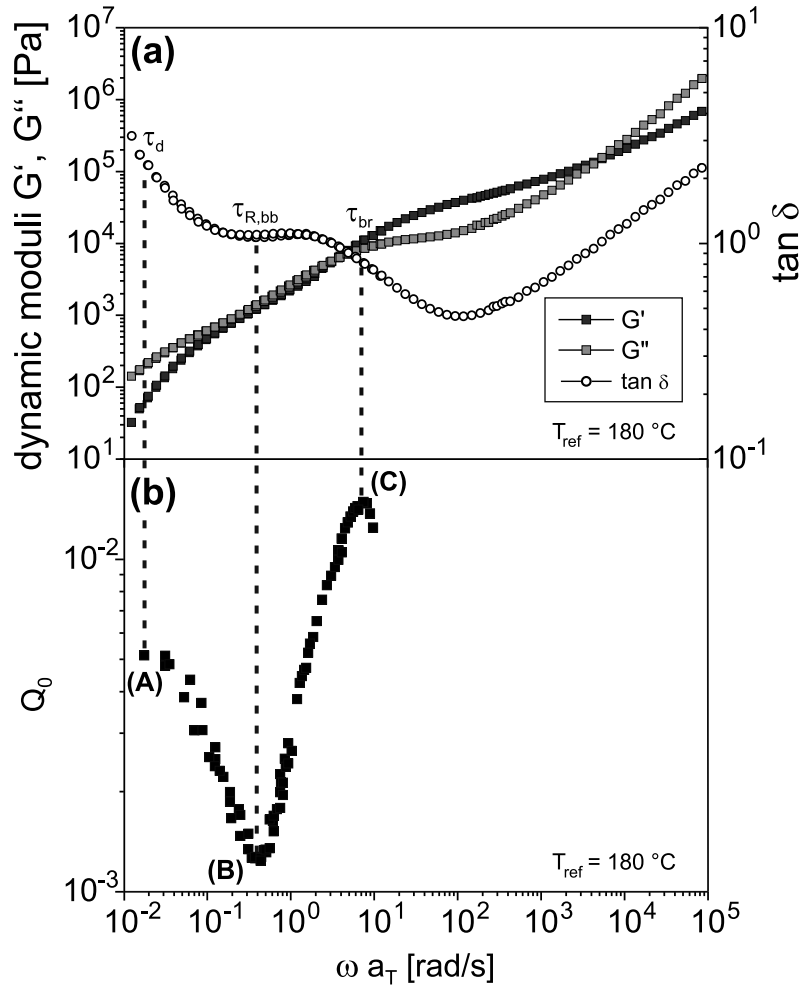
Figure 5.9: Comparison between the linear (a) and the non-linear (b) mastercurve of CK106 (197k-14-42k), (T_{ref} = 180 °C). The maxima and minima of the non-linear mastervurve correspond to relaxation processes known from the linear mastercurve, whose relaxation times can be directly extracted from the experiment. (A) reptation time τ_d, (B) backbone Rouse time $\tau_{R,bb}$ and plateau modulus $G_{N,bb}^0$, (C) branch relaxation time τ_{br}.

process. The experimental access to this minimum is difficult so far. The combination of low temperatures, which are necessary to access this frequency region and the excitation at large strain amplitudes leads to high emerging torques, exceeding the maximum limit of the transducer. Further improvement of the measurement technique is necessary to access this frequency range. As earlier mentioned in the extensional viscosity section, the instrinsic non-linear mastercurve can be used to explain the extensional behavior of branched polymers, Fig. 5.10. In case the Hencky strain rate $\dot{\epsilon}_H$ exceeds the reptation time τ_d, which is indicated by the first maximum (A) of the instrinsic non-linear mastercurve, strain hardening can be observed. Hencky strain rates $\dot{\epsilon}_H$ lower than the reptation

Table 5.1: Comb relaxation times

sample	$\tau_{d,\ exp.}$ [a] [s]	$\tau_{d,\ theory}$ [b] [s]	$\tau_{R,bb,\ exp.}$ [a] [s]	τ_{br} [a] [s]
62k	0.0093	0.004[b] 0.0093[c]	-	-
197-14-42k	50.76	1.231	2.690	0.135
275k-5-42k	14.29	11.44	0.445	0.022
275k-25-26k	44.64	-	0.436	-
275k-29-47k	93.46	0.853	2.139	0.053

[a]: Determined by the minima and maxima of the instrinsic non-linear mastercurve at 180 °C

[b]: Determined using $\eta_0 = \tau_d \cdot G_N^0$, see section B.3 for details.

[c]: Determined using the Likhtman-McLeish model [Likhtman 02]

time τ_d, will result in a linear behavior. For $\dot{\epsilon}_H$ lower than the Rouse time of the backbone $\tau_{R,bb}$, ($\dot{\epsilon}_H < \tau_R$), corresponding to the minimum (B), a plateau for the combs with higher amount of branches (q > 14, combs CK106 and C642) at the maximum is reached. For higher Hencky strain rates, which are exceeding the Rouse time $\tau_{R,bb}$, the transient extensional viscosity will decrease instead, after reaching a maximum in strain hardening. This is indicated by a downturn of the transient extensional viscosity after reaching a maximum.

The slope of the line between the maximum (A) and the minimum (B) gives an indication of the rate of the relaxation process, Fig. 5.10a. The slope of the comb C642 (275k-29-47k) is higher than for the comb CK106 (197k-14-42k), so the relaxation process should proceed faster for C642 (275k-29-47k). This can be observed in the trend of the strain hardening factor in Fig. 4.10, while for CK106 (197k-14-42k) the SHF is almost constant, it decreases in the case of C642 (275k-29-47k) for $\dot{\epsilon}_H > 0.3$ s^{-1}. Furthermore this effect can be observed on the difference of the strain hardening maximum Fig. 5.10b. For CK106 (197k-14-42k) at steady state a plateau for $\dot{\epsilon}_H \leq 0.3$ s^{-1} and a maximum with subsequent decrease in η_E^+ at higher Hencky strain rate ($\dot{\epsilon}_H > 0.3$ s^{-1}) is observed. While for C642 (275k-29-47k) the maximum with subsequent decrease in η_E^+ already occurs at $\dot{\epsilon}_H = 0.3$ s^{-1}, as expected from the SHF-factor decrease determined in Fig. 4.10. Due to the faster relaxation process of C642 (275k-29-47k) in contrast to CK106 (197k-14-42k) the maximum with subsequent decrease comes earlier into the picture.

In the extensional rheology section, it was already mentioned that the extensional data

of the two combs CK106 (197k-14-42k) and C642 (275k-29-47k) are almost similar. This can also be observed by the comparison with the instrinsic non-linear mastercurve. The overlay of the extensional measurements as well as the instrinsic non-linear mastercurve of CK106 (197k-14-42k) and C642 (275k-29-47k) are illustrated in Fig. 5.10. Though the two combs are different, according to the number of branches (a factor of two difference), they show the same effect in two different non-linear measurement techniques. On one hand this gives proove to the assumption, that for a certain number of branches, the backbone stretching reaches a maximum and therefore the amount of possible strain hardening is limited. In this case the optimal number of branches would be in the range of 10 to 30 (approx. 1 mol-%) for a backbone molecular weight of 200-300 kg/mol. On the other hand it shows the comparability between the different non-linear measurement techniques and the possibility of the instrinsic non-linear mastercurve to give a better physical understanding of the processes taking place in the non-linear regime.

The different relaxation times obtained from the intrinsic non-linear mastercurve are listed in table 5.1. The theoretical reptation time $\tau_{d,theory}$ was obtained using:

$$\eta_0 = \tau_d \cdot G_N^0 \tag{5.10}$$

for the case of the combs, the zero shear viscosity η_0 and the plateau modulus G_N^0 were determined using the data of the linear mastercurves. The theoretical reptation time $\tau_{d,theory}$ for the linear polymer was also determined using the Likhtman-McLeish model [Likhtman 02]. Since the Eq. 5.10 is based on the Doi-Edwards theory, the theoretically calculated values are only valid for the case of linear polymers and do therefore not correspond with the experimental values determined from the intrinsic non-linear mastercurves. Only in the case of CK123 with a low branching degree of only 5 branches, the experimental and theoretical values are comparable. However for the linear polymer, the reptation time calculated using the Likhtman-McLeish model is identical with the value obtained from the intrinsic non-linear mastercurve. The value determined by Eq. 5.10 differs by a factor of about 2, which is still comparable with the experimental value. The huge difference between the experimental and the theoretical values of the comb polymers is a result of the restriction of the theoretical approach to linear polymers. The comparability of the theoretical and experimental values of the linear polymer gives besides the pom-pom prediction another proove for the accurate determination of the reptation time using the intrinsic non-linear mastercurve. Relaxation times can be thereby obtained for complex architectures, which are not accessible using linear measurements or models.
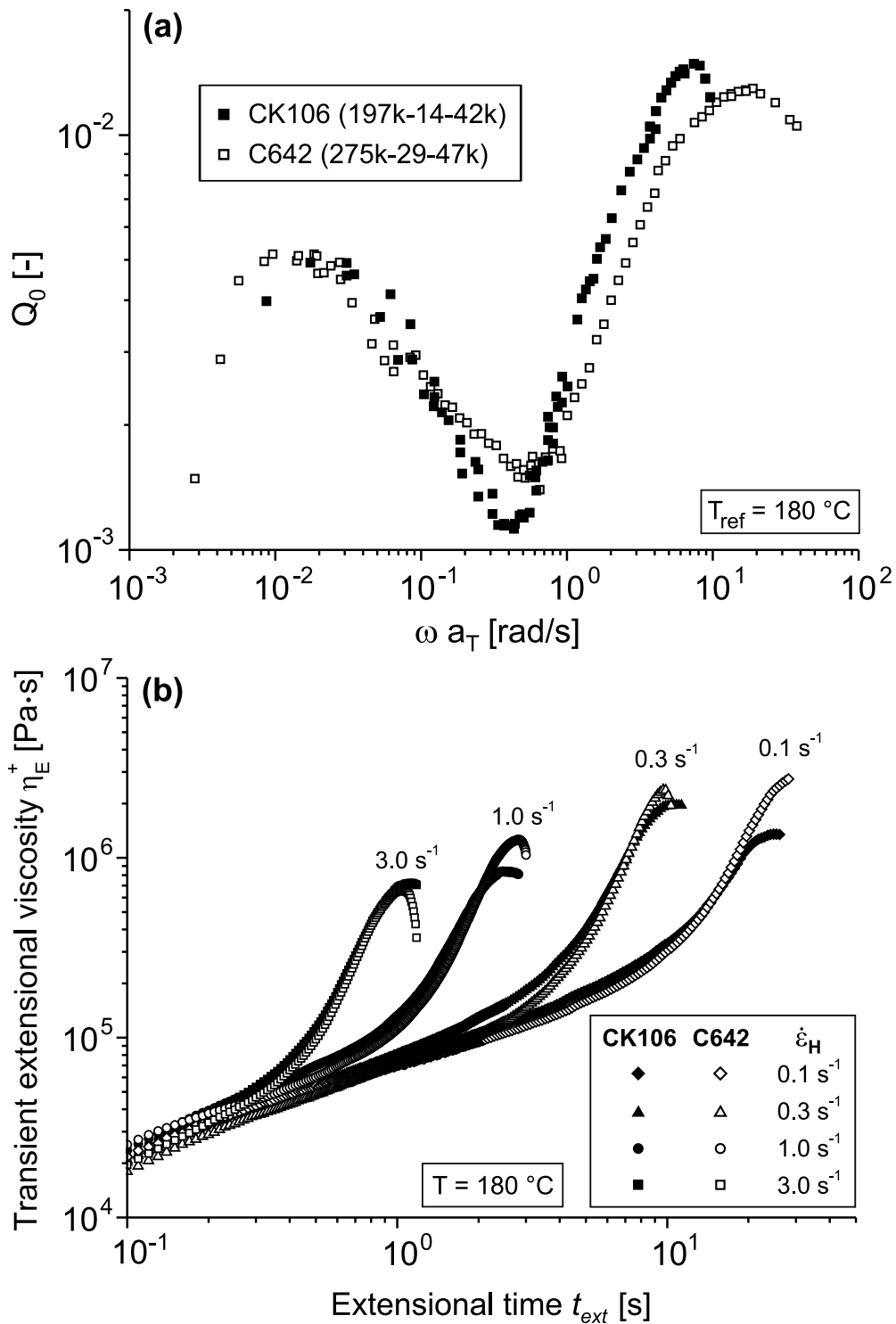
Figure 5.10: Comparison of two combs with different number of branches, CK106 (197k-14-42k) and C642 (275k-29-47k), measured with two different non-linear rheological techniques. (a) Intrinsic non-linear mastercurve obtained using the non-linear parameter Q_0 in combination with FT-Rheology and (b) transient extensional viscosity curves obtained by uniaxial extensional rheology. The two combs show in each case similar behavior, giving an indication for a limiting number of branches.

5.3   Conclusion

Using the non-linear parameter Q_0, obtained via a square scaling law from FT-Rheology an intrinsic non-linear mastercurve could be created and correlated with the relaxation processes of the linear mastercurve. From the instrinsic non-linear mastercurve different relaxation times (reptation time and Rouse time of the backbone and branches) can be directly extracted from the corresponding maxima and minima. The experimental access-ability to relaxation times opens up the possibility for a better physical understanding of the underlying relaxation processes and for the improvement of linear and non-linear modeling.

Chapter 6

Modeling and Simulations

Modeling and simulations have a high significance in polymer rheology, since rheological properties can be predicted, which is especially important for polymer processing. Furthermore rheological data of polymers, where a certain structure is not available, can be predicted and compared with experimental data to elucidate structural effects. In this chapter two different non-linear models, the molecular stress function (MSF) model and the Pom-Pom model are used. The MSF model was applied to the experimental data of the extensional rheology measurements to examine the applicability of the model for those systems. To validate the comparability of the synthesized model comb systems with commercial branched polymers, the parameters obtained for both systems were compared with each other. The Pom-Pom model was used to predict the strain hardening behavior as well as the non-linear mastercurves depending on the number and molecular weight of the branches. The predictions were performed by M.Eng. Deepak Ahirwal using home-written Matlab programs and the IRIS [Winter 08] software.

6.1   Molecular Stress Function (MSF) Model

6.1.1   Fundamentals

The molecular stress function (MSF) model can be used to describe quantitatively the non-linear rheology of branched polymers in uniaxial extension. Using this approach steady state and transient extensional viscosities can be modeled and the molecular structure be correlated to the energy parameter f_{max}^2. The MSF model, developed by Wagner et al. [Wagner 92, Wagner 03, Wagner 04] is a single tube segment model. The tube diameter a is assumed to be independent of the orientation of the tube segment and decreases from its equilibrium value a_0 to a value $a(t)$ with increasing uniaxial deformation, Fig. 6.1.
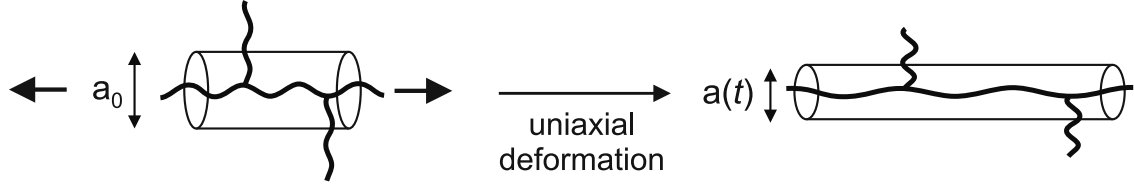
Figure 6.1: Influence of uniaxial deformation on the tube diameter a.

The extra stress tensor of the MSF model is given by:

$$\bar{\bar{\sigma}}(t) = \int\limits_{-\infty}^{t} m(t - t') f^2 \bar{\bar{S}}_{DE}^{IA}(t, t') dt' \tag{6.1}$$

with $m(t - t')$ as the linear-viscoelastic memory function, which is described by the sum of the discrete relaxation modes.

$$m(t - t') = \sum_{i=1}^{N} \left(\frac{G_i}{\tau_i} \right) \exp(-t - t')/\tau_i \tag{6.2}$$

G_i and τ_i can be calculated from oscillatory shear data. The strain measure $\bar{\bar{S}}_{DE}^{IA}$ represents the affine rotation of the tube segments originated from the assumption of independent allignment (IA), which was proposed by Doi and Edwards (DE) [Doi 78].

$$\bar{\bar{S}}_{DE}^{IA}(t, t') = 5 \left(\frac{\bar{u}'\bar{u}'}{u'^2} \right) = 5\bar{\bar{S}}(t, t') \tag{6.3}$$

with $\bar{\bar{S}} = \bar{\bar{S}}(t, t')$ as the relative second-order orientation tensor and $\bar{u}'\bar{u}'$ as the dyad of the deformed unit vector $\bar{u}' = \bar{u}'(t, t')$. The parameter f_{max}^2 is related to the maximum strain energy which can be stored in a polymeric system and determines the steady state value of the viscosity in extensional flow [Wagner 05]. By the addition of the interchain pressure term [Marrucci 04] an evolution equation for constant extension rate in uniaxial extensional flow is obtained:

$$\frac{\partial f^2}{\partial t} = \dot{\epsilon}_H \cdot \frac{\beta f^2}{1 + \frac{\beta - 1}{f^4}} \left(S_{11} - S_{33} - \frac{f(f^3 - 1)}{f_{max}(f_{max}^3 - 1)} \sqrt{S_{11} + \frac{1}{2}} \right) \tag{6.4}$$

with the Hencky strain rate $\dot{\epsilon}_H$ in the deformation direction as well as the components S_{11} and S_{33} of the orientation tensor $\bar{\bar{S}}$ in the parallel and perpendicular stretch direction. The parameter β reflects the backbone and branch entanglements and is therefore defined by the topology of the polymer, Eq. 6.5.

$$\beta = 1 + \frac{q \cdot M_{w,br}}{M_{w,bb}} \tag{6.5}$$

A value of $\beta = 1$ represents the case of a linear chain and $\beta > 1$ is related to the additional contribution of branch entanglements. It determines the slope of the elongational viscosity after the inception of strain hardening and is equivalent to the ratio of the molar mass of the branched polymer to the molar mass of the backbone [Wagner 03, Wagner 04].

6.1.2 MSF model applied to model combs

The values of β in table 6.1 were determined for the comb systems using Eq. 6.5. For the numerical solution of the Eqs. (6.1) and (6.4) a home-written Matlab program was applied to fit the parameter f_{max}^2 to the transient extensional viscosity η_E^+ data.

Table 6.1: Parameters of the MSF model.

sample #	sample name	β	f_{max}^2
CK106	197k-14-42k	2.5	32.5
CK123	275k-5-42k	2.1	7.84
CK128	197k-14-15k	2.1	14.4
CK132	197k-29-15k	2.5	42.3
C642	275k-29-47k	2.8	38.4

Good agreement was found between the experimental data and the model predictions for the transient extensional viscosity behavior, also a sharp transition from the transient to the steady state could be observed, Figs. 6.2 and 6.3. But since branch point withdrawal [Wagner 08] was not considered only a plateau can be evaluated at steady state, a possible downturn is not taken into account.

In Fig. 6.2 the MSF model prediction was applied to a series of comb polymers with different number of branches, but similar molecular weight of the backbones and the branches. For the combs with higher number of branches CK106 (197k-14-42k) and C642 (275k-29-47k) the prediction corresponds well with the transient extensional viscosity, also the steady state extensional viscosity could be well predicted. For the comb with lower amount of branches CK123 (275k-5-42k), the predicted transient extensional viscosity is conform with the experimental data. But since the steady state extensional viscosity is getting lower with decreasing extension rate, the f_{max}^2 value does not show good correspondence with the experimental maximum.

For comb polymers with high number of branches, but only slightly entangled branches (CK128 and CK132), Fig. 6.3, the predicted transient extensional viscosity corresponds well only for higher extension rates. In contrast to the combs with well-entangled
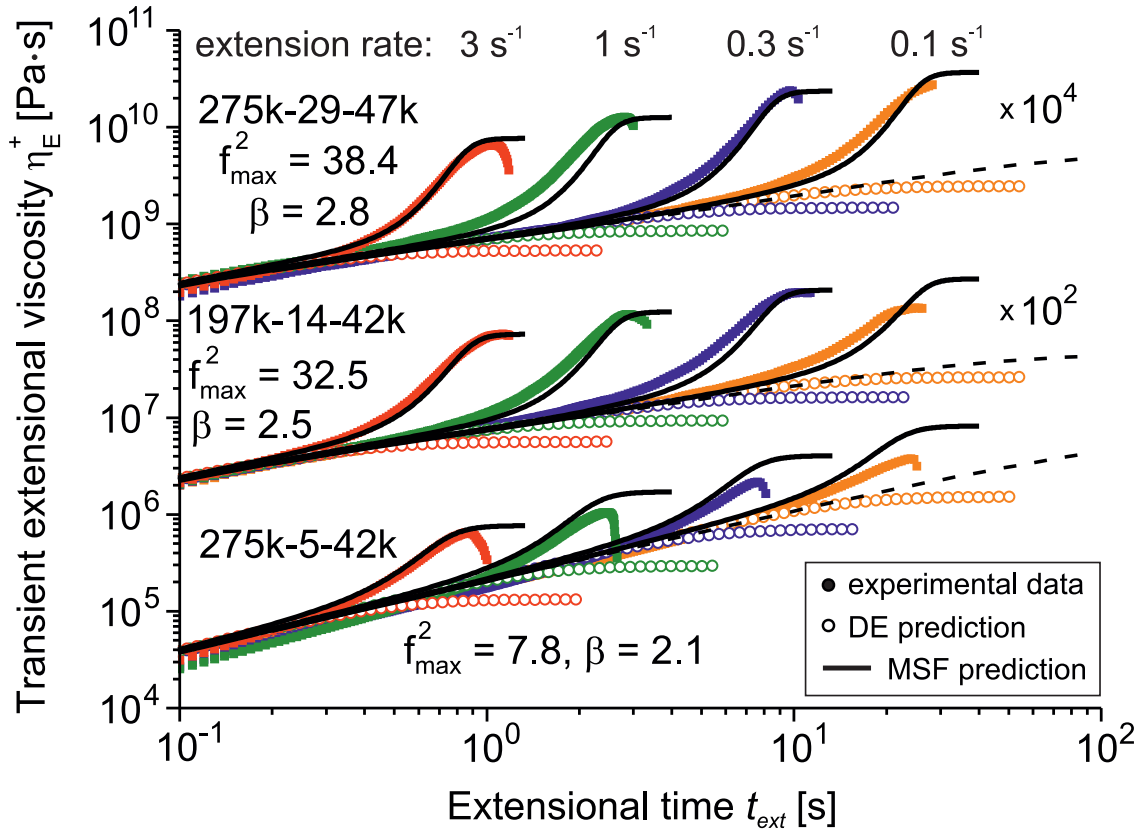
Figure 6.2: Extensional rheology measurements of combs with different number of branches. The number of branches is varied (5, 14 and 29 branches) via appropriate synthesis. The MSF model prediction corresponds well with the experimental data, only for the comb with low amount of branches CK123 (275k-5-42k), where the steady state extensional viscosity is getting lower with decreasing extension rate the f_{max}^2 value does not correspond well with the maximum.

branches a major difference in the predicted f_{max}^2 value can be observed for low extension rates. Due to the low molecular weight of the branches, the combs behave like a linear polymer at low extension rates, which is not considered by the constant f_{max}^2 value applied.

Wagner et al. [Wagner 08] found a correlation between the parameter f_{max}^2 and the topology, the lower f_{max}^2 the more linear is the polymer, which indicates a reduced stretch of the backbone and a lower steady state extensional viscosity. This is also the case for the examined comb polymers, the f_{max}^2 is dependend on the molecular weight and the number of the branches. The f_{max}^2 value decreases with decreasing number and molecular weight of the branches. For a high number of branches (CK132 and C642) with 29 branches each, the f_{max}^2 value is predominantly influenced by the number of branches, although the molecular weight differs by a factor of 3. For a lower number of branches, as in the case of the combs CK106 and CK128, where the number of branches
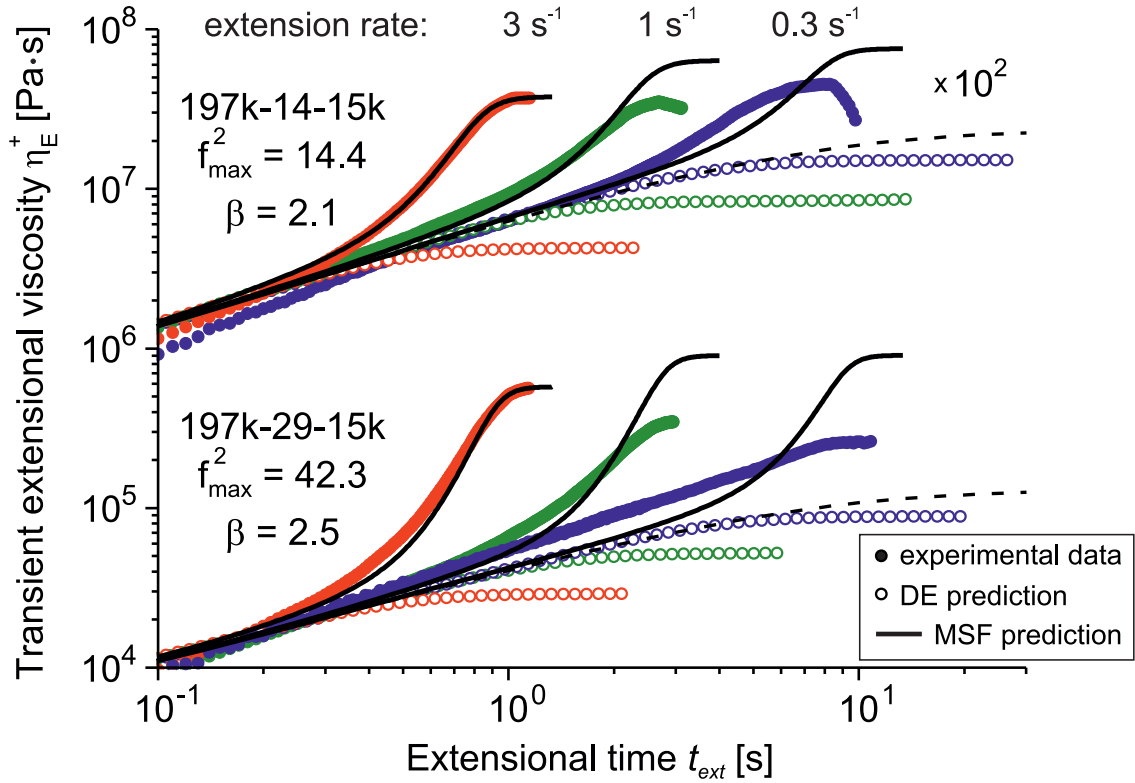
Figure 6.3: Extensional rheology measurements of combs with different number of slightly entangled branches. The transient extensional as well as the steady state extensional viscosity prediction differs from the experimental data for lower extension rates.

and the molecular weight of the backbone is identical, the branch molecular weight has an extensive influence on the f_{max}^2 value. So it can be concluded that the f_{max}^2 value is predominantly influenced, in the case of a comb with a high number of branches, by the number of branches and in the case of a comb with a low number of branches, by the molecular weight of the branches.

The f_{max}^2 value is directly comparable with the strain hardening factor (SHF), since both values depend on the ratio between the steady state extensional viscosity η_E and the Doi-Edwards (DE) behavior. This is illustrated in Fig. 6.4, with the SHF values of the highest extension rate ($\dot{\epsilon}_H = 3 \ s^{-1}$). The f_{max}^2 and the SHF values are comparable in this case. Since the f_{max}^2 value is the same for all extension rates, a comparison with lower extension rates would instead be misleading.

6.1.3 Comparison with commercial LDPE

To compare the extensional properties of the model comb polymers a commercial LDPE, with a low amount of long-chain branching, was used as a benchmark material. The used
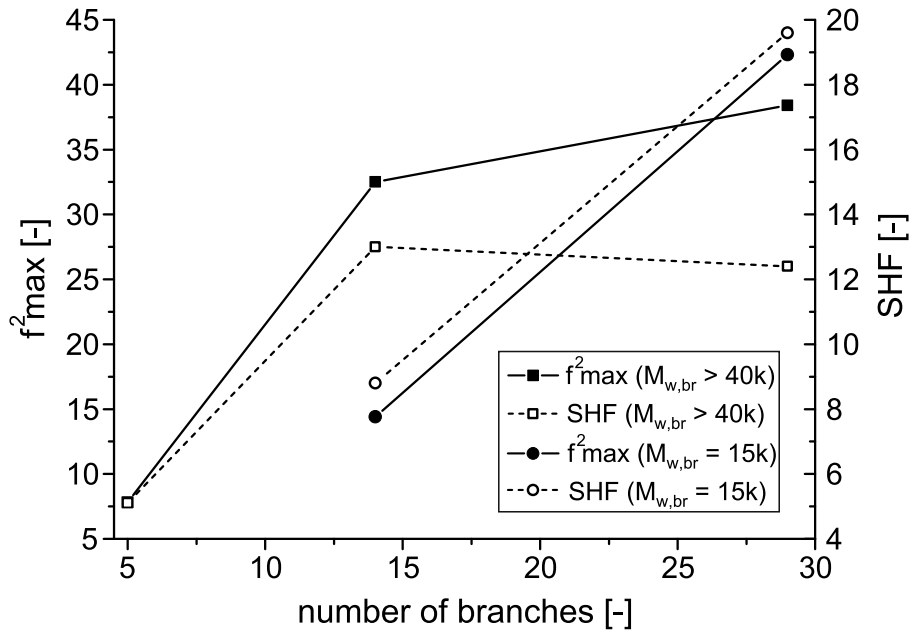
Figure 6.4: Comparison of the f^2_{max} and the SHF values of the highest extension rate ($\dot{\epsilon}_H = 3\ s^{-1}$) with the number of branches.
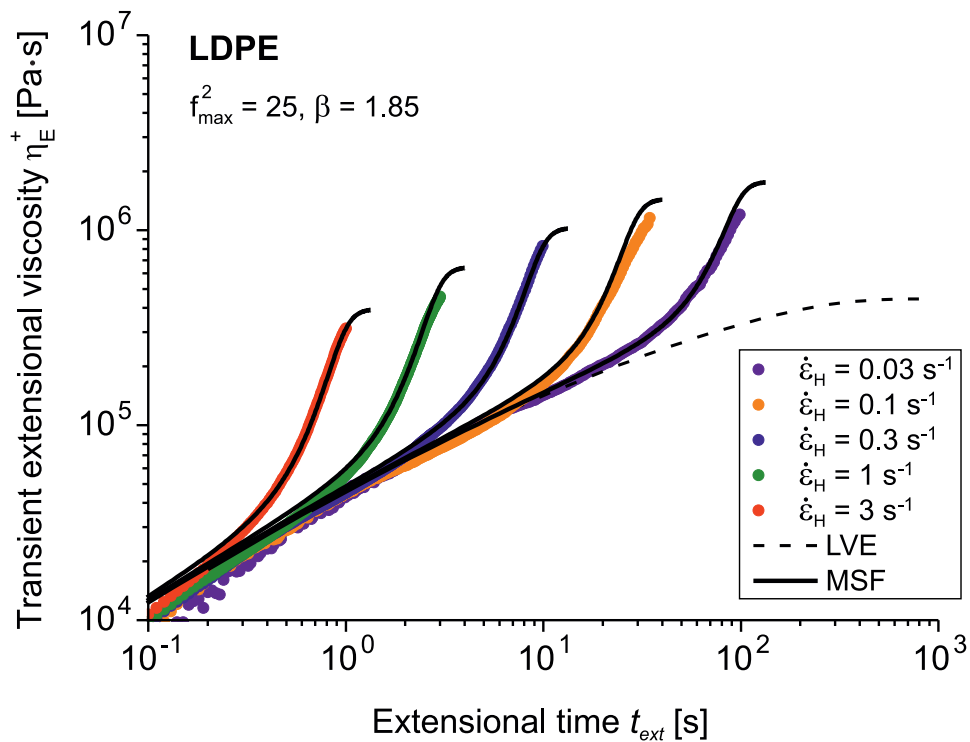
Figure 6.5: Extensional rheology measurements of a commercial LDPE with a low amount of long-chain branching (LCB/1000CH$_2$ = 0.24). The filled spheres stand for the experimental data, the dashed line for the LVE prediction and the straight line for the MSF model prediction.

LDPE was kindly provided by the company Lyondell-Basell. The molar mass distribution of the sample was measured using SEC-MALLS (M_w = 366.96 [kg/mol], M_n = 49.629 [kg/mol], PDI = 7.4, LCB/1000CH$_2$ = 0.24).

For the LDPE a pronounced strain hardening behavior can be observed for all extension rates applied, the deviation from the linear viscoelastic (LVE) behavior is for all extension rates approximately the same, Fig. 6.5. A steady state extensional viscosity is not reached thus far, due to the low Hencky strain (ϵ_H = 3) used. Though the underlying molecular structure is unknown, it can be concluded, using the obtained MSF parameters, that the LDPE sample is only sparsely branched, due to the low β value of 1.85, in contrast to the model combs with β values ranging from 2.1 to 2.8. An important criteria for the comparison between commercial LDPE and model comb systems is however the amount of resulting strain hardening. The f_{max}^2 value for the LDPE sample (f_{max}^2 = 25) is in the range of the results for the model comb systems (f_{max}^2 = 7.8 - 42.3), thus it can be concluded that the branching degree chosen for the model comb system is comparable with the degree of branching for commercial LDPE polymers. Therefore the results obtained with the model combs are very useful for the better understanding of the influence of branching in commercial polymers.

6.2   Pom-Pom Model

6.2.1   Fundamentals

A non-linear viscoelastic model for the description of multiple branched polymers was developed by McLeish and Larson [McLeish 98], the so-called Pom-Pom model. A Pom-Pom molecule consists of a backbone with two terminal branching points (at each end of the backbone chain) with a various number of branches q (in the case of $q = 2$ at each end, a H-polymer is reached), Fig. 6.6. This is the simplest molecule that contains multiple branch points allowing segments of the molecule to become 'buried' and causing a hierarchy of relaxation processes. The Pom-Pom model is used to describe the backbone orientation and stretch for monodisperse Pom-Pom polymers, which gives access to backbone orientation and backbone stretch time. Therefore the Pom-Pom model can be used to predict the amount of strain hardening, which was determined to be dependent on the number of branches q per branch point [McLeish 98, Larson 01].

The Pom-Pom model contains three basic time constants: the backbone reptation time τ_b, the backbone stretch time τ_s, and the branch relaxation time τ_a:

$$\tau_b[\zeta_c, t] = \frac{4}{\pi^2} Z_b^2 \varphi_b \tau_a[\zeta_c, t] q \tag{6.6}$$

$$\tau_s = Z_b \tau_a(1) q \tag{6.7}$$

$$\tau_a(x) = t_{pre} \exp\left(\nu Z_a \left[\zeta^2 - (1 - \varphi_b)\frac{2\zeta^3}{3}\right]\right) \tag{6.8}$$

Z_a is the number of entanglements of each branch, which is defined as $Z_a = M_a/M_e$ where M_a is the molecular weight and M_e is the entanglement molecular weight of a branch, Z_b is the number of entanglements of the backbone respectively. The volume fraction of the backbone φ_b is defined as $\varphi_b = Z_b/(Z_b + 2 \cdot q \cdot Z_a)$. ζ is a coordinate, which is leading from
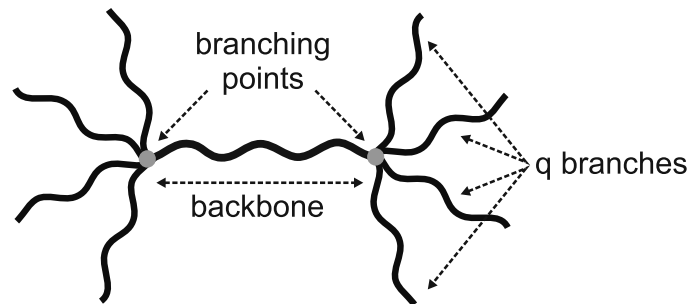
Figure 6.6: Schematic illustration of the Pom-Pom structure.

the tip of the branch inwards along the branch, with $\zeta = 1$ at the branch point. τ_a (ζ) is the relaxation time of the branch located at the position ζ. The parameter ν has a value of 3/2 when using the Graessley-Fetters definition of M_e, while $\nu = 15/8$ is used for the Ferry definition of M_e.

The backbone stretch time (τ_s) is the time taken for the path length of the backbone to return from some displaced length to its equilibrium length. The backbone reptation time or orientation relaxation time (τ_d) is the average time it takes the backbone to reptate, via its branch points diffusing along the backbone tube, out of a tube of unstretched length. The two dominant relaxation processes, the backbone stretch and reorientation are determined from the branch disentanglement time.

The original differential form by McLeish and Larson [McLeish 98] was improved with the local branch-point displacement by Blackwell et al. [Blackwell 00]. The modification of the backbone reorientation time for very fast non-linear flows was proposed by Lee et al. [Lee 01], the set of revised Pom-Pom Model equations are:

$$\text{Stress tensor:} \qquad \bar{\bar{\sigma}} = G_0 \varphi_b^\beta \lambda^2(t) \bar{\bar{S}}(t) \qquad\qquad (6.9)$$

$$\text{Orientation tensor:} \qquad \bar{\bar{S}}(t) = \bar{\bar{A}}/tr\bar{\bar{A}} \qquad\qquad (6.10)$$

$$\dot{\bar{\bar{A}}} - \kappa \cdot \bar{\bar{A}} - \bar{\bar{A}} \cdot \kappa = -\frac{1}{\tau_d}\left(\bar{\bar{A}} - I\right) \qquad\qquad (6.11)$$

$$\text{Stretch:} \quad \frac{D\lambda(t)}{Dt} = \lambda(t)\kappa : \bar{\bar{S}} - \frac{1}{\tau_s}[\lambda(t) - 1]\exp(v^*(\lambda(t) - 1)) \quad (6.12)$$

$$\text{Time Scales:} \quad \tau_s = \frac{5}{2}\, q\, s_{bb}\, \varphi_b^{\beta - 1}\, \tau_a \qquad \tau_d = \frac{75}{2\pi^2}\, q\, s_{bb}^2\, \varphi_b^{2(\beta - 1)}\, \tau_a \quad (6.13)$$

$$\text{Reversing Flow Correction:} \ \frac{1}{\tau_d^*} = \begin{cases} \dfrac{1}{\tau_d} & \text{for } 1 \leq \lambda \leq q \\[2mm] \dfrac{1}{\tau_d} + \dfrac{\dot{\lambda}}{\lambda} - \kappa : \bar{\bar{S}} & \text{for } \lambda < 1 \end{cases} \qquad (6.14)$$

where s_{bb} and s_{br} is the number of entanglements of the backbone and the branches, $v^* = 2/(q - 1)$ and $\beta = 2$ (dilution factor assumed to be $\alpha = 1$) [McLeish 02].

6.2.2 Strain hardening behavior of Pom-Pom polymers

The prediction of the Pom-Pom constitutive model in extensional rheology is examined with particular focus on the strain hardening factor (SHF) behavior with increasing number and molecular weight of the branches for the Pom-Pom molecule. In Fig. 6.7a the number of branches was changed for a Pom-Pom with constant molecular weight of the backbone and the branches. An increase with Hencky strain rate $\dot{\epsilon}_H$ as well as with the number of branches q at constant Hencky strain rate $\dot{\epsilon}_H$ was observed qualitatively as an effect on the SHF. The increase with $\dot{\epsilon}_H$ can be explained using the stretching equation,
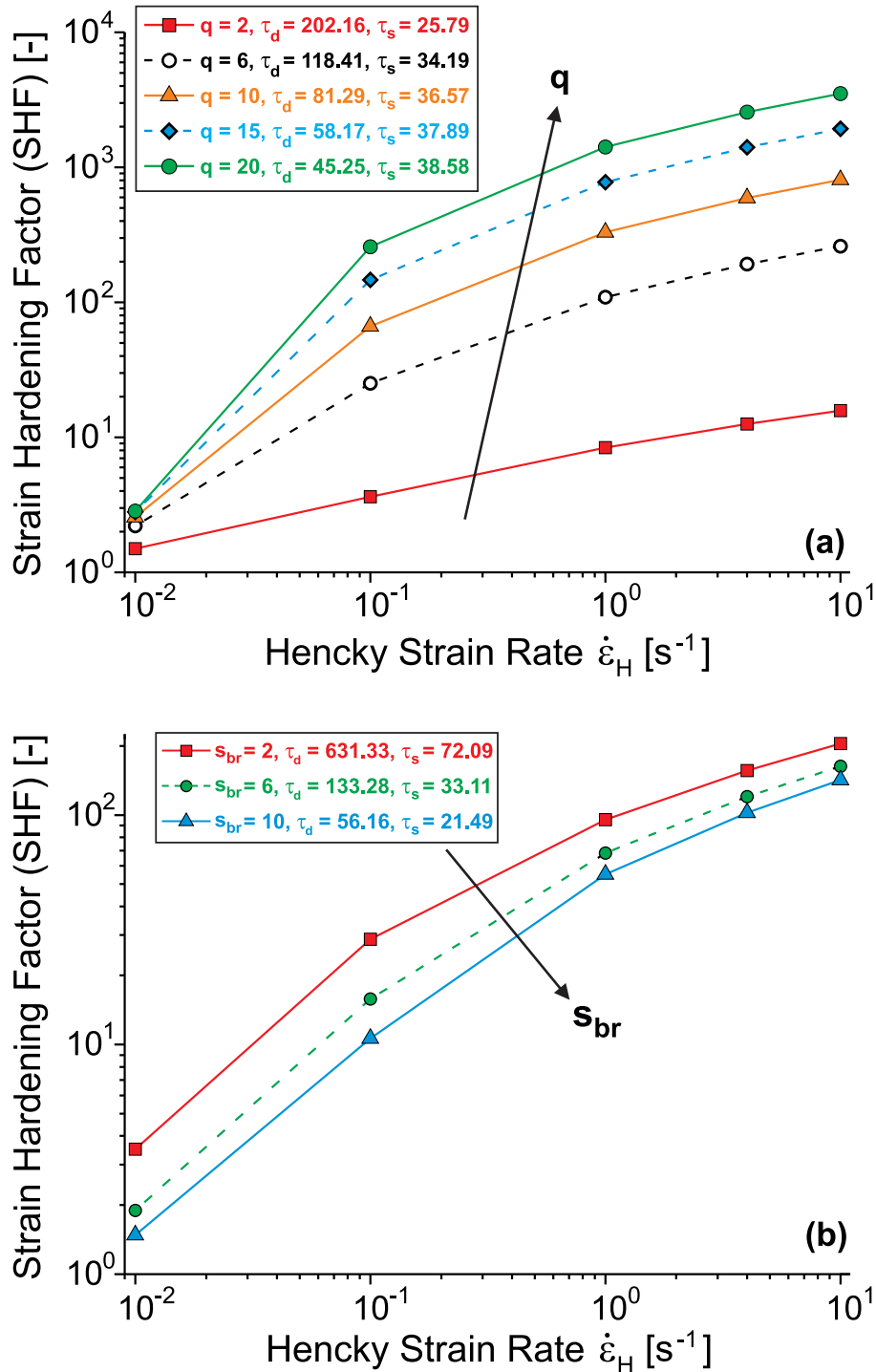
Figure 6.7: Pom-Pom model simulations of the influences on the strain hardening factor (SHF): (a) Effect of changing number of the branches q, the number of entanglements of the backbone $s_{bb} = 14$ and the branches $s_{br} = 6$ are kept constant; (b) Effect of changing molecular weight of the branches, the number of entanglements of the backbone $s_{bb} = 14$ and the number of branches $q = 5$ are kept constant.

where the first term is $\lambda\kappa\cdot S$ or $\lambda\dot{\epsilon}(S_{11}-S_{22})$, so with increasing $\dot{\epsilon}_H$ the large chain stretch can be sustained at steady state. In the case of the increase of the number of branches the separation of two time scales decreases and stretching time τ_s is increased, in turn the stretching of the Pom-Pom molecule would occur earlier. In Fig. 6.7b the Pom-Pom branch molecular weight is changed instead, the backbone molecular weight and the number of branches are constant. The first observation could be explained in a similar way as before, as the branch molecular weight is increased, the backbone fraction in the molecule is decreasing, in turn τ_s is decreasing as this time scale is directly proportional to the backbone fraction φ_b, so SHF is decreasing subsequently.

The Pom-Pom model can also be used to explain the steady state extensional viscosity behavior. As the backbone of the Pom-Pom becomes maximum stretched, the tension in the backbone is high enough to pull the branches into the tube of the backbone. This maximum is reached for extension rates $\dot{\epsilon}_H$ equal to the inverse of the stretching time τ_s, the stress reaches a constant value and a plateau of the steady state extensional viscosity occurs. As the extension rate is further increased $\dot{\epsilon}_H > \tau_s^{-1}$ the steady state extensional viscosity decreases, since the stress is constant ($\eta_E \propto \dot{\epsilon}_H^{-1}$ for $\sigma = $ const.) [Dealy 06]. This phenomenom was reported by Archer and Juliani [Archer 04] for Pom-Pom architectures and McLeish et al. [McLeish 99] for H-polymers.

6.2.3 Pom-Pom prediction of the Q_0 parameter

The prediction of the Pom-Pom constitutive model in LAOS was examined using the nonlinear parameter Q_0 for different model parameters. In Fig. 6.8a the qualitative behavior of the Q_0 parameter with changing molecular weight of the Pom-Pom branches is shown. There is always an occurrence of a maximum at the reptation frequency $1/\tau_d$ observable, with increasing molecular weight of the branches the maximum value decreases. In Fig. 6.8b the behavior of Q_0 with increasing number of branches q is shown, here $q = 1$ belongs to the linear topology which shows in contrast to the branched architectures no decrease of Q_0 after reaching the maximum. Similar trends as in the previous case, but a more prominent decrease in the maximum value was observed. In both cases, the increase of the number of branches q or of the molecular weight of the branches, the separation between two time scales decreased and in turn stretching of the polymer backbone chain would be dominant, which is responsible for the decrease in the Q_0 maximum.
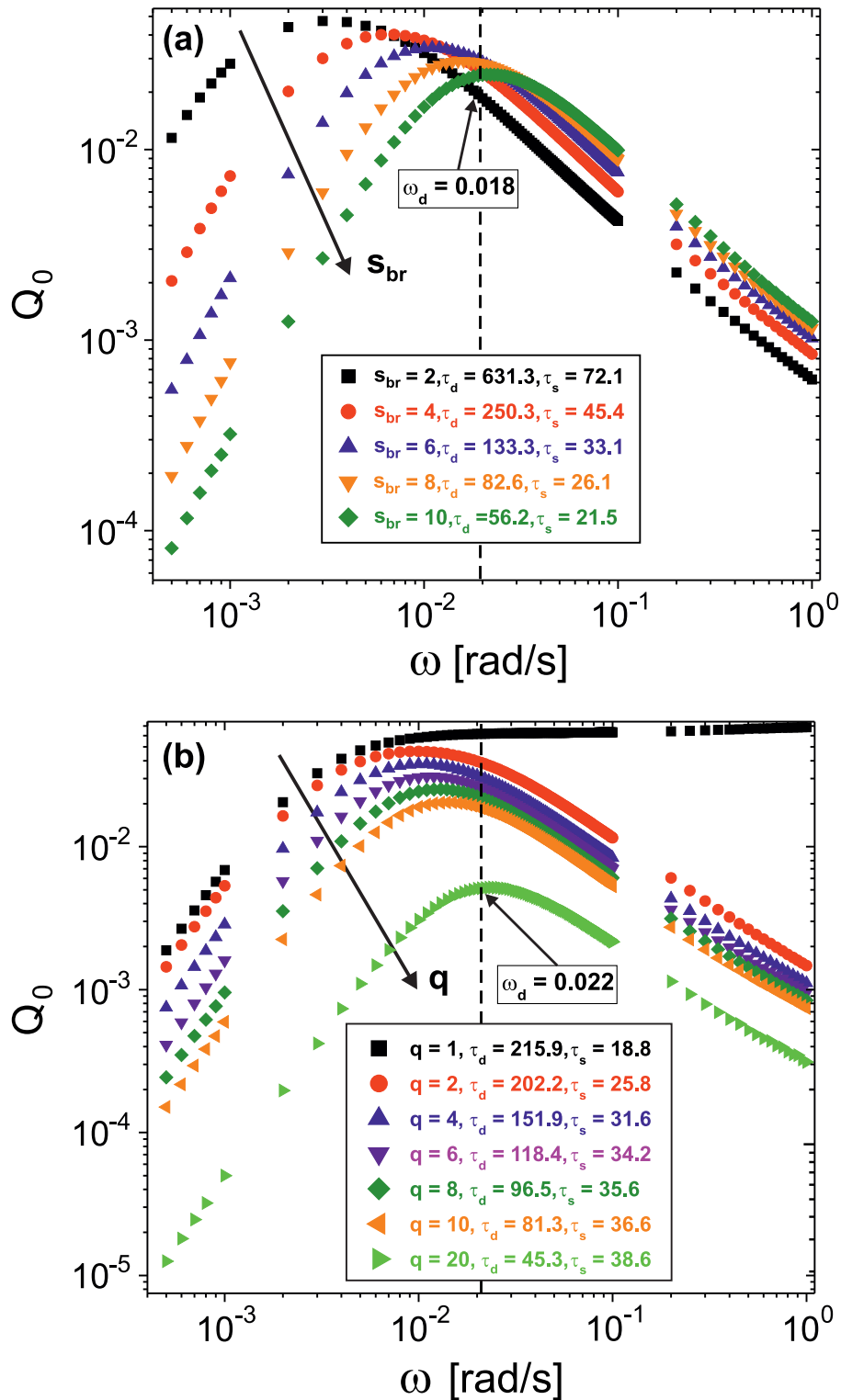
Figure 6.8: Pom-Pom model simulations of the non-linear parameter Q_0: (a) Effect of changing molecular weight of the branches, the number of entanglements of the backbone $s_{bb} = 14$ and the number of branches $q = 5$ is kept constant; (b) Effect of the number of branches, the number of entanglements of the backbone $s_{bb} = 14$ and of the branches $s_{br} = 6$ is kept constant.

6.3 Conclusion

The molecular stress function (MSF) model is useful to predict the extensional behavior of branched polymers. In the case of comb polymers with a high number of well-entangled branches the MSF prediction agreed well with the transient extensional viscosity as well as with the transition to the steady state extensional viscosity. For comb polymers with a low number of branches or slightly entangled ones, the prediction differs from the experimental data, especially for low extension rates. The steady state extensional viscosity decreases with decreasing extension rate, so that the constant f_{max}^2 value is not useful for this type of comb polymers. By the comparison with a commercial branched polymer, in this case a slightly branched LDPE, with the model comb polymers examined, a good correspondence could be found for the MSF parameters. Thus it can be concluded that the results obtained from the model comb polymers can be useful for the determination of branching and extensional properties of commercial branched polymers.

The prediction of the strain hardening behavior using the Pom-Pom model, gives similar results to what can be observed for the model comb polymers. The increase in strain hardening is predominantly dependent on the number of branches and an extensive increase can be found for the transition from two to six branches, which is in good aggreement with the findings for the comb polymers. From the analysis of the simulated non-linear mastercurves it can be concluded that it is a very useful tool to evaluate experimentally the reptation time (τ_d) and which in turn could provide another degree of freedom in correctly modeling the linear and non-linear rheology of any given architecture.

Chapter 7

Summary

The existence of random long chain branching (LCB) in commercial polymers strongly influences the (non-)linear rheological and processing properties of polymer melts. The correlation between the properties and the underlying molecular structure for commercial polymers (especially LDPE) is difficult, due to broad polydispersities and the almost unknown topology. Due to its high sensitivity towards the molecular structure, rheology is a promising method for the investigation of the influences and for the quantification of long-chain branching.

For a better understanding of the extent of branching, it is necessary to correlate rheological properties with the structure of well defined model topologies to determine the influences of the underlying structure.

Therefore new syntheses methods were developed, which are suitable for the synthesis of model branched polymers with well-defined structures and low branching degrees, to assure comparability to commercial branched polymers. By the usage of poly(p-methylstyrene) (PpMS) as comb backbone the number of branching points were well controlled via selective bromination of the methyl group and degrees of functionalization of 0.1-1 mol-% were achieved. Due to its similarity to styrene, p-methylstyrene allowed the independent anionic polymerization of the backbone and the branches with well defined molecular weights and low polydispersities. Alternatively polystyrene (PS) model combs with lower polydispersities and functionalization degrees, in comparison to PpMS, were synthesized. Though the grafting yield in the case of the PS combs was not quantitative, well-characterized and defined PS model combs were obtained. The polystyrene backbones, with acetyl-groups used as branching points, allow further coupling methods, due to its accessability to other functional groups.

Various rheological measurement techniques, in the linear and non-linear regime, were evaluated to correlate the degree of branching with the rheological properties. In the

linear regime, the reduced van Gurp-Palmen plot was applied to the data obtained in small amplitude oscillatory shear (SAOS) experiments. A linear correlation of the volume fraction of the branches with the value of the reduced modulus, corresponding to the minimum of the backbone relaxation, was found, Fig. 3.21. Even for low branching degrees (two branches per backbone) a deviation from the behavior of linear polymers was determined using the van Gurp-Palmen plot.

In the non-linear regime two different rheological measurement techniques were used, on one hand extensional rheology and on the other hand shear rheology under large amplitude oscillatory shear (LAOS) in combination with FT-Rheology. The knowledge of the non-linear rheological behavior of branched polymers is of substantial interest, since during the polymer processing large and rapid deformations are applied which result in a highly non-linear mechanical behavior.

Using extensional rheological measurements it could be concluded that the number as well as the molecular weight of the branches have an influence on the strain hardening behavior of branched polymers. The strain hardening factor increases linearly with increasing number of branches. However at a certain number of branches a maximum is reached, where the number of branches has only a low influence on the strain hardening. This was the case for combs with the number of branches in the range from 14 to 29, with molecular weights above the critical molecular weight ($M_{w,br} > M_c$, with $M_c \approx$ 35 kg/mol). By lowering the number of branches a lower limit for strain hardening can be reached. This is the case for a comb with only two branches per backbone, where slight strain hardening can only be observed for the highest extension rate ($\dot{\epsilon}_H = 3 \text{ s}^{-1}$) applied. The number of branches, when the transition from slight to extensive strain hardening takes place, is in the range between 3 and 4 branches per backbone. Although the number of branches has an influence on the strain hardening behavior, the steady state extensional viscosity is not influenced by the number of branches. Similar values of the steady state extensional viscosity were found for combs with branching degrees varying from 5 to 29 branches.

The molecular weight of the branches needs to be at least slightly entangled ($M_e > M_{w,br}$ $< M_c$) to contribute to the strain hardening, which increases with molecular weight of the branches. The comb polymers with slightly entangled branches ($M_{w,br} \approx 15$ kg/mol) showed a linear increase of the strain hardening behavior with the extension rate, while no decrease was observed for the extension rates applied. In contrast to this, combs with well entangled branches ($M_{w,br} > 40$ kg/mol) showed a decrease of strain hardening with extension rates, exceeding the inverse Rouse time of the backbone due to branch relaxation. This result is important for industrial processes, where extensional flows play

a major role and intense strain hardening even at high extension rates is desired.

Using the non-linear parameter Q_0, obtained via a square scaling law from FT-Rheology, intrinsic non-linear mastercurves were created and correlated with the relaxation processes of the linear mastercurve. From the intrinsic non-linear mastercurve different relaxation times (reptation time and Rouse time of the backbone) could be directly extracted from the corresponding maxima and minima. The correspondence of the reptation time could be confirmed via Pom-Pom model simulations. The experimental accessability to relaxation times opens up the possibility for a better physical understanding of the underlying relaxation processes and can be furthermore used to improve linear and non-linear modeling.

To predict the extensional behavior of branched polymers, the molecular stress function (MSF) model was used. In the case of comb polymers with a high number of well-entangled branches the MSF prediction agreed well with the transient extensional viscosity as well as with the transition to the steady state extensional viscosity. For comb polymers with a low number of branches or slightly entangled ones, the prediction differs from the experimental data, especially for low extension rates. The steady state extensional viscosity decreases with decreasing extension rate, so that the constant f_{max}^2 value is not useful for this type of comb polymers. By the comparison with a commercial branched polymer, a good correspondence was found for the MSF parameters. Due to this comparability, the rheological results obtained from the model comb polymers can be used for the determination of branching and extensional properties of commercial branched polymers.

The Pom-Pom model was used for the prediction of the strain hardening behavior. A depedency between the increase in strain hardening and the number of branches was found. An extensive increase was found for the transition from two to six branches, which is in good aggreement with the findings for the comb polymers. From the analysis of the simulated non-linear mastercurves it was concluded that it is a very useful tool to evaluate experimentally the reptation time (τ_d) and which in turn could provide another degree of freedom in correctly modeling the linear and non-linear rheology.

The developed syntheses methods make model comb polymers accessible, which are comparable to long-chain branched commercial polymers. Especially the synthesized combs with a high number (> 1 mol-%) of slightly entangled branches ($M_e \approx M_{w,br} < M_c$) showed superior rheological properties in extensional flow in comparison to combs with well entangled branches ($M_{w,br} > M_c$).

Comparing the different rheological measurement techniques, each of them can give valuable informations on the branching degree, so far only a semi-quantitative determi-

nation is possible. However, the results obtained from the used rheological techniques in combination with simulations can help to fundamentally understand the rheology of complex polymer structures.

Comparison of the comb synthesis methods:

- *Poly(p-methylstyrene) (PpMS) based combs*:

  Advantages:

    ⋄ Controlled number of branching points (> 0.5 mol-%) can be introduced.
    ⋄ Quantitative conversion of the branching points during comb formation.
    ⋄ High amount of sample (approx. 2-5 g) accessible, sufficient to perform several rheological measurements.
    ⋄ Well-defined structures with known branching degree can be achieved using ^{1}H-NMR and SEC-MALLS as characterization methods.

  Disadvantages:

    ⋄ Lithium-bromide exchange as side reaction during comb formation.
    ⋄ Time consuming purification for seperation of excess branches.
    ⋄ Solvent (CCl_4) for bromination is carcinogenic (restricted usage).

- *Polystyrene (PS) based combs*:

  Advantages:

    ⋄ A wider range of a controlled number of branching points (0.1-10 mol-%) can be introduced in contrast to PpMS.
    ⋄ Accessability to other functional groups.
    ⋄ High amount of sample (approx. 2-5 g) accessible, sufficient to perform several rheological measurements.
    ⋄ Well-defined structures with known branching degree can be achieved using ^{1}H-NMR and SEC-MALLS as characterization methods.

  Disadvantages:

    ⋄ Enolate formation as side reaction during comb formation.
    ⋄ No quantitative conversion of the branching points during the comb formation.
    ⋄ Time consuming purification for seperation of excess branches.

Comparison of the rheological measurement techniques:

- *Shear rheology in the linear regime:*

  Advantages:

  ⋄ Low amount of sample necessary (15-50 mg).

  ⋄ Easy to perform.

  ⋄ Medium time exposure for the measurement (a few hours).

  ⋄ Determination of linear model parameters.

  ⋄ Linear measurements can be complemented or predicted using linear models.

  Abilities for the investigation of branched structures:

  ⋄ Differentiation between branched and linear topology even for low branching degrees possible. A comb polymer with two branches, however only for branch molecular weights higher than the critical molecular weight, could be distinguished from a linear polymer using the van-Gurp Palmen plot.

  ⋄ Only semi-quantitative correlation between the rheological measurement and the structure can be made. Using the reduced van Gurp Palmen plot, the volume fraction of the branches or the backbone respectively can be determined.

- *Extensional rheology:*

  Advantages:

  ⋄ Strain hardening can be investigated in constrast to shear measurements.

  ⋄ Easy to perform.

  ⋄ Low time exposure for the measurement (minutes).

  Disadvantages:

  ⋄ High amount of sample necessary (approx. 100-200 mg per sample).

  ⋄ Inhomogeneous flow can give misleading results.

  Abilities for the investigation of branched structures:

  ⋄ High sensitivity: low branching degrees can be determined. Even two branches showed the occurrence of strain hardening at the highest applied extension rate ($\dot{\epsilon}_H = 3$ s^{-1}).

⋄ Dependence of the strain hardening on the branching degree can be used to determine the number of branches. For branches with molecular weights higher than the critical molecular this is limited.

⋄ Improvements of non-linear models (e.g. MSF-model).

• ***Shear rheology in the non-linear regime:***

Advantages:

⋄ Low amount of sample necessary (15-60 mg).

Disadvantages:

⋄ Time consuming (several hours).

⋄ Experience necessary for optimal measurement conditions.

⋄ Low branching degrees are difficult to access. A comb with five branches (branching degree 0.2 mol-%), showed only a slight minimum, difficult to differentiate from linear structure.

⋄ Access to branching relaxation regime limited due to torque transducer.

Abilities for the investigation of branched structures:

⋄ Linear and branched architectures can be differentiated for branching degrees > 0.2 mol-%.

⋄ Access to relaxation times for branched structures and to relaxation phenomena in the non-linear regime.

Chapter 8

Outlook

The investigations performed so far provide an insight into the dynamics and rheological properties of long-chain branched polymers. However, the conditions used in polymer processing were not investigated using model branched polymers so far. This is the result of the lack of adequat amounts of sample, which are necessary to perform measurements under processing conditions and as well to perform further in-depth rheological measurements. The synthesis of high amounts (> 10 g) of polystyrene based combs is so far limited, due to side reactions taking place during the comb formation and the further separation from excess branches. Thus the comb formation needs to be optimized with regard to the functional groups and grafting procedures used.

The synthesis of further comb structures with branching degrees in the range from 5 to 30 branches is also necessary to determine the limit for an ideal number of branches. Since it was observed that in the range from 14 to 29 branches, a limit for the number of branches is reached, where a further increase does not have an effect on the rheological properties. The comb polymers with slightly entangled branches showed superior extensional properties in the investigated range. A high amount of strain hardening without successive decrease at higher extension rates ($\dot{\epsilon}_H = 3$ s^{-1}) was observed in contrast to long-chain branched combs. The further synthesis and comparison of the rheological properties of long- ($M_{w,br} > M_c$) and short-chain branched ($M_e > M_{w,br} < M_c$) combs is therefore also of fundamental interest.

To get a detailed picture of the underlying dynamics of the backbone and the branches of the comb architectures, the synthesis of well-defined, isotopically labeled model combs is required. Multiple quantum NMR spectroscopy can be used as a measurement technique to separate between the backbone and the branch motion to study the molecular chain dynamics in detail.

For the better correlation of the rheological properties of comb architectures in the linear

regime, the experimental data can be complemented using simulated linear data. For this purpose linear models, e.g. the BoB (branch on branch) or hierarchical model are available. The simulated data can be used to improve and to validate the current findings in the linear regime.

The existence of the steady state behavior and the successive downturn of the extensional viscosity in extensional rheological measurements is still a subject of discussion. The monitoring of the sample during the extensional measurement could give evidence to the origin of the steady state behavior, possibly caused by inhomogeneous flow at the end of the extension.

FT-Rheology is a very useful tool to obtain the relaxation times of branched polymers. The branch relaxation regime is so far not accessible, due to the high torque emerging at the low temperatures necessary to access the branch relaxation regime. By the usage of a rubber tester in combination with FT-Rheology, this issue could be circumvented. However higher sample amounts (4 g per sample) are necessary for the measurements.

Appendix A

Materials and Methods

A.1 Synthesis steps

A.1.1 Monomer and solvent purification

Styrene (Acros, 99 %) and p-Methylstyrene (Acros, 98 %) was purified by distillation at reduced pressure after stirring over calcium hydride (CaH_2) (Acros, 93 %) overnight, then distilled from dibutylmagnesium (Aldrich, 1 M in heptane) into precalibrated ampoules and degassed afterwards by three successive freezing-evacuation-thawing cycles. 1,1-diphenylethylene (DPE) (Acros, 99 %) was purified by titration with n-butyllithium (n-BuLi) (Acros, 2.2 M in cyclohexane) until a red color is persistently formed and then distilled into precalibrated ampoules. Styrene, p-Methylstyrene and DPE were stored under argon at -20 °C until needed. Tetrahydrofuran (THF) (Acros, 99+ %) was distilled first from CaH_2, then from sodium benzophenone and stored over sodium benzophenone on the vacuum line prior to use. Toluene (Acros, 99.5 %) was distilled from CaH_2 and stored over living polystyrene on the vacuum line prior to use. Chloroform ($CHCl_3$) was distilled from CaH_2 prior to use. Sec-Butyllithium (s-BuLi) (Aldrich, 1.4 M in cyclohexane), n-BuLi (Acros, 2.2 M in cyclohexane), Carbon tetrachloride (CCl_4, Acros, 99 %), 2,2'-azobisisobutyronitrile (AIBN, Sigma-Aldrich, 98 %), N-bromosuccinimide (NBS, Acros, 99 %), Acetylchloride (AcCl, Fluka, 99 %), Aluminiumchloride (Sigma-Aldrich, 1 M in nitrobenzene), Methyltriphenylphosphonium bromide (PPh_3MeBr, Acros, 98 %), Potassium tert-butoxide (KtOBu, Acros, 1.7M in THF), Lithium aluminum hydride ($LiAlH_4$, Sigma-Aldrich, 1M in THF), Chlorotrimethylsilane (TMS-Cl, Acros, 98 %), Lithium bromide (LiBr, Acros, 99+%) and Acetonitrile (Acros, 99.9 % Extra Dry) were used as received.

A.1.2 Backbone and side chain polymerization

Anionic polymerization of styrene and grafting procedures were performed using high-vacuum techniques. The ampoules and the polymerization reactor were equipped with high-vacuum PTFE stopcocks and ground glass joints. To introduce the reagents, the ampoules were mounted directly on the reactor. The dry solvents were introduced directly from the solvent reservoir on the vacuum line into the reactor. The polystyrene (PS) backbone and the branches were prepared by polymerization at room temperature of styrene with s-BuLi as initiator and toluene as solvent. In the case of the backbone, the residual anions were terminated using degassed methanol, after complete conversion of the monomer. The polymerization of the branches was performed in an ampoule with high-vacuum PTFE stopcocks and ground glass joints. After completion of the polymerization only a sample was removed using a syringe and terminated with degassed methanol for the characterization of the branches.

A.1.3 Bromination of Poly(p-methylstyrene)

To introduce a small amount of bromomethyl groups (1 mol-%) to the PpMS backbone, N-bromosuccinimide (NBS) was used as brominating agent. In a typical reaction, PpMS (5g, 197,000 g/mol) was dissolved in 200 ml of carbon tetrachloride (CCl_4) at 60 °C, then NBS (73 mg, 0.41 mmol) and 2,2'-azobisisobutyronitrile (AIBN) (5 mg, 0.03 mmol) were added and the solution was stirred under reflux. After approximately 5 h the CCl_4 was removed under reduced pressure, the polymer dissolved in tetrahydrofuran (THF) and then precipitated in methanol, redissolved in THF and precipitated once more. To remove residual amounts of solvents, the polymer was first dried under vacuum at 45 °C and then freeze-dried from cyclohexane. ^{1}H NMR ($CDCl_3$): δ = 4.40 ppm (s, 2H, -CH_2Br).

A.1.4 Acetylation of polystyrene

To achieve a small number of branching points (< 1 mol-%), acetyl-groups were introduced via Friedel-Crafts-Acetylation to the PS backbone [Janata 02]. Acetylchloride was used as acetylation agent. In a typical reaction, to achieve 20 braching points (acetyl groups) on the PS backbone, PS (5.00 g, 200,000 g/mol) was dissolved in 50 ml of dry chloroform ($CHCl_3$), then a solution of acetylchloride (AcCl) (0.07 ml, 0.50 mmol) and aluminiumchloride (1 M in nitrobenzene) (1.00 ml, 0.05 mmol) in 50 ml chloroform was added and the solution was stirred at room temperature for approximately 5 h. The polymer was then precipitated in methanol, redissolved in THF and precipitated once more. To remove residual amounts of solvents, the polymer was first dried under vacuum at

45 °C and then freeze-dried from cyclohexane. ^{1}H NMR (CDCl$_3$): δ = 2.51 ppm (d, 3H, -CH$_3$), 7.4-7.7 ppm (m, 2H, benzyl protons in m-position).

A.1.5 Polystyrene comb synthesis

The partially acetylated PS backbone was introduced into a Schlenk flask, dissolved in dry THF (< 5 % w/v), cooled down to approx. -70 °C with an acetone/dry-ice cooling bath and connected via a transfer cannula with the reactor. Dry THF was then transferred into the reactor, cooled down to approx. -70 °C and the living PS side chains were added. The temperature was maintained at approx. -70 °C and the living side chains were titrated with the solution of the acetylated PS solution over approximately 30 minutes. Stirring was continued for 1 h and the residual living side chains were terminated with degassed methanol. The comb was separated from the unreacted side chains by precipitation/fractionation in a THF-methanol mixture. Successful fractionation was confirmed by size exclusion chromatography (SEC) for the fractionated and non-fractionated samples.

A.1.6 Poly(p-methylstyrene) comb synthesis

The partially brominated PpMS backbone was introduced into a Schlenk flask, dissolved in dry THF (< 5 % w/v), cooled down to approx. -70 °C with an acetone/dry-ice cooling bath and connected via a transfer cannula with the reactor. Dry THF was then transferred into the reactor, cooled down to approx. -70 °C and the living PpMS side chains were added. The temperature was maintained at approx. -70 °C and the living side chains were titrated with the solution of the brominated PpMS over approximately 30 minutes. Stirring was continued for 1 h and the residual living side chains were terminated with degassed methanol. The comb was separated from the unreacted side chains by precipitation/fractionation in a THF-methanol mixture. Successful fractionation was confirmed by size exclusion chromatography (SEC) for the fractionated and non-fractionated samples.

A.1.7 Wittig-transformation

In a typical reaction, Methyltriphenylphosphonium bromide (PPh$_3$MeBr, 0.058 g, 0.16 mmol) were added to a preheated three-neck flask and dried under high vacuum. THF (50 ml, anhydrous) and Potassium tert-butoxide (KtOBu, 0.09 ml, 0.153 mmol) were added. The solution was heated under reflux for 8 h until the PPh$_3$MeBr was completely dissolved. A solution of acetylated PS (1.00 g, M$_w$ = 262,000 g/mol, 35 acetyl groups) in 20 ml THF (anhydrous) were slowly added under ice cooling. The turbid yellow ylid-solution turned to grey. The solution was left under stirring over night. Afterwards the

reaction was terminated by the addition of Aceton. The polymer was then precipitated in methanol, redissolved in THF and precipitated once more. To remove residual amounts of solvents, the polymer was dried under vacuum at 45 °C. ^{1}H NMR (CDCl$_3$): δ = 5.02 & 5.31 ppm (s, 2H, =CH$_2$).

A.1.8   Reduction of the acetyl-group

In a typical reaction, LiAlH$_4$ (0.4 ml, 0.4 mmol) and 50 ml THF (anhydrous) were added to a preheated schlenk flask. Under stirring a solution of acetylated PS (1 g, 262,000 g/mol, 35 acetyl groups) in 100 ml THF (anhydrous) was added dropwise. Afterwards the reaction was terminated by the addition of degassed Methanol. The polymer was then precipitated in an excess of Methanol, redissolved in THF and precipitated once more. To remove residual amounts of solvents, the polymer was dried under vacuum at 45 °C. ^{1}H NMR (CDCl$_3$): δ = 4.78 ppm (s, 1H, -CH). According to ^{1}H-NMR measurements the conversion to reduction proceeds in a quantitative conversion.

A.1.9   Conversion of the hydroxy group to a bromine

In a typical reaction, hydroxylated PS (0.5 g, 189,000 g/mol, 50 hydroxy-groups) was dissolved in CHCl$_3$ (50 ml, anhydrous) in a preheated 250 ml schlenk flask. To the solution, TMS-Cl (1.7 ml, 13 mmol), LiBr (1.15 g, 13 mmol) and acetonitril (30 ml) were added and stirred overnight. Afterwards a HCl solution (2 ml, 0.1 ml) was added and the solution was filtered to remove non-dissolved LiBr. The polymer solution was then precipitated in an excess of methanol, redissolved in THF and precipitated once more. To remove residual amounts of solvents, the polymer was dried under vacuum at 45 °C. ^{1}H NMR (CDCl$_3$): δ = 4.99 ppm (s, 1H, -CHCl) and δ = 5.14 ppm (s, 1H, -CHBr).

A.2   Characterization methods

A.2.1   NMR-spectroscopy

Quantitative ^{1}H-NMR spectroscopy was performed in deuterated chloroform (CDCl$_3$) at 30 °C using a Bruker DRX 500 spectrometer. Spectra were obtained at 500 MHz and 512 scans. The number of acetyl groups on the polystyrene backbone was calculated by the ratio of the peak integrals of the CH$_3$ protons adjacent to the carbonyl group at 2.51 ppm and the five aromatic protons located between 6 and 7.5 ppm. The number of bromomethyl (-CH$_2$Br) groups on the Poly(p-methystyrene) backbone was calculated by

the ratio of the peak integrals of the CH_2 protons adjacent to the bromine at 4.40 ppm and the four aromatic protons located between 6 and 7.5 ppm.

A.2.2 Size exclusion chromatography (SEC)

Size exclusion chromatography (SEC) was performed for the linear backbone before and after acetylation, the side chains, the raw comb product and the fractionated comb. The absolute weight-average molecular weight (M_w) and polydispersity index (PDI) of the combs was determined by SEC-MALLS (multiangle laser light scattering). The SEC instrument consisted of an Agilent 1100 pump, an Agilent 1200 Differential Refractive Index (DRI) and UV detector, a WGE Dr. Bures ETA-2010 viscometer and a PSS SLD 7000 MALLS detector with two PSS SDV Lux 8×300 mm columns (10^3 and 10^5 Å pore size). The polymers were analyzed in THF at 25 °C and a flow rate of 1 ml/min. Static light scattering experiments were performed for the comparison with the SEC-MALLS on a PSS SLD 7000 MALLS detector at seven different angles in THF at 25 °C.

A.2.3 dn/dc

The dn/dc values where measured in toluene and THF with a refractometer dn/dc 2010 from PSS, Mainz, Germany. Typically six concentrations of the polymer from 2-10 g/l were used to determine the dn/dc values.

A.2.4 Rheological measurements

Rheological measurements were conducted for oscillatory shear and uniaxial extensional flow on an ARES rotational rheometer from TA Instruments. Oscillatory shear measurements were carried out in parallel plate geometry (8 and 13 mm, gap ≈ 1 mm) in a temperature range from 130 to 230 °C using a frequency range from 10^{-1} to 10^2 rad/s for each temperature. To determine the linear viscoelastic region, strain sweep experiments were performed before the frequency sweep tests at small amplitude oscillatory shear (SAOS). The master curves were obtained using time-temperature superposition (TTS), which was found to be valid for all combs that were investigated. The horizontal shift factors were fitted independently for the PS and PpMS with the WLF function: $\log a_T = [-C_1(T-T_{ref})]/[C_2 + T - T_{ref}]$. The extensional experiments were performed at 180 °C using the Extensional Viscosity Fixture (EVF) from TA Instruments with strain rates between 0.1 and 3 s^{-1}. Non-linear data was obtained on an ARES G2 rotational rheometer from TA Instruments, with implemented FT-Rheology module, in medium (MAOS) and large oscillatory shear (LAOS). Strain sweep experiments were performed using cone plate ge-

ometries (8 and 13 mm, $\alpha = 0.1$ rad) in a temperature range from 170 to 230 °C. Strain amplitudes in a range from 10 to 75 % in a frequency range from 0.2 to 20 rad/s were applied for each temperature. The samples were press-molded under vacuum at 190 °C into 8 and 13 mm discs (shear), respectively $20 \times 10 \times 1$ mm rectangular bars (extension).

Appendix B

Rheological Data

B.1 Determination of the plateau modulus $\mathbf{G}_N^0$

The plateau modulus G_N^0 of the backbones were determined for the linear and comb polymers using the storage modulus value of the frequency which is corresponding to the minimum in $\tan \delta$. The plateau modulus for the diluted backbone $G_N^0(\Phi)$ of the comb polymers corresponds to the first minimum of $\tan \delta$ at low frequencies. The differences between the plateau modulus of the backbone of a comb and the corresponding linear backbone polymer are illustrated in Fig. B.1. The values of G_N^0 and $G_N^0(\Phi)$ are listed in table B.1.

B.2 Entanglement molecular weight $\mathbf{M}_e$ of PpMS

The entanglement molecular weight (M_e) of PpMS is about 24400 g/mol. M_e was calculated using

$$M_e = \frac{4}{5} \cdot \frac{\rho R T}{G_N^0} \tag{B.1}$$

with a plateau modulus G_N^0 = 120400 Pa, derived from the backbone mastercurve of the linear PpMS LK95 (M_w = 197.000 g/mol), at T_{ref} = 453 K (180 °C), ρ = 0.976 g/cm^3 and the gas constant R = 8.31 J/K·mol.

B.3 Determination of the reptation time

The reptation times were calculated using the Eqs. (B.2) and (B.3) [Dealy 06]. The discrete relaxation spectrum parameter set G_i, τ_i was obtained from the linear mastercurves using the IRIS software [Winter 08]. The discrete relaxation spectrum parameter set G_i,

τ_i are listed in the tables B.2 and B.2 and the plateau modulus G_N^0 can be found in table B.1 for the linear and comb polymers.

$$\eta_0 = \sum_{i=1}^{N} G_i \tau_i \qquad (B.2)$$

$$\tau_d = \frac{12}{\pi^2} \cdot \frac{\eta_0}{G_N^0} \qquad (B.3)$$

Table B.1: Plateau moduli of the comb and linear polymers.

sample #	sample name	$G_N^{0\,(a)}$ [Pa] linear backbone	$G_N^0(\Phi)^{(b)}$ [Pa] comb
LK93	275k (linear)	225700	-
LK95	197k (linear)	120400	-
LK330k	262k (linear)	207300	-
CK106	197k-14-42k	120400	7800
CK123	275k-5-42k	225700	49700
CK128	197k-14-15k	120400	23900
CK132	197k-29-15k	120400	14900
CK158	262k-2-17k	207300	182100
CK159	262k-2-37k	207300	206500
C632$^{(c)}$	275k-25-26k	210000	14700
C642$^{(c)}$	275k-29-47k	210000	5400

[a]: Plateau moduli of the corresponding linear backbone of the combs.

[b]: Plateau moduli of the diluted comb polymer backbones.

[c]: Model comb samples synthesized by Roovers [Roovers 79].
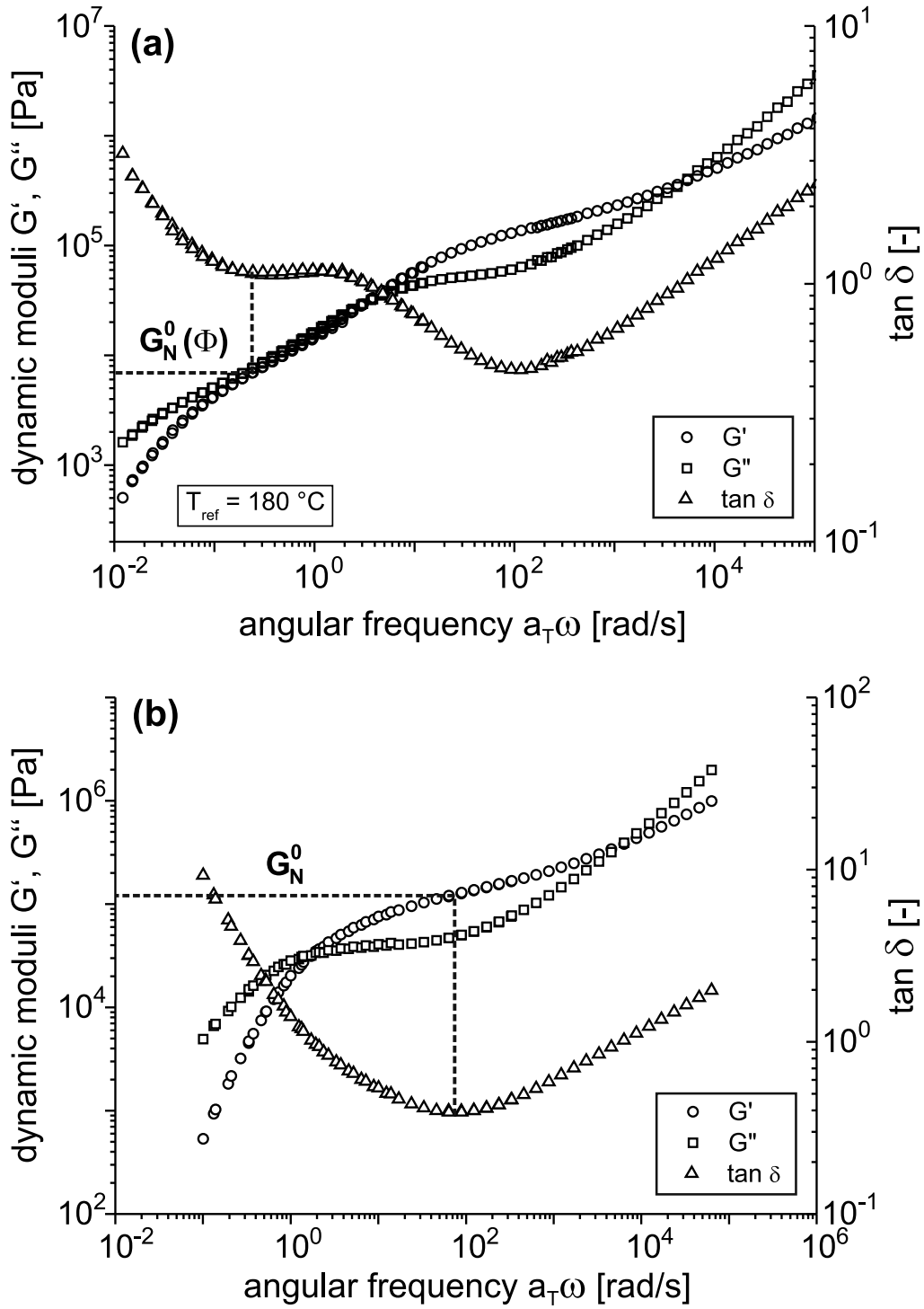
Figure B.1: Determination of the plateau modulus using the storage modulus value of the frequency which is corresponding to the minimum in tan δ. (a) Determination of the plateau modulus for the diluted backbone $G_N^0(\Phi)$ of the comb CK106 and (b) the plateau modulus G_N^0 for the corresponding linear backbone LK95 of the comb CK106.

Table B.2: Discrete relaxation spectrum parameter set G_i, τ_i of the model comb samples.

CK106 (197k-14-42k)		CK123 (275k-5-42k)		CK128 (197k-14-15k)		CK132 (197k-29-15k)	
G_i	τ_i	G_i	τ_i	G_i	τ_i	G_i	τ_i
5.12E+07	5.98E-07	3.14E+07	4.02E-07	4.09E+07	7.52E-07	5.69E+07	8.45E-07
8.35E+05	2.06E-05	7.48E+05	9.42E-06	6.56E+05	2.21E-05	8.81E+05	3.13E-05
2.86E+05	1.50E-04	2.67E+05	4.77E-05	2.57E+05	1.26E-04	2.77E+05	3.29E-04
1.10E+05	1.21E-03	1.24E+05	2.01E-04	1.20E+05	7.41E-04	1.31E+05	3.88E-03
5.60E+04	8.14E-03	6.42E+04	9.39E-04	8.23E+04	3.64E-03	3.83E+04	2.93E-02
6.12E+04	5.35E-02	5.52E+04	4.88E-03	3.69E+04	1.78E-02	1.22E+04	2.93E-01
3.35E+04	2.68E-01	5.69E+04	2.03E-02	1.61E+04	9.77E-02	3.92E+03	5.60E+00
8.06E+03	1.85E+00	4.42E+04	7.88E-02	1.11E+04	5.14E-01	5.71E+03	1.71E+00
4.25E+03	1.13E+01	3.04E+04	3.06E-01	9.38E+03	2.25E+00	2.92E+02	2.47E+01
1.67E+03	4.80E+01	1.64E+04	1.16E+00	5.79E+03	6.73E+00		
		1.39E+04	4.46E+00	3.50E+02	3.16E+01		
		1.26E+04	1.82E+01				
		1.28E+04	7.38E+01				
		5.64E+03	2.32E+02				

Table B.3: Discrete relaxation spectrum parameter set G_i, τ_i of the model comb samples.

CK158 (262k-2-17k)		CK159 (262k-2-37k)		C642 (275k-29-42k)		LK62 (62k linear)	
G_i	τ_i	G_i	τ_i	G_i	τ_i	G_i	τ_i
8.72E+06	1.95E-06	2.37E+07	6.54E-07	8.29E+04	1.22E-03	7.48E+06	2.14E-06
3.54E+05	2.91E-05	6.20E+05	1.55E-05	1.64E+07	1.10E-06	1.92E+05	5.96E-05
1.57E+05	1.63E-04	2.33E+05	8.92E-05	2.79E+05	3.43E-05	9.21E+04	2.23E-04
6.03E+04	8.83E-04	8.92E+04	4.59E-04	6.59E+04	8.97E-02	7.03E+04	9.10E-04
3.51E+04	3.93E-03	4.40E+04	2.23E-03	8.69E+04	1.31E-02	4.75E+04	3.09E-03
2.81E+04	1.72E-02	4.12E+04	1.38E-02	1.73E+05	1.53E-04	6.73E+04	7.78E-03
3.71E+04	8.36E-02	4.38E+04	7.51E-02	5.27E+03	4.78E+00	9.26E+01	1.69E-01
4.30E+04	4.22E-01	4.52E+04	3.94E-01	1.82E+04	5.11E-01		
4.31E+04	2.07E+00	4.80E+04	2.11E+00	2.98E+03	4.61E+01		
3.02E+04	6.51E+00	2.90E+04	6.85E+00	5.79E+03	6.73E+00		
2.30E+03	2.71E+01	6.45E+03	3.14E+01				
6.42E+01	2.26E+02	2.67E+02	1.97E+02				

Appendix C

Glossary

Abbreviations

AIBN	2,2'-Azobis(2-methylpropionitril)
bb	backbone
br	branch
n-BuLi	n-Butyllithium
s-BuLi	sec-Butyllithium
DPE	1,1-Diphenylethylen
DPHLi	1,1-Diphenylhexyllithium
G'	storage modulus
G"	loss modulus
G*	complex modulus
G_{red}	reduced complex modulus (G^*/G_N^0)
G_N^0	plateau modulus
M_c	critical molecular weight
M_e	entanglement molecular weight
M_n	number average molecular weight
M_w	weight average molecular weight
MeCN	acetonitril
MeOH	methanol

MWD	molecular weight distribution
NBS	N-Bromsuccinimid
P_n	degree of polymerization
PDI	polydispersity index
pMS	p-methylstyrene
PpMS	poly(p-methylstyrene)
PpMS-Li	poly(p-methylstyryl)lithium
PS	polystyrene
PSLi	polystyryllithium
rt	room temperature
THF	tetrahydrofuran
TMEDA	N,N,N',N'-tetramethylethylendiamin
V_H	hydrodynamic volume
TTS	time temperature superposition
vGP	van Gurp-Palmen

Symbols

δ	phaseangle	η_E^+	transient extensional viscosity
$\dot{\epsilon}_H$	Hencky strain rate	η_E	steady state extensional viscosity
ϵ_H	Hencky strain	ω	amplitude frequency
γ	deformation	σ	shear stress
$\dot{\gamma}$	shear rate	τ_d	reptation time
λ	relaxation time	τ_R	Rouse time
η	shear viscosity	$tan\delta$	loss factor

Bibliography

[Altares Jr. 65]   T. Altares Jr., D. P. Wyman, V. R. Allen, K. Meyersen. *J. Polym. Sci. - A* **3**(12), 4131–4151 (1965).

[Archer 04]   L. A. Archer, Juliani. *Macromolecules* **37**(3), 1076–1088 (2004).

[Bach 03]   A. Bach, K. Almdal, H. K. Rasmussen, O. Hassager. *Macromolecules* **36**(14), 5174–5179 (2003).

[Ball 89]   R. C. Ball, T. C. B. McLeish. *Macromolecules* **22**(4), 1911–1913 (April 1989).

[Barner-Kowoll 08]   C. Barner-Kowollik (eds.). Handbook of RAFT polymerization. Wiley-VCH, Weinheim (2008).

[Barnes 98]   H. A. Barnes, J. F. Hutton, K. Walters. An introduction to rheology. Rheology series ; 3. Elsevier, Amsterdam, 6. impr.. edition (1998).

[Binder 08]   W. H. Binder, R. Sachsenhofer. *Macromol. Rapid Commun.* (2008).

[Blackwell 00]   R. J. Blackwell, T. C. B. McLeish, O. G. Harlen. *J. Rheol.* **44**(1), 121–136 (2000).

[Burchard 80]   W. Burchard, M. Schmidt, W. H. Stockmayer. *Macromolecules* **13**(5), 1265–1272 (1980).

[Burghelea 11]   T. I. Burghelea, Z. Starý, H. Münstedt. *J. Non-Newtonian Fluid Mech.* **166**(19-20), 1198 – 1209 (2011).

[Butz 06]   T. Butz. Fourier transformation for pedestrians. Springer, Berlin (2006).

[Cameron 81]   G. G. Cameron, M. Y. Qureshi. *Macromol. Rapid Commun.* **2**(4), 287–291 (1981).

[Camps 87]   M. Camps, M. Chatzopoulos, J.-M. Camps, J.-P. Montheard. *Polym. Rev.* **27**(3), 505–557 (1987).

[Chalk 69]   A. J. Chalk, T. J. Hoogeboom. *J. Polym. Sci., Part A: Polym. Chem.* **7**(9), 2537–2545 (1969).

[Chambon 08]   P. Chambon, C. M. Fernyhough, K. Im, T. Chang, C. Das, J. Embery, T. C. B. McLeish, D. J. Read. *Macromolecules* **41**(15), 5869–5875 (2008).

[Cloizeaux 88]   J. des Cloizeaux. *EPL* **5**(5), 437 (1988).

[Clouet 79]   G. Clouet, J. Brossas. *Makromol. Chem.* **180**(4), 867–874 (1979).

[Colby 90]   R. H. Colby, M. Rubinstein. *Macromolecules* **23**(10), 2753–2757 (1990).

[Daniels 01]   D.R. Daniels, T.C.B. McLeish, B.J. Crosby, R.N. Young, C.M. Fernyhough. *Macromolecules* **34**(20), 7025–7033 (2001).

[Das 06]   C. Das. *J. Rheol.* **50**(2), 207 (2006).

[Dealy 06]   J. M. Dealy, R. G. Larson. Structure and rheology of molten polymers. Hanser, Munich (2006).

[Dealy 09]   J. M. Dealy, D. Plazek. *Rheol. Bull.* **78**, 16–31 (2009).

[DesLauriers 07] P. J. DesLauriers, M. P. McDaniel. *J. Polym. Sci., Part A: Polym. Chem.* **45**(15), 3135–3149 (2007).

[Doi 78]   M. Doi, S. F. Edwards. *J. Chem. Soc., Faraday Trans. 2* **74**, 1802–1817 (1978).

[Doi 80]   M. Doi, N. Y. Kuzuu. *J. Polym. Sci. Polym. Lett. Ed.* **18**(12), 775–780 (1980).

[Doi 86]   M. Doi, S. F. Edwards. The theory of polymer dynamics. Oxford University Press (1986).

[Elias 05]   H.-G. Elias. Macromolecules, Volume 1: Chemical structures and syntheses. Wiley, Weinheim (2005).

[Falk 73]   J. Falk, R. Schlott, D. Hoeg, J. Pendleton. *Rubber Chem. Technol.* **46**, 1044 (1973).

[Fernyhough 01] C.M. Fernyhough, R.N. Young, D. Poche, A.W. Degroot, F. Bosscher. *Macromolecules* **34**(20), 7034–7041 (2001).

[Ferri 99]   D. Ferri, P. Lomellini. *J. Rheol.* **43**(6), 1355–1372 (1999).

[Ferry 80]   J. D. Ferry. Viscoelastic properties of polymers. John Wiley & Sons, Inc. (1980).

[Fetters 94]   L. J. Fetters, D. J. Lohse, D. Richter, T. A. Witten, A. Zirkel. *Macromolecules* **27**(17), 4639–4647 (1994).

[Fetters 99]   L. J. Fetters, D. J. Lohse, S. T. Milner, W. W. Graessley. *Macromolecules* **32**(20), 6847–6851 (1999).

[Franck a]   A. Franck. The ARES-EVF: Option for Measuring Extensional Viscosity of Polymer Melts (APN002). Product Information, TA Instruments.

[Franck b]   A. Franck. Elongation viscosity of pololefine and polystyrene melts, measured with the EVF for ARES (AAN020). Application Note, TA Instruments.

[Fujimoto 70]   T. Fujimoto, H. Narukawa, M. Nagasawa. *Macromolecules* **3**(1), 57–64 (1970).

[Gabriel 03]   C. Gabriel, H. Münstedt. *J. Rheol.* **47**(3), 619–630 (2003).

[Gahleitner 01] M. Gahleitner. *Prog. Polym. Sci.* **26**(6), 895 – 944 (2001).

[García-Fran 01] C. A. García-Franco, S. Srinivas, D. J. Lohse, P. Brant. *Macromolecules* **34**(10), 3115–3117 (2001).

[Gennes 71] P. G. de Gennes. *J. Chem. Phys.* **55**(2), 572 (1971).

[Gennes 75] P. G. de Gennes. *J. Phys.* **36**(12), 1199–1203 (1975).

[Giacomin 98] A.J. Giacomin, J.M. Dealy. Rheological Measurement, Ch. 11, pp. 327–356. Springer (1998).

[Glasse 83] M.D. Glasse. *Prog. Polym. Sci.* **9**(2-3), 133 – 195 (1983).

[Gnanou 89] Y. Gnanou, P. Lutz. *Makromol. Chem.* **190**(3), 577–588 (1989).

[Graessley 79] W. W. Graessley, J. Roovers. *Macromolecules* **12**(5), 959–965 (1979).

[Graessley 80] W. W. Graessley. *J. Polym. Sci. Polym. Phys. Ed.* **18**(1), 27–34 (1980).

[Gurp 98] M. van Gurp, J. Palmen. *Rheol. Bull.* **67**, 5–8 (1998).

[Hadjichristid 00a] N. Hadjichristidis, H. Iatrou, S. Pispas, M. Pitsikalis. *J. Polym. Sci., Part A: Polym. Chem.* **38**(18), 3211–3234 (2000).

[Hadjichristid 00b] N. Hadjichristidis, M. Xenidou, H. Iatrou, M. Pitsikalis, Y. Poulos, A. Avgeropoulos, S. Sioula, S. Paraskeva, G. Velis, D. J. Lohse, D. N. Schulz, L. J. Fetters, P. J. Wright, R. A. Mendelson, C. A. García-Franco, T. Sun, C. J. Ruff. *Macromolecules* **33**(7), 2424–2436 (2000).

[Hepperle 05] J. Hepperle, H. Münstedt, P. Haug, C. Eisenbach. *Rheol. Acta* **45**(2), 151–163 (2005).

[Hepperle 06] J. Hepperle, H. Münstedt. *Rheol. Acta* **45**(5), 717–727 (2006).

[Heymans 00] N. Heymans. *Macromolecules* **33**(11), 4226–4234 (2000).

[Hirao 96] A. Hirao, M. Hayashi, S. Nakahama. *Macromolecules* **29**(10), 3353–3358 (1996).

[Hirao 09] A. Hirao, K. Murano, R. Kurokawa, T. Watanabe, K. Sugiyama. *Macromolecules* **42**(20), 7820–7827 (2009).

[Hong 99] K. Hong, D. Uhrig, J. W. Mays. *Curr. Opin. Solid State Mater. Sci.* **4**(6), 531–538 (1999).

[Hoyle 10] C. E. Hoyle, C. N. Bowman. *Angew. Chem.* **122**(9), 1584–1617 (2010).

[Hsieh 96] H. L. Hsieh, R. P. Quirk. Anionic polymerization: principles and practical applications. Plastics engineering; 34. Dekker, New York (1996).

[Hyun 09] K. Hyun, M. Wilhelm. *Macromolecules* **42**(1), 411–422 (2009).

[Hyun 10] K. Hyun, M. Wilhelm. *KGK* pp. 123–129 (2010).

[Hyun 11] K. Hyun, M. Wilhelm, C. O. Klein, K. S. Cho, J. G. Nam, K. H. Ahn, S. J. Lee, R. H. Ewoldt, G. H. McKinley. *Prog. Polym. Sci.* **36**(12), 1697 – 1753 (2011).

[Inkson 99]   N. J. Inkson, T. C. B. McLeish, O. G. Harlen, D. J. Groves. *J. Rheol.* **43**(4), 873–896 (1999).

[Inkson 06]   N.J. Inkson, R.S. Graham, T.C.B. McLeish, D.J. Groves, C.M. Fernyhough. *Macromolecules* **39**(12), 4217–4227 (2006).

[Islam 01]   M. T. Islam, Juliani, L. A. Archer, S. K. Varshney. *Macromolecules* **34**(18), 6438–6449 (2001).

[Janata 02]   M. Janata, B. Masar, L. Toman, P. Vlcek, P. Polická, J. Brus, P. Holler. *React. Funct. Polym.* **50**(1), 67–75 (2002).

[Janzen 99]   J. Janzen, R. H. Colby. *J. Mol. Struct.* **485-486**, 569 – 584 (1999).

[Kapnistos 05]   M. Kapnistos, D. Vlassopoulos, J. Roovers, L.G. Leal. *Macromolecules* **38**(18), 7852–7862 (2005).

[Kapnistos 09]   M. Kapnistos, K. M. Kirkwood, J. Ramirez, D. Vlassopoulos, L. G. Leal. *J. Rheol.* **53**(5), 1133–1153 (2009).

[Kirkwood 09]   K. M. Kirkwood, L. G. Leal, D. Vlassopoulos, P. Driva, N. Hadjichristidis. *Macromolecules* **42**(24), 9592–9608 (2009).

[Klimke 06]   K. Klimke, M. Parkinson, C. Piel, W. Kaminsky, H. W. Spiess, M. Wilhelm. *Macromol. Chem. Phys.* **207**(4), 382–395 (2006).

[Koutalas 05]   G. Koutalas, H. Iatrou, D. J. Lohse, N. Hadjichristidis. *Macromolecules* **38**(12), 4996–5001 (2005).

[Krieger 73]   I. M. Krieger, T.-F. Niu. *Rheol. Acta* **12**, 567–571 (1973).

[Larson 99]   R. G. Larson. The structure and rheology of complex fluids. Oxford University Press, New York (1999).

[Larson 01]   R. G. Larson. *Macromolecules* **34**(13), 4556–4571 (2001).

[Lee 01]   K. Lee, M. R. Mackley, T. C. B. McLeish, T. M. Nicholson, O. G. Harlen. *J. Rheol.* **45**(6), 1261–1277 (2001).

[Lee 05]   J.S. Lee, R.P. Quirk, M.D. Foster. *Macromolecules* **38**(13), 5381–5392 (2005).

[Li 01]   J. Li, M. Gauthier. *Macromolecules* **34**(26), 8918–8924 (2001).

[Likhtman 02]   A. E. Likhtman, T. C. B. McLeish. *Macromolecules* **35**(16), 6332–6343 (2002).

[Liu 11]   J. Liu, W. Yu, C. Zhou. *J. Rheol.* **55**(3), 545–570 (2011).

[Lohse 02]   D. J. Lohse, S. T. Milner, L. J. Fetters, M. Xenidou, N. Hadjichristidis, R. A. Mendelson, C. A. García-Franco, M. K. Lyon. *Macromolecules* **35**(8), 3066–3075 (2002).

[Macosko 94]   C. W. Macosko. Rheology: principles, measurements, and applications. VCH, New York (1994).

[Malpass 10]   D. B. Malpass. Introduction to Industrial Polyethylene: Properties, Catalysts, and Processes. John Wiley & Sons (2010).

[Marrucci 85]   G. Marrucci. *J. Polym. Sci. Polym. Phys. Ed.* **23**(1), 159–177 (1985).

[Marrucci 96]   G Marrucci. *J. Non-Newtonian Fluid Mech.* **62**(2-3), 279 – 289 (1996).

[Marrucci 04]   G. Marrucci, G. Ianniruberto. *Macromolecules* **37**(10), 3934–3942 (2004).

[McLeish 88]   T. C. B. McLeish. *EPL* **6**(6), 511 (1988).

[McLeish 98]   T. C. B. McLeish, R. G. Larson. *J. Rheol.* **42**(1), 81–110 (1998).

[McLeish 99]   T. C. B. McLeish, J. Allgaier, D. K. Bick, G. Bishko, P. Biswas, R. Blackwell, B. Blottiere, N. Clarke, B. Gibbs, D. J. Groves, A. Hakiki, R. K. Heenan, J. M. Johnson, R. Kant, D. J. Read, R. N. Young. *Macromolecules* **32**(20), 6734–6758 (1999).

[McLeish 02]   T. C. B. McLeish. *Adv. Phys.* **51**(6), 1379–1527 (2002).

[Meissner 94]   J. Meissner, J. Hostettler. *Rheol. Acta* **33**, 1–21 (1994).

[Mezger 06]   Thomas Mezger. The rheology handbook: for users of rotational and oscillatory rheometers. Vincentz Network, Hannover, 2., rev. ed.. edition (2006).

[Milner 97]   S. T. Milner, T. C. B. McLeish. *Macromolecules* **30**(7), 2159–2166 (1997).

[Milner 98]   S. T. Milner, T. C. B. McLeish. *Phys. Rev. Lett.* **81**(3), 725–728 (1998).

[Monrabal 94]   B. Monrabal. *J. Appl. Polym. Sci.* **52**(4), 491–499 (1994).

[Mori 99]   S. Mori, H. G. Barth. Size exclusion chromatography. Springer laboratory. Springer, Berlin (1999).

[Morton 70]   M. Morton, L. J. Fetters, R. A. Pett, J. F. Meier. *Macromolecules* **3**(3), 327–332 (1970).

[Münstedt 75]   H. Münstedt. *Rheol. Acta* **14**, 1077–1088 (1975).

[Münstedt 79]   H. Münstedt. *J. Rheol.* **23**(4), 421 (1979).

[Münstedt 80]   H. Münstedt. *J. Rheol.* **24**(6), 847 (1980).

[Münstedt 06]   H. Münstedt, S. Kurzbeck, J. Stange. *Polym. Eng. Sci.* **46**(9), 1190–1195 (2006).

[Neidhöfer 03] T. Neidhöfer, M. Wilhelm, B. Debbaut. *J. Rheol.* **47**(6), 1351–1371 (2003).

[Neidhöfer 04] T. Neidhöfer, S. Sioula, N. Hadjichristidis, M. Wilhelm. *Macromol. Rapid Commun.* **25**(22), 1921–1926 (2004).

[Nielsen 06]   J. K. Nielsen, H. K. Rasmussen, M. Denberg, K. Almdal, O. Hassager. *Macromolecules* **39**(25), 8844–8853 (2006).

[Odian 04]   G. Odian. Principles of polymerization. Wiley-Interscience, Hoboken, NJ, 4th. edition (2004).

[Olah 80]   G. A. Olah, B. G. B. Gupta, R. Malhotra, S. C. Narang. *J. Org. Chem* **45**(9), 1638–1639 (1980).

[Park 04]   S. J. Park, R. G. Larson. *Macromolecules* **37**(2), 597–604 (2004).

[Peacock 00]   A. J. Peacock. Handbook of polyethylene: structures, properties, and applications. Dekker, New York (2000).

[Pearson 84]   D. S. Pearson, E. Helfand. *Macromolecules* **17**(4), 888–895 (1984).

[Pepper 53]   K. W. Pepper, H. M. Paisley, M. A. Young. *J. Chem. Soc.* pp. 4097 – 4105 (1953).

[Podzimek 01a] S. Podzimek, T. Vlcek. *J. Appl. Polym. Sci.* **82**(2), 454–460 (2001).

[Podzimek 01b] S. Podzimek, T. Vlcek, C. Johann. *J. Appl. Polym. Sci.* **81**(7), 1588–1594 (2001).

[Pryke 02]   A. Pryke, R. J. Blackwell, T. C. B. McLeish, R. N. Young. *Macromolecules* **35**(2), 467–472 (2002).

[Quirk 82]   R. P. Quirk, W.-C. Chen. *Makromol. Chem.* **183**(9), 2071–2076 (1982).

[Quirk 84]   R. P. Quirk, W.-C. Chen. *J. Polym. Sci., Part A: Polym. Chem.* **22**(11), 2993–3000 (1984).

[Quirk 03]   Roderic P. Quirk, Bumjae Lee. *Macromol. Chem. Phys.* **204**(14), 1719–1737 (2003).

[Quirk 07]   R. P. Quirk, C. Garcés, M. J. Polce, C. Wesdemiotis. *Polym. Prepr.* **48**, 169 (2007).

[Radke 96]   W. Radke. *Synthese von Kammpolymeren und deren Charakterisierung durch GPC mit Lichtstreu- und Viskositätsdetektion*. Dissertation, Johannes Gutenberg Universität, Mainz (1996).

[Radke 05]   W. Radke, A.H.E. Müller. *Macromolecules* **38**(9), 3949–3960 (2005).

[Rahlwes 77]   D. Rahlwes, J. E. L. Roovers, S. Bywater. *Macromolecules* **10**(3), 604–609 (1977).

[Rasmussen 05] H. Rasmussen. *J. Rheol.* **49**(2), 369 (2005).

[Roovers 75]   J. Roovers. *Polymer* **16**(11), 827–832 (1975).

[Roovers 79]   J. Roovers. *Polymer* **20**(7), 843–849 (1979).

[Roovers 81]   J. Roovers, W. W. Graessley. *Macromolecules* **14**(3), 766–773 (1981).

[Roovers 84]   J. Roovers. *Macromolecules* **17**(6), 1196–1200 (1984).

[Schlatter 05] G. Schlatter, G. Fleury, R. Muller. *Macromolecules* **38**(15), 6492–6503 (2005).

[Schulze 01]   J. S. Schulze, T. P. Lodge, C. W. Macosko, J. Hepperle, H. Münstedt, H. Bastian, D. Ferri, D. J. Groves, Y. H. Kim, M. Lyon, T. Schweizer, T. Virkler, E. Wassner, W. Zoetelief. *Rheol. Acta* **40**, 457–466 (2001).

[Schulze 05]   D. Schulze, T. Roths, C. Friedrich. *Rheol. Acta* **44**(5), 485–494 (2005).

[Sentmanat 04]   M. L. Sentmanat. *Rheol. Acta* **43**, 657–669 (2004).

[Sentmanat 05]   M. L. Sentmanat. *J. Rheol.* **49**(3), 585 (2005).

[Shaw 94]   M. T. Shaw, W. H. Tuminello. *Polym. Eng. Sci.* **34**(2), 159–165 (1994).

[Spitael 04]   P. Spitael, C. W. Macosko. *Polym. Eng. Sci.* **44**(11), 2090–2100 (2004).

[Stadler 09]   F. Stadler, J. Kaschta, H. Münstedt, F. Becker, M. Buback. *Rheol. Acta* **48**, 479–490 (2009).

[Szwarc 68]   M. Szwarc. Carbanions living polymers and electron transfer processes. Interscience Publ., New York (1968).

[Takaki 79]   M. Takaki, R. Asami, Y. Kuwata. *Macromolecules* **12**(3), 378–382 (1979).

[Trinkle 01]   S. Trinkle, C. Friedrich. *Rheol. Acta* **40**(4), 322–328 (2001).

[Trinkle 02]   S. Trinkle, P. Walter, C. Friedrich. *Rheol. Acta* **41**(1), 103–113 (2002).

[Trouton 06]   F. T. Trouton. *Proc. R. Soc. London, Ser. A* **77**(519), 426–440 (1906).

[Tuminello 86]   W. H. Tuminello. *Polym. Eng. Sci.* **26**(19), 1339–1347 (1986).

[Vega 07]   D. A. Vega, S. T. Milner. *J. Polym. Sci., Part B: Polym. Phys.* **45**(23), 3117–3136 (2007).

[Vittorias 07a]   I. Vittorias, M. Parkinson, K. Klimke, B. Debbaut, M. Wilhelm. *Rheol. Acta* **46**, 321–340 (2007).

[Vittorias 07b]   I. Vittorias, M. Wilhelm. *KGK* **60**, 112–120 (2007).

[Wagner 79]   M. H. Wagner, T. Raible, J. Meissner. *Rheol. Acta* **18**, 427–428 (1979).

[Wagner 92]   M. Wagner. *J. Rheol.* **36**(1), 1 (1992).

[Wagner 00]   M. H. Wagner, H. Bastian, P. Hachmann, J. Meissner, S. Kurzbeck, H. Münstedt, F. Langouche. *Rheol. Acta* **39**, 97–109 (2000).

[Wagner 03]   M. Wagner. *J. Rheol.* **47**(3), 779 (2003).

[Wagner 04]   M. H. Wagner, J. Hepperle, H. Münstedt. *J. Rheol.* **48**(3), 489–503 (2004).

[Wagner 05]   M. H. Wagner, S. Kheirandish, K. Koyama, A. Nishioka, A. Minegishi, T. Takahashi. *Rheol. Acta* **44**, 235–243 (2005).

[Wagner 08]   M. H. Wagner, V. H. Rolon-Garrido. *J. Rheol.* **52**(5), 1049–1068 (2008).

[Wang 10]   Z. Wang, X. Chen, R. G. Larson. *J. Rheol.* **54**(2), 223–260 (2010).

[Watanabe 99]   H. Watanabe. *Prog. Polym. Sci.* **24**(9), 1253 – 1403 (1999).

[Wilhelm 98]   M. Wilhelm, D. Maring, H.-W. Spiess. *Rheol. Acta* **37**, 399–405 (1998).

[Wilhelm 02]   M. Wilhelm. *Macromol. Mater. Eng.* **287**(2), 83–105 (2002).

[Williams 55] M. L. Williams, R. F. Landel, J. D. Ferry. *J. Am. Chem. Soc.* **77**(14), 3701–3707 (1955).

[Winter 86] H. Winter. *J. Rheol.* **30**(2), 367 (1986).

[Winter 08] H. H. Winter. *AIP Conf. Proc.* **1027**, 1387–1389 (2008).

[Wood-Adams 00a] P. M. Wood-Adams, J. M. Dealy. *Macromolecules* **33**(20), 7481–7488 (2000).

[Wood-Adams 00b] P. M. Wood-Adams, J. M. Dealy, A. W. deGroot, O. D. Redwine. *Macromolecules* **33**(20), 7489–7499 (2000).

[Worsfold 72] D. J. Worsfold, S. Bywater. *Macromolecules* **5**(4), 393–397 (1972).

[Wu 04] C. Wu (eds.). Handbook of size exclusion chromatography and related techniques. Dekker, New York, 2nd, rev. and exp. edition (2004).

[Yamaguchi 02] M. Yamaguchi, K.-I. Suzuki. *J. Appl. Polym. Sci.* **86**(1), 79–83 (2002).

[Yurasova 94] T. A. Yurasova, T. C. B. McLeish, A. N. Semenov. *Macromolecules* **27**(24), 7205–7211 (1994).

[Zhang 03] M. Zhang, S. E. Wanke. *Polym. Eng. Sci.* **43**(12), 1878–1888 (2003).

[Zimm 48a] B. Zimm. *J. Chem. Phys.* **16**(12), 1099 (1948).

[Zimm 48b] B. Zimm. *J. Chem. Phys.* **16**(12), 1093 (1948).

[Zimm 49] B. Zimm. *J. Chem. Phys.* **17**(12), 1301–1314 (1949).

ACKNOWLEDGMENT

Life is like a long road with many crossroads along the way and sometimes we are unsure which way to go, where we will pass by or where our way will eventually lead. However, on our way we are not alone. On this part of the road, I met many people who I want to thank for helping me to find the right direction and for their company during this time thereby making this a pleasent journey. I am deeply indepted to ...

Prof. Dr. Manfred Wilhelm for the opportunity to work in his group, his continual interest and support at each stage of my work, for giving me the opportunity to go to the USA and Greece for research stays and for the freedom he provided me to follow my own ideas.

Prof. Dimitris Vlassopoulos (University of Crete) for the chance to work in his group and for his kind hospitality and support during my research stay at FORTH. I also want to thank Helen Lentzakis, Antje Larsen, Kiki, Uli Jonas, Rossana Pasquino, Frank Snijkers and Simon Rogers for their support and the good times together during my stay in Crete.

Prof. Haskell Beckham (Georgia Institute of Technology) for the opportunity to work in his group, the freedom he gave me to explore my own ideas and for his kind hospitality and support during my research stay. I especially want to thank Matthew Ryan Kincer and his family, Kara King and Kristy Wentz for their hospitality and support during my stay in Atlanta. They helped me to feel at home and gave me an unforgettable experience.

Dr. Vitor Barroso as my rheology mentor, for introducing me to the mysteries of rheology and his support during my work.

The *AK Wilhelm* for the great atmosphere and the pleasant time I had during my PhD. I especially want to thank Christopher Klein, Kathrin Reinheimer, Ingo Naue, Thomas Meins, Vitor Barroso and Arrate Huegun Mutiloa for their friendship and the good times we had together. I want to acknowledge Miriam Cziep for supporting me with the development of the synthesis methods and for the nice conversations that made the lab work much more pleasant. I also want to thank my lab colleagues Alicia Malek and Thomas Meins for their help and the pleasant work environment in the lab.

CURRICULUM-VITAE

PERSONAL DETAILS:

Name:	Michael Kempf
Date of birth:	18.10.1979
Place of birth:	Landau in der Pfalz

UNIVERSITY:

08/07-12/11	Ph.D. thesis under the supervision of Prof. Dr. Manfred Wilhelm at the Institute for Chemical Technology and Polymerchemistry, Karlsruhe Institute of Technology (KIT). Topic: "Synthesis and Rheology of Model Comb Polymer Architectures."
03/10-07/10	Research stay at the research group of Prof. Dimitris Vlassopoulos, Foundation of Research and Technology Hellas (FORTH) in Heraklion, Greece.
08/08-12/08	Research stay at the research group of Prof. Haskell Beckham at the Georgia Institute of Technology in Atlanta, USA. Supported by a stipend from the Karlsruhe House of Young Scientists (KHYS).
10/00-07/07	Chemistry studies, University of Karlsruhe, Diploma in Chemistry, 2007. Diploma thesis at the research group of Prof. Dr. Manfred Wilhelm at the Max-Planck Institute for Polymer Research in Mainz, Germany. Topic: "Synthesis und rheological investigation of atactic Poly(para-Methylstyrol) comb architectures."

MILITARY SERVICE:

07/99-04/00	Military service at the 4th tank artillery batallion 345, Kusel, Germany.

SCHOOL EDUCATION:

08/90-06/99	Alfred-Grosser Gymnasium, Bad Bergzabern, Germany. Abitur 1999.